CHAPTER 8
THE DYNAMIC PROCESS RESPONSE TO STEP CHANGES IN FURNACE OPERATING PARAMETERS

This chapter describes a series of experiments conducted with the ISFP model. The purpose of these experiments was to study the influence of step changes in furnace operating parameters on the dynamic behaviour of the furnace wall, freeze lining, crust and slag bath. The focus was on the following aspects:

- Freeze lining and crust thickness.
- Temperature distribution through the furnace wall, freeze lining and crust.
- Time lag in temperature response of the refractory brick wall relative to the time when conditions changed in the slag bath.
- Liquid slag temperature.
- Composition distribution through the freeze lining and crust.
- Liquid slag composition.

In addition to the above list, metal bath composition data, off-gas composition data, heat loss data and reactor power data are also presented to provide a comprehensive set of results for each experiment.

8.1 EXPERIMENTAL SETUP

The model flow diagram used for all experiments in this chapter is shown in Figure 58 (page 116). The geometry and dimensions used are all the same as those given in paragraph 5.3.1 (page 90).

A single steady state was generated and used for all experiments conducted in this chapter. The details of this steady state are as follows:

- Inputs
  - ElectricalPower: 21,715 kW
  - IlmeniteFeed: 20,000 kg/h
  - ReductantFeed: 1,700 kg/h
- Contents
  - IsoMod1:
    - Temperature: 1,589 °C
  - SlagBath:
    - Mass: 225,859 kg
    - Composition: 14.7-54.0-31.9 (FeO-TiO_2-Ti_2O_3 mass percentages)
  - MetalBath:
    - Mass: 323,002 kg
    - Composition: 2 mass percent carbon. Trace amounts of O, Ti and TiO. Balance as Fe.
  - ReductantInBath:
    - Mass: 52.4 kg
  - FurnaceFreeboard:
    - Mass: 30.9 kg
    - Composition: 98.8-1.2 (CO-CO_2 volume percentages)
  - FurnaceWall:
    - Freeze lining thickness: 76.3 mm
    - Freeze lining mass: 7,992 kg
  - Crust:
    - Crust thickness: 0 mm
- Outputs
  - HeatLoss1: 161.5 kW
  - HeatLoss2: 434.8 kW

- FurnaceWall: 280 kW
- Crust: 2,631 kW
- SlagTap: 11,842 kg/h
- MetalTap: 6,151 kg/h
- Offgas: 3,707 kg/h

The effective thermal conductivity of the liquid slag was assumed to be 0.005 kW/(m.°C).

All experiments were run for a period of 24 hours, or until the freeze lining had been melted away completely.

8.2 EXPERIMENTS

The parameters that were varied over the series of experiments include the following:

- Ilmenite feed rate.
- Reductant feed rate.
- Electrical power.

The set of experiments with the various parameters of interest to each experiment are listed in Table 23 below. The set of 20 experiments consists of 4 subsets.

EXPERIMENT NO.	ILMENITE FEED RATE CHANGE	ILMENITE FEED RATE	REDUCTANT FEED RATE CHANGE	REDUCTANT FEED RATE	ELECTRICAL POWER CHANGE	ELECTRICAL POWER
8.1	−20,000 kg/h	0 kg/h	−1,700 kg/h	0 kg/h	−	21,715 kW
8.2	−	20,000 kg/h	−1,700 kg/h	0 kg/h	−	21,715 kW
8.3	−	20,000 kg/h	+ 1 kg/t ilm.	1,720 kg/h	−	21,715 kW
8.4	−	20,000 kg/h	−1 kg/ton ilm.	1,680 kg/h	−	21,715 kW
8.5	−	20,000 kg/h	+ 2 kg/ton ilm.	1,740 kg/h	−	21,715 kW
8.6	−	20,000 kg/h	−2 kg/ton ilm.	1,660 kg/h	−	21,715 kW
8.7	−	20,000 kg/h	−	1,700 kg/h	+ 5 kWh/ton ilm.	21,815 kW
8.8	−	20,000 kg/h	−	1,700 kg/h	−5 kWh/ton ilm.	21,615 kW
8.9	−	20,000 kg/h	−	1,700 kg/h	+ 10 kWh/ton ilm.	21,915 kW
8.10	−	20,000 kg/h	−	1,700 kg/h	−10 kWh/ton ilm.	21,515 kW
8.11	−	20,000 kg/h	+ 1 kg/ton ilm.	1,720 kg/h	+ 5 kWh/ton ilm.	21,815 kW
8.12	−	20,000 kg/h	−1 kg/ton ilm.	1,680 kg/h	−5 kWh/ton ilm.	21,615 kW
8.13	−	20,000 kg/h	+ 2 kg/ton ilm.	1,740 kg/h	+ 10 kWh/ton ilm.	21,915 kW
8.14	−	20,000 kg/h	−2 kg/ton ilm.	1,660 kg/h	−10 kWh/ton ilm.	21,515 kW
8.15	−	20,000 kg/h	+ 5 kg/ton ilm.	1,800 kg/h	+ 25 kWh/ton ilm.	22,215 kW
8.16	−	20,000 kg/h	−5 kg/ton ilm.	1,600 kg/h	−25 kWh/t ilm	21,215 kW
8.17	−	20,000 kg/h	+ 10 kg/ton ilm.	1,900 kg/h	+ 50 kWh/ton ilm.	22,715 kW
8.18	−	20,000 kg/h	−10 kg/ton ilm.	1,500 kg/h	−50 kWh/ton ilm.	20,715 kW
8.19	−	20,000 kg/h	+ 10 kg/ton ilm.	1,900 kg/h	+ 52 kWh/ton ilm.	22,755 kW
8.20	−	20,000 kg/h	−10 kg/ton ilm.	1,500 kg/h	−53 kWh/ton ilm.	20,655 kW

Table 23 – List of experiments conducted for CHAPTER 8.

The first subset consists of experiments 8.1 and 8.2. The objective of these experiments was to investigate the influence of two severe operational errors on the process. In experiment 8.1 all feed was stopped while maintaining the initial power input. In experiment 8.2 only the reductant feed was stopped and the initial ilmenite feed rate and electrical power was maintained.

The second subset consists of experiments 8.3 to 8.10. The aim of these experiments was to determine the influence on the process of independent adjustment of the reductant feed rate and electrical power operating parameters. Increasing and decreasing adjustments were made to both operating parameters. It

was reported by Pistorius (1999) that energy and reductant inputs cannot be changed independently while maintaining stable process conditions. It was further suggested in that work that the ratio between reductant and energy change must be 1 kg:5 kWh. Therefore, each 1kg/(ton ilmenite) reductant change must be combined with a 5 kWh/(ton ilmenite) energy change. The second subset of experiments therefore ignored this suggestion. The impact of the changes were expected to be clear because the steady state initial condition used by all of the experiments represented stable operating conditions.

The third subset included experiments 8.11 to 8.18. These experiments aimed to test the validity of the 1 kg:5 kWh ratio proposed by Pistorius (1999). Experiments covered both increases and decreases in reductant and energy operating parameters. The magnitudes of the changes were also varied to study dynamic process responses further.

The results of the third subset showed excellent agreement with the 1:5 ratio proposed by Pistorius (1999). At large operating parameter changes the freeze lining thickness did however vary. In the fourth and last subset it was attempted to adjust the 1 kg:5 kWh ratio so that very little variation in freeze lining thickness occurred over the duration of the experiment.

8.3 EXPERIMENTAL RESULTS

The results from each experiment are presented below using a series of graphs marked from (a) to (n). The set of graphs is presented consistently for all experiments in this chapter. For this reason each graph type in the set is explained below. A discussion of the experimental results follows after the graphical presentation of the results of all experiments conducted as part of this chapter.

(a) Freeze Lining Thickness and Isotherm Graph

Refer to paragraph 6.3, item (a) on page 139 for details.

(b) Freeze Lining Composition Graph

This graph shows the composition of the freeze lining as a function of position within the freeze lining at the point in time when the freeze lining thickness was at its maximum.

The composition of the solid slag is presented by showing both the distribution of mass between phases (rutile and pseudobrookite), and by showing the distribution of mass between constituents of a specific phase. The phases are separated by a thick solid line, and the constituents within a phase are separated by a thin solid line. The rutile phase is always plotted in the lower part of the graph, and pseudobrookite above it.

Refer to paragraph 6.3, item (e) on page 140 for more details.

(c) Crust Thickness Graph

This graph shows the thickness of the solid slag crust as a function of time.

(d) Crust Composition Graph

This graph shows the composition of the crust as a function of crust thickness at the point in time when the crust thickness was at its maximum.

This graph is presented similarly to graph (b). Refer to that paragraph above for more details.

(e) Temperature Response Time Delay Graph

Refer to paragraph 6.3, item (c) on page 139 for details.

(f) Liquid Slag Temperature Graph

Refer to paragraph 6.3, item (b) on page 139 for details.

(g) Liquid Slag Composition Graph

Refer to paragraph 6.3, item (d) on page 140 for details.

(h) Liquid Slag Composition Ternary Graph

Refer to paragraph 6.3, item (f) on page 141 for details.

(i) Liquid Metal Composition Graph

This graph shows the variation (with time) of the liquid metal C, O and Ti content. Carbon content is expressed in mass percentage and oxygen and titanium content in parts per million (ppm) by mass.

(j) Off-gas Composition Graph

This graph shows the variation (with time) of off-gas composition. Firstly the CO and CO_2 contents are give in volume percentage. The bottom-most sub-graph shows the variation of the logarithm of the oxygen partial pressure.

(k) Reactor Power Graph

Each of the four reactors in the model flow sheet (Figure 58, page 116) describes one or more chemical reactions. The net enthalpy change calculated by the Gibbs-free-energy minimisation in each reactor is always endothermic. The power indicated on this graph is therefore the rate at which energy is consumed by each of the reactors.

(l) Heat Loss Graph

This graph presents time series heat loss data of the process. It consists of three sub-graphs. The 'Upper' sub-graph shows the sum of the Crust conductor module and HeatLoss1 energy output module heat losses. This represents all radiation and convection losses from the slag bath surface. The 'Middle' sub-graph shows the heat loss calculated by the FurnaceWall conductor module. This only describes heat lost through the portion of the sidewall that is covered by the freeze lining. The 'Lower' sub-graph shows the heat loss represented by the HeatLoss2 energy output module. This heat loss includes heat lost through the portion of the sidewalls below the freeze lining and heat lost through the furnace hearth.

(m) Energy Balance Error Graph

Refer to paragraph 6.3, item (g) on page 141 for details.

(n) Mass Balance Error Graph

Refer to paragraph 6.3, item (h) on page 142 for details.

Fluctuations are present in many of the signals presented in graphs (i), (j) and (k). These fluctuates were caused by the method used to regulate the liquid slag composition close to the stoichiometric M_3O_5 line. See paragraphs 5.6.8a (page 125) and 5.6.8b (page 129) for details about the approach used.

8.3.1 Experiment 8.1

ILMENITE FEED RATE CHANGE	ILMENITE FEED RATE	REDUCTANT FEED RATE CHANGE	REDUCTANT FEED RATE	ELECTRICAL POWER CHANGE	ELECTRICAL POWER
−20,000 kg/h	0 kg/h	−1,700 kg/h	0 kg/h	-	21,715 kW

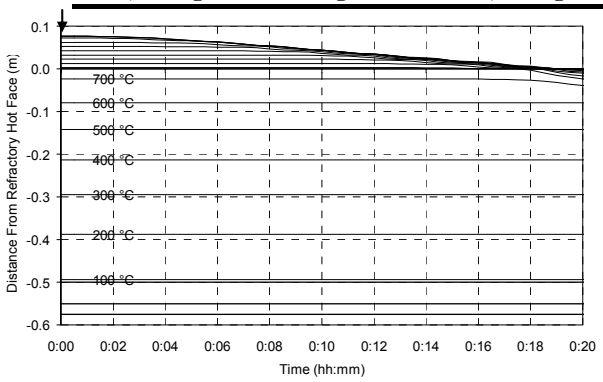

(a)

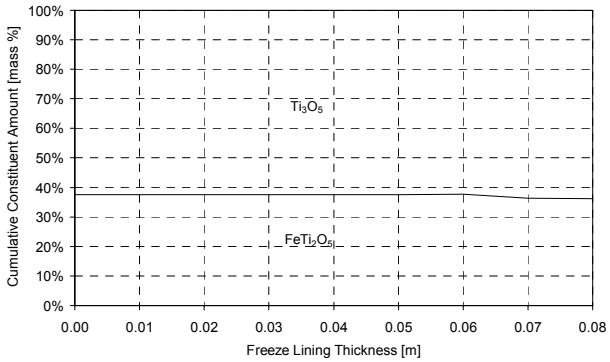

(b)

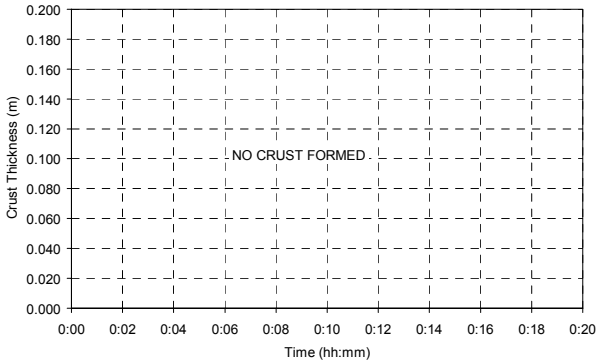

(c)

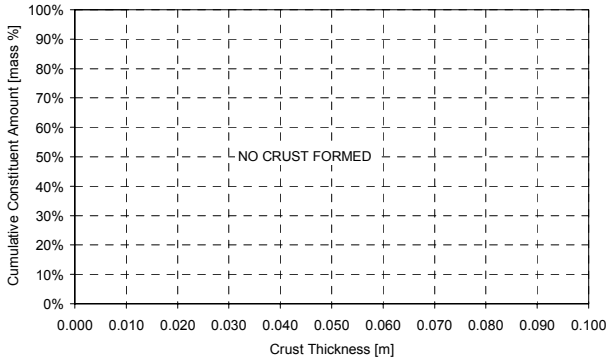

(d)

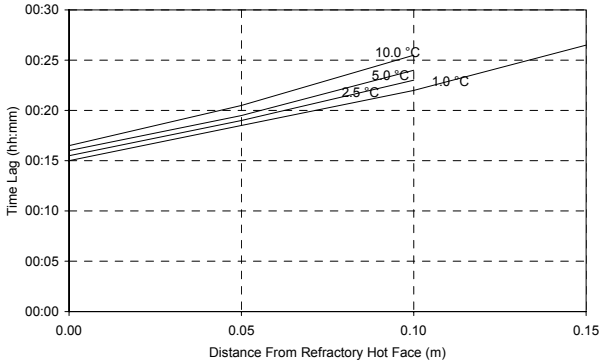

(e)

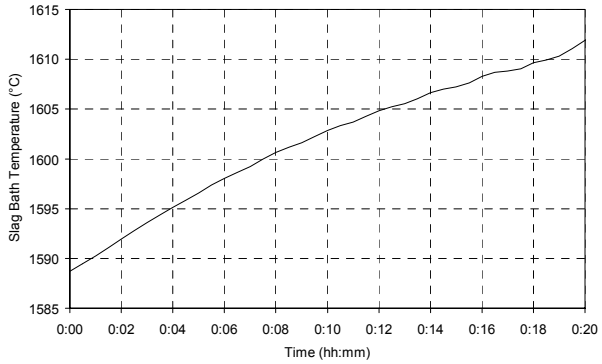

(f)

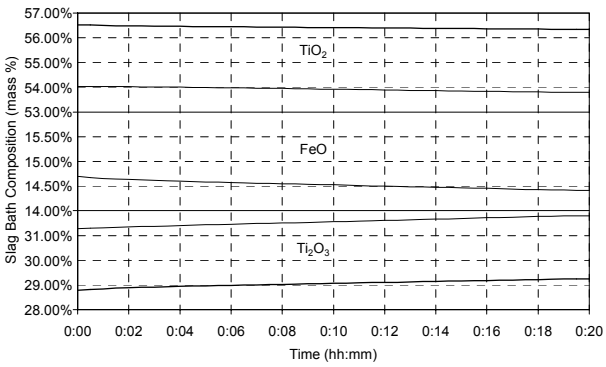

(g)

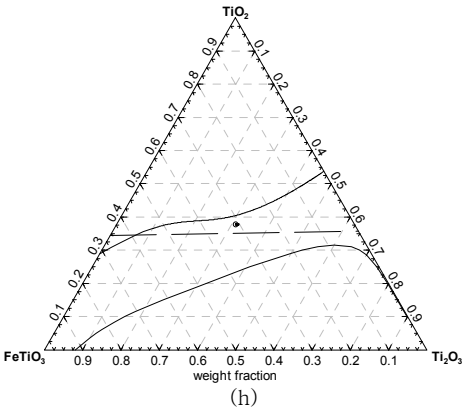

(h)

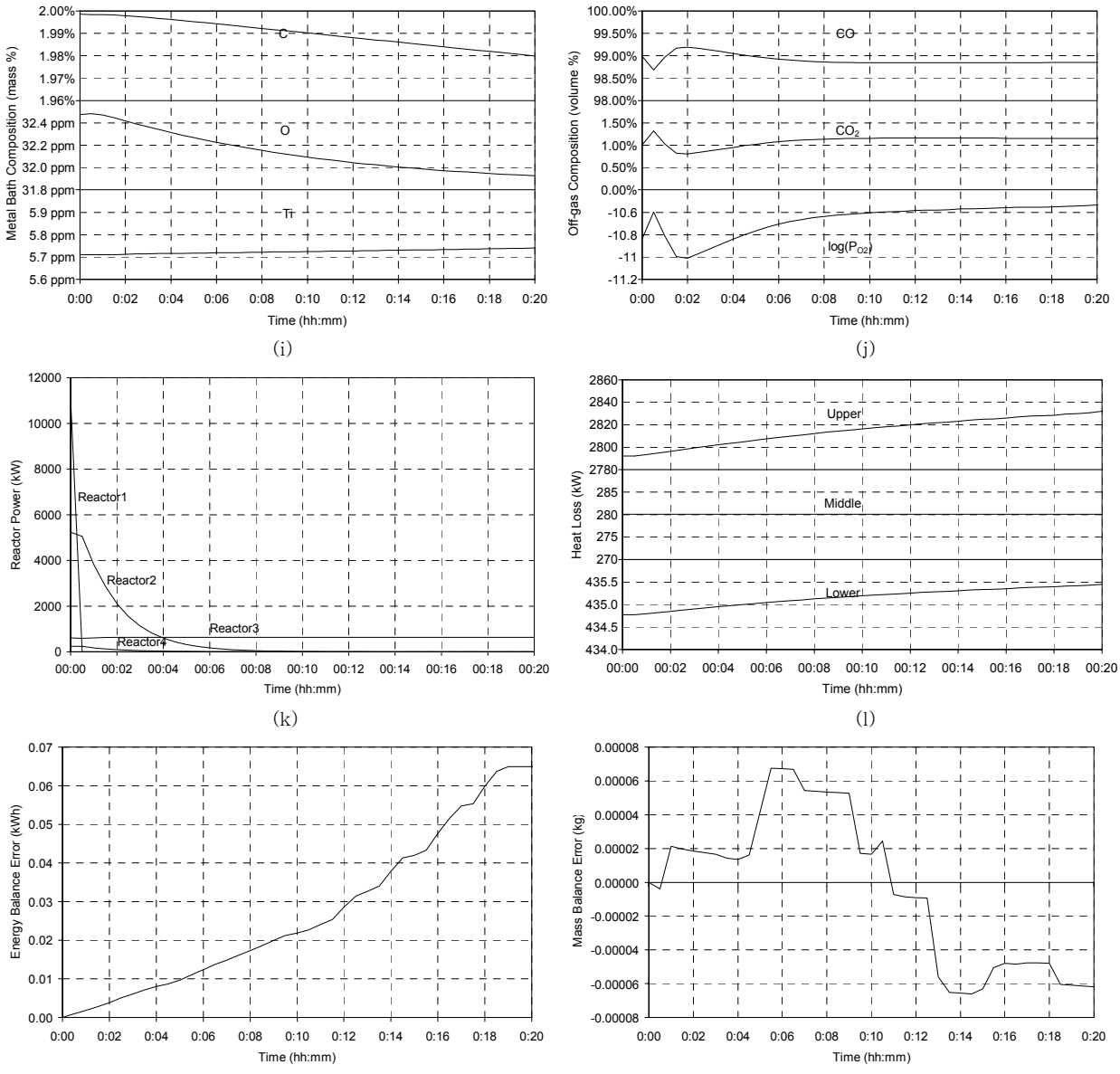

Figure 121 – Experiment 8.1 results.

8.3.2 Experiment 8.2

ILMENITE FEED RATE CHANGE	ILMENITE FEED RATE	REDUCTANT FEED RATE CHANGE	REDUCTANT FEED RATE	ELECTRICAL POWER CHANGE	ELECTRICAL POWER
–	20,000 kg/h	−1,700 kg/h	0 kg/h	–	21,715 kW

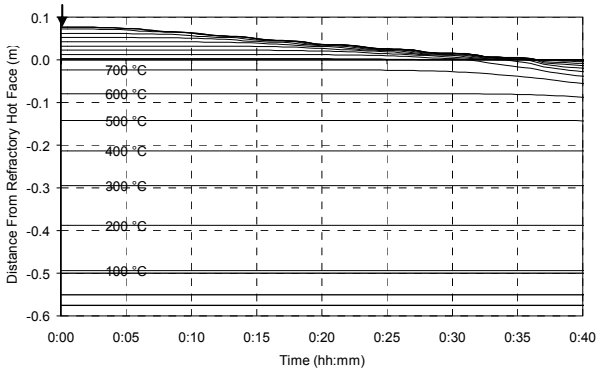

(a)

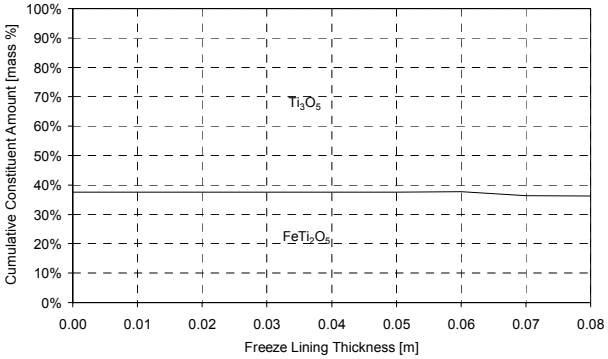

(b)

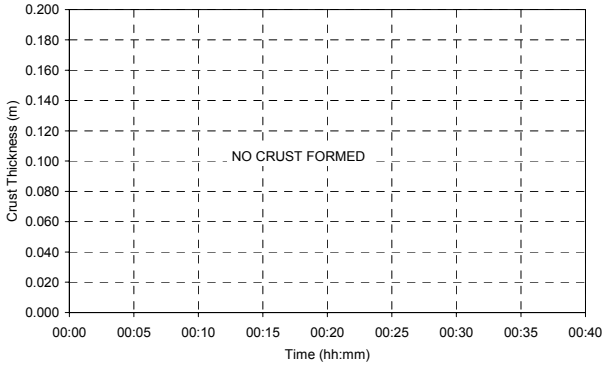

(c)

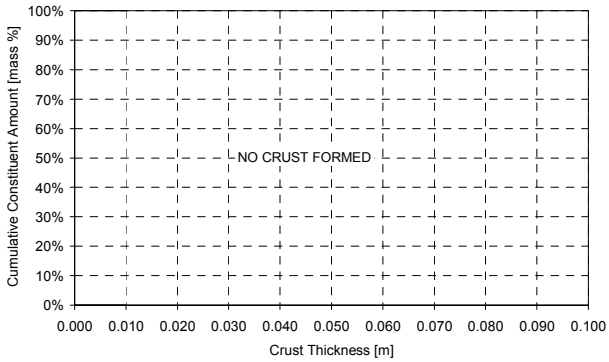

(d)

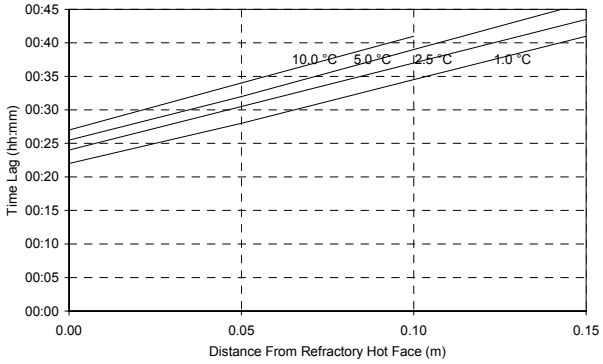

(e)

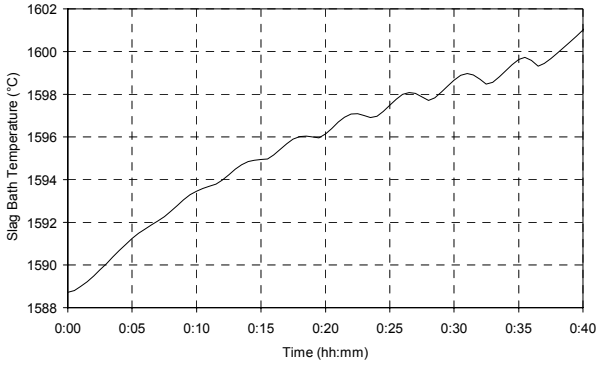

(f)

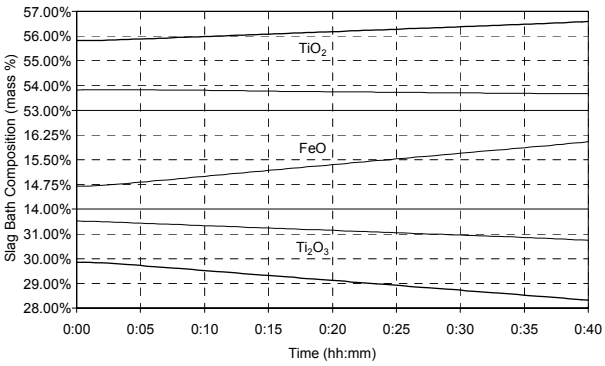

(g)

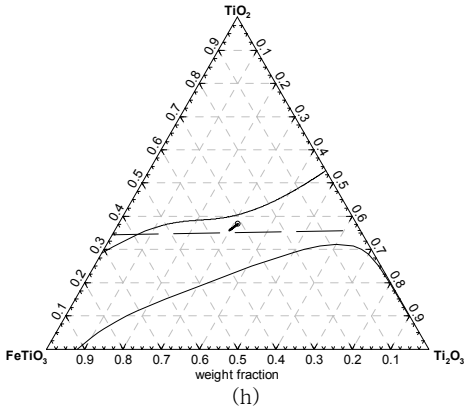

(h)

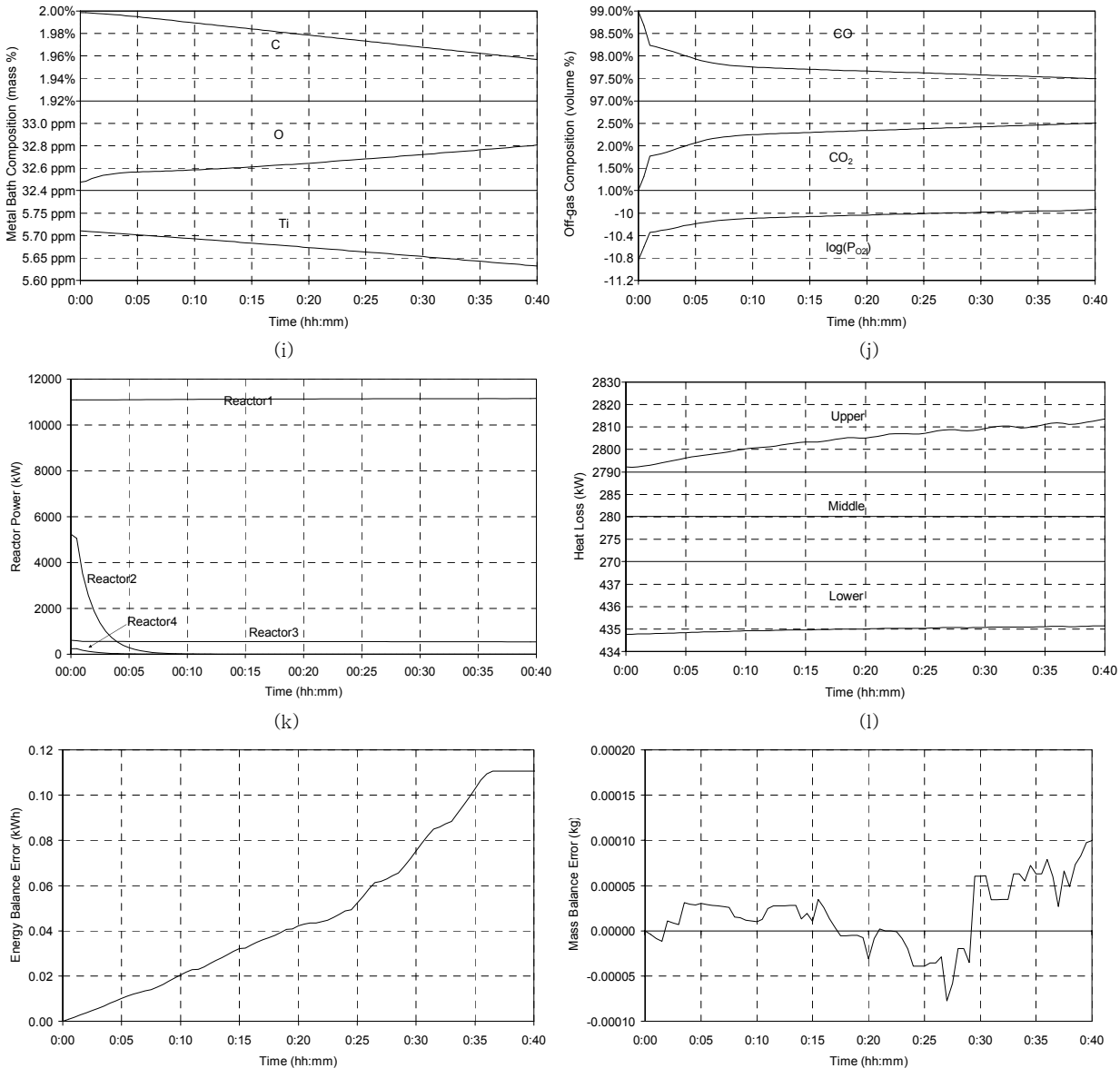

Figure 122 – Experiment 8.2 results.

8.3.3 Experiment 8.3

ILMENITE FEED RATE CHANGE	ILMENITE FEED RATE	REDUCTANT FEED RATE CHANGE	REDUCTANT FEED RATE	ELECTRICAL POWER CHANGE	ELECTRICAL POWER
–	20,000 kg/h	+ 1 kg/t ilm.	1,720 kg/h	–	21,715 kW

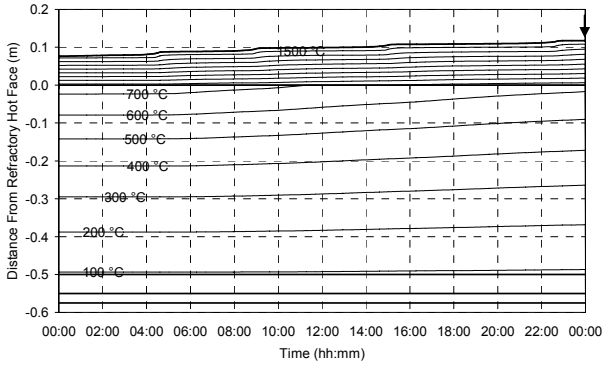

(a)

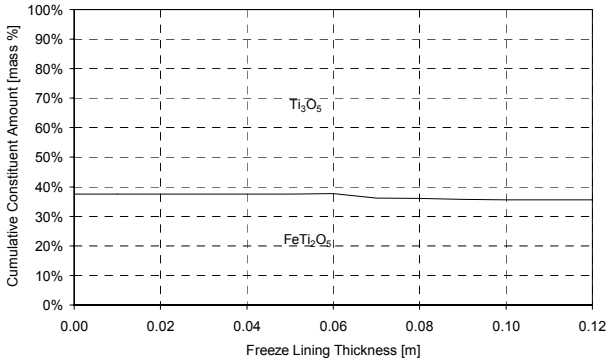

(b)

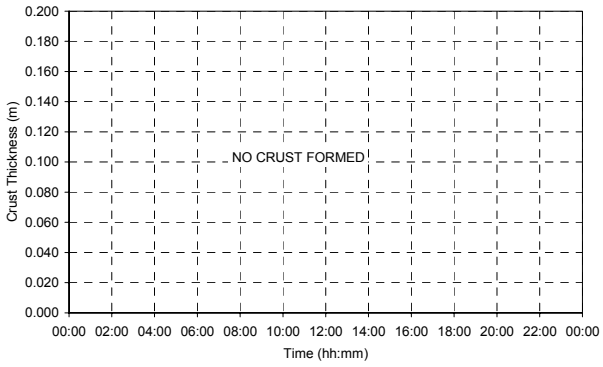

(c)

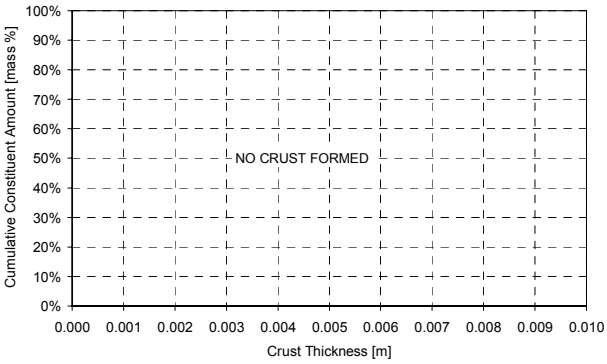

(d)

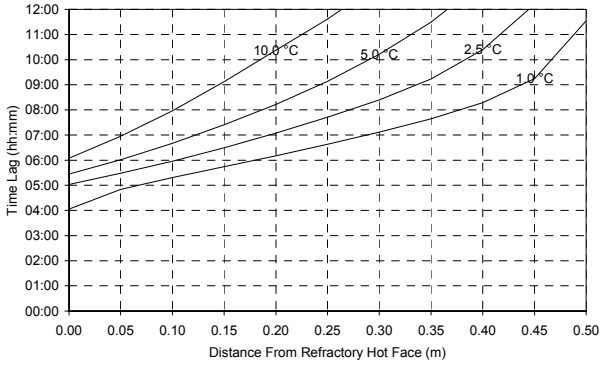

(e)

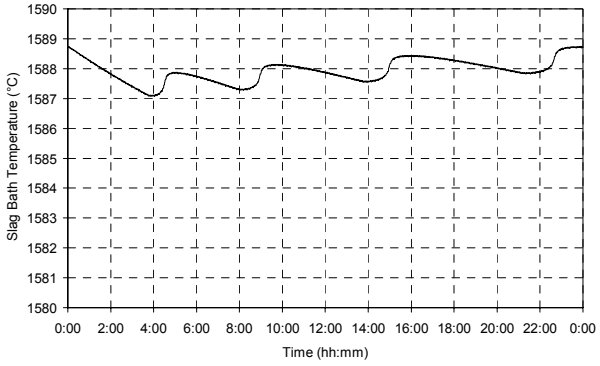

(f)

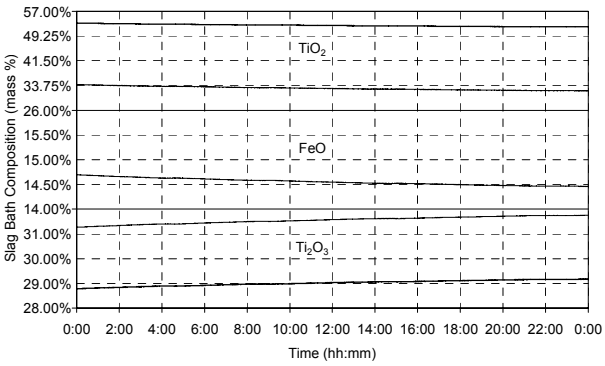

(g)

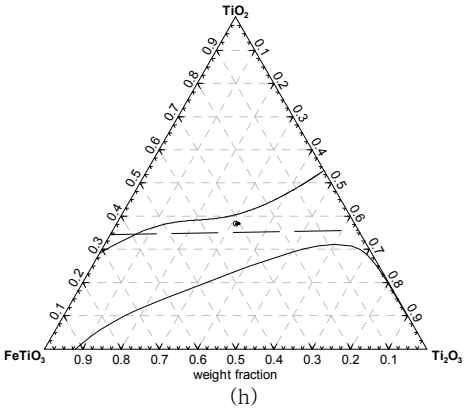

(h)

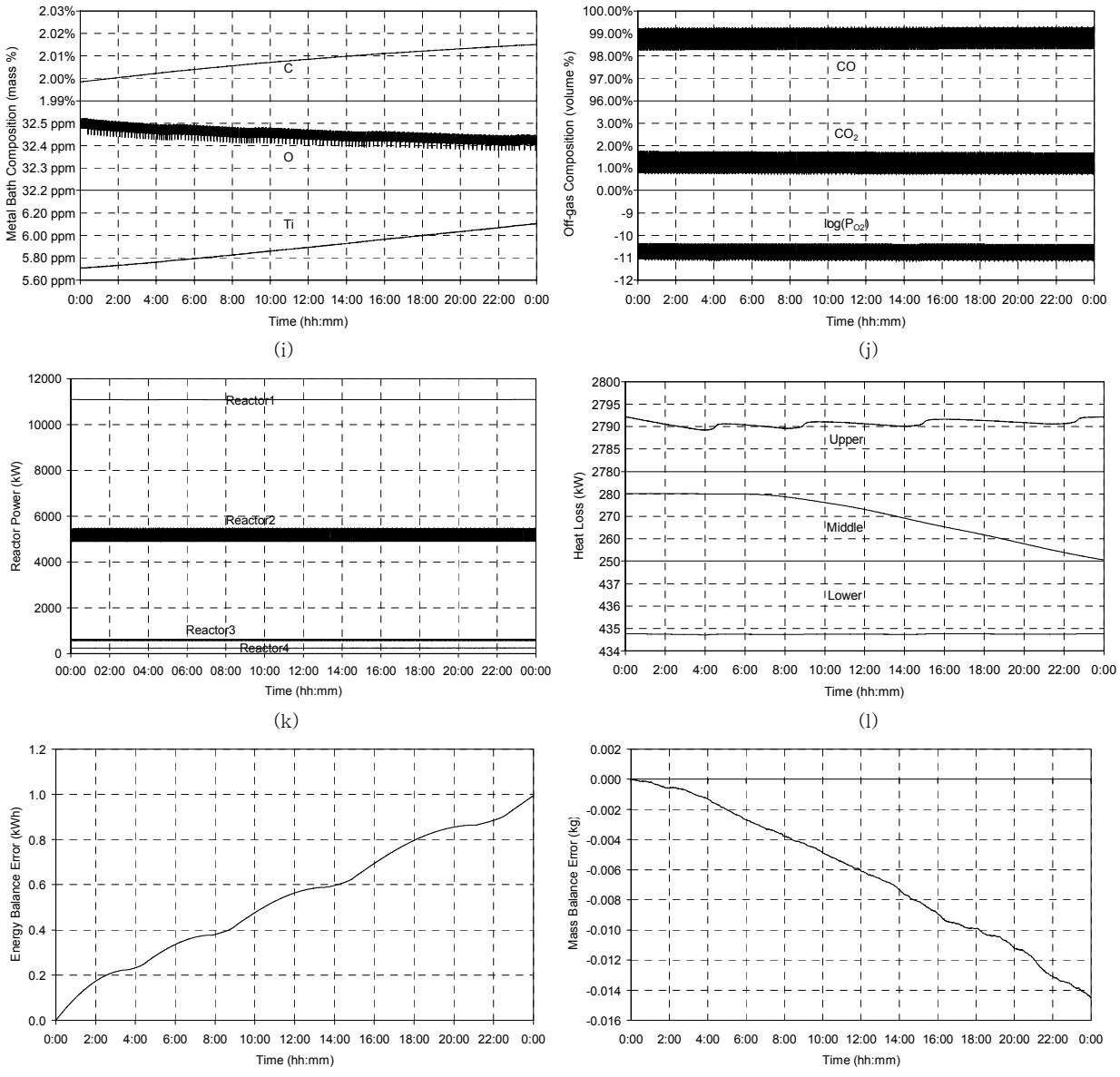

Figure 123 – Experiment 8.3 results.

8.3.4 Experiment 8.4

ILMENITE FEED RATE CHANGE	ILMENITE FEED RATE	REDUCTANT FEED RATE CHANGE	REDUCTANT FEED RATE	ELECTRICAL POWER CHANGE	ELECTRICAL POWER
–	20,000 kg/h	−1 kg/ton ilm.	1,680 kg/h	–	21,715 kW

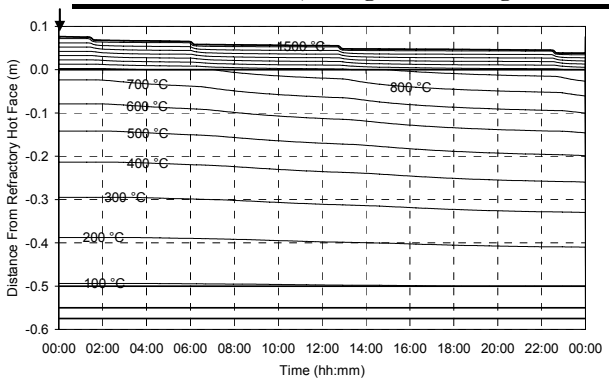

(a)

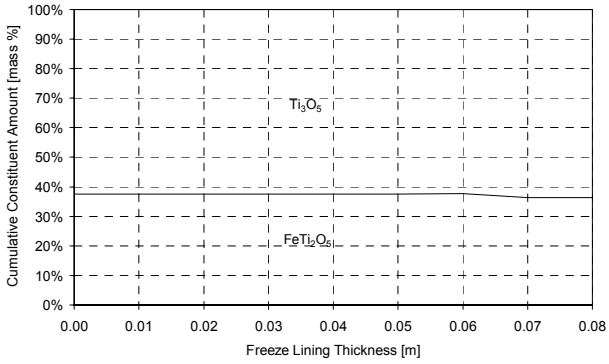

(b)

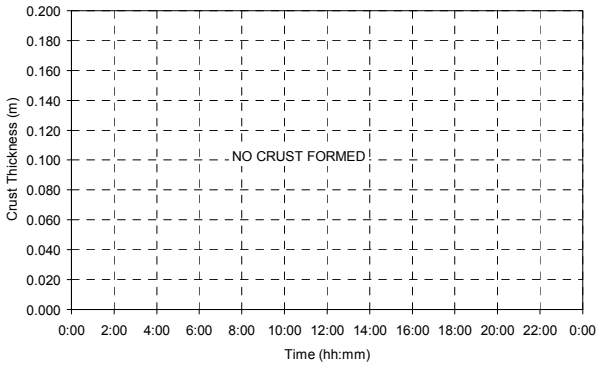

(c)

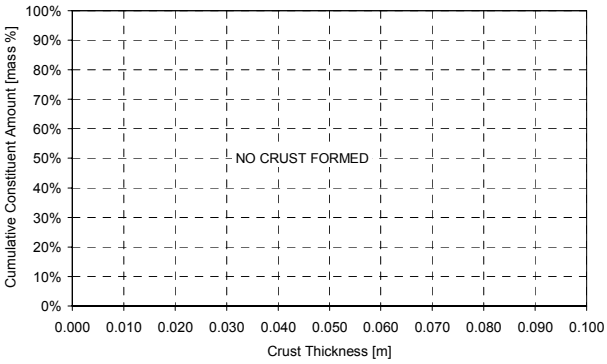

(d)

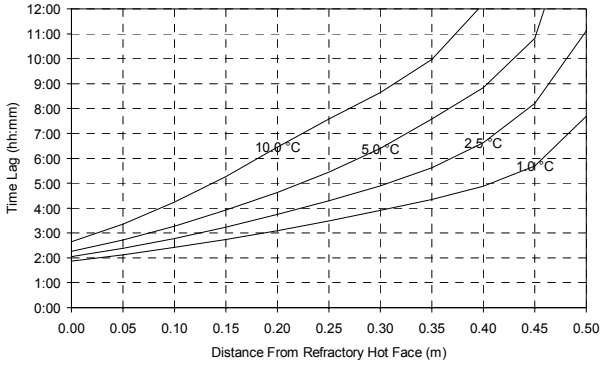

(e)

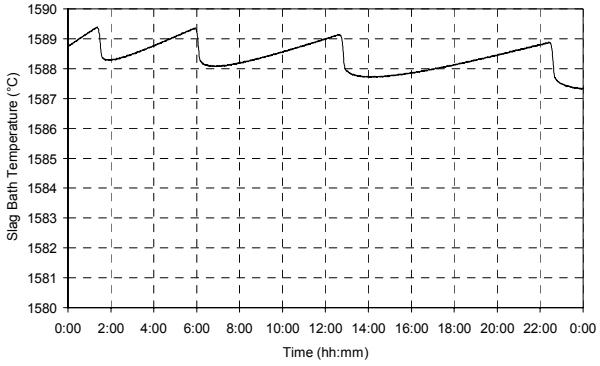

(f)

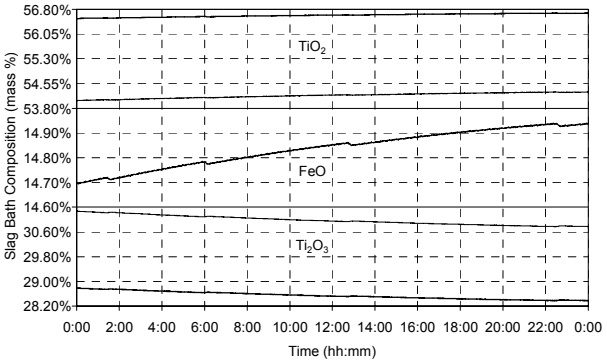

(g)

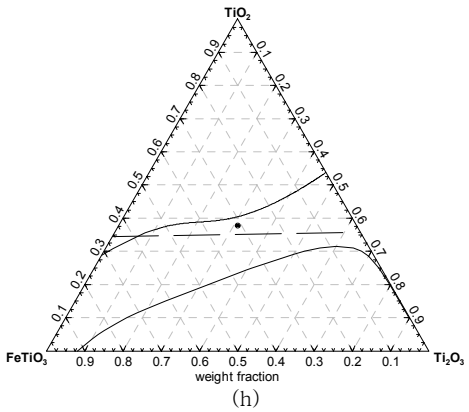

(h)

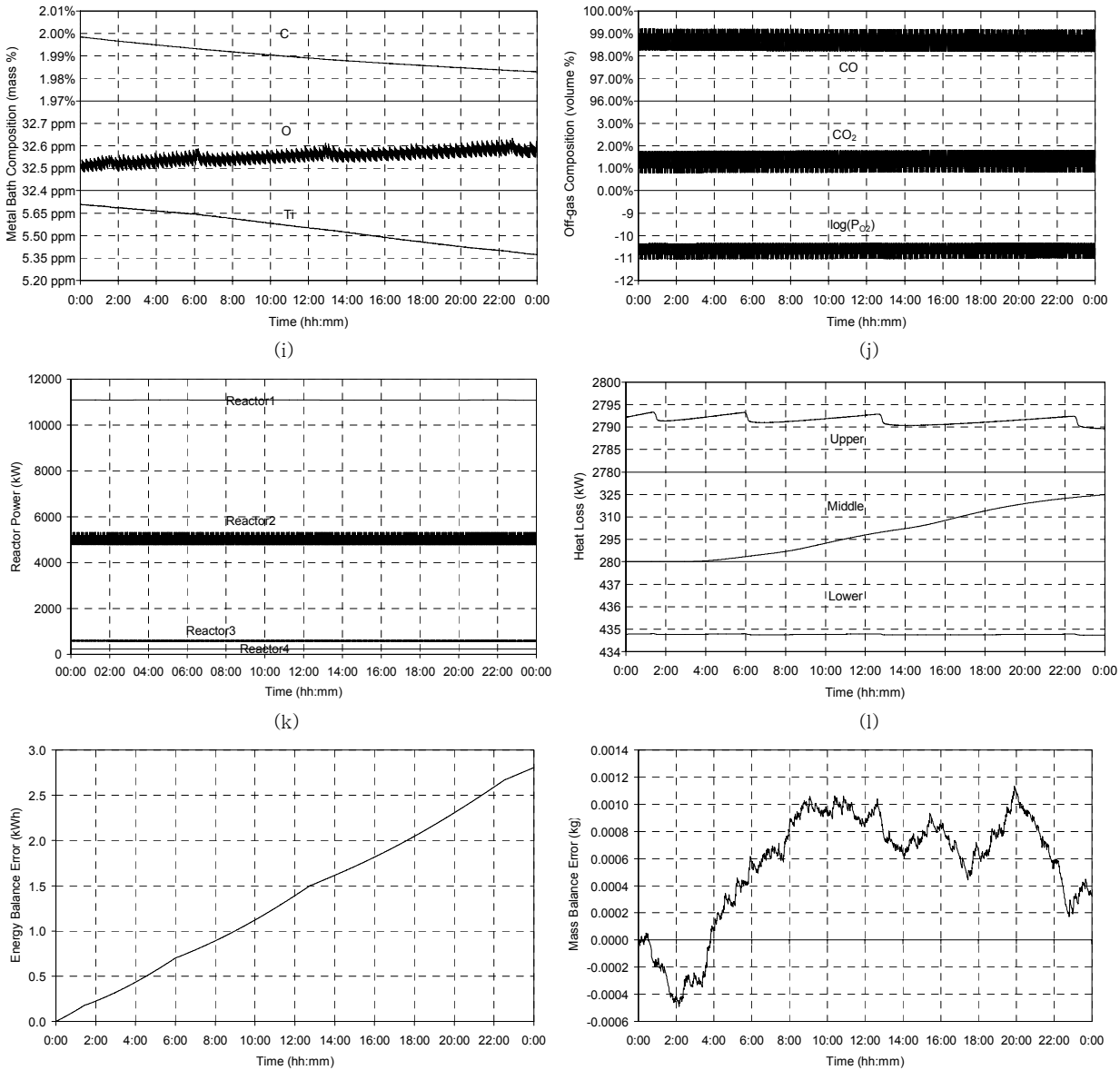

Figure 124 – Experiment 8.4 results.

8.3.5 Experiment 8.5

ILMENITE FEED RATE CHANGE	ILMENITE FEED RATE	REDUCTANT FEED RATE CHANGE	REDUCTANT FEED RATE	ELECTRICAL POWER CHANGE	ELECTRICAL POWER
–	20,000 kg/h	+ 2 kg/ton ilm.	1,740 kg/h	–	21,715 kW

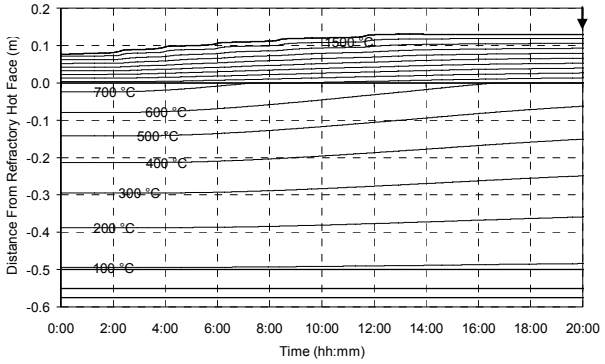

(a)

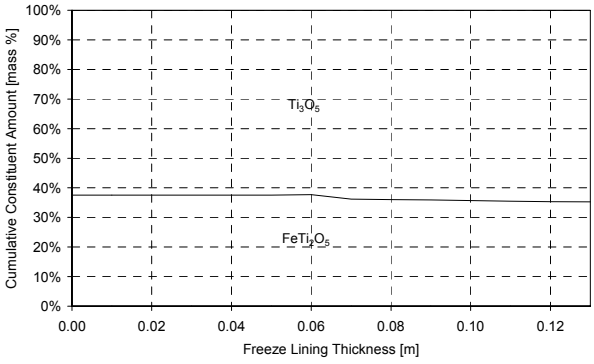

(b)

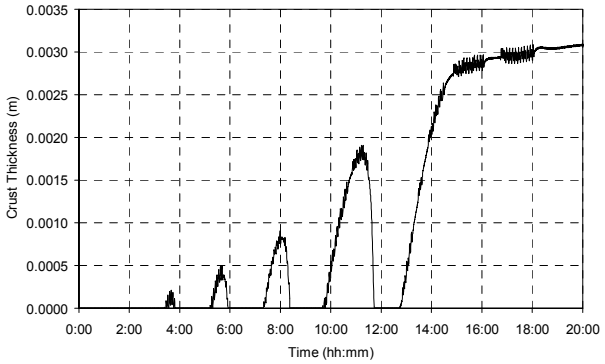

(c)

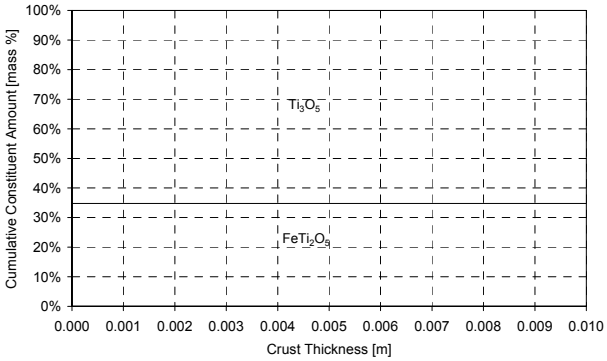

(d)

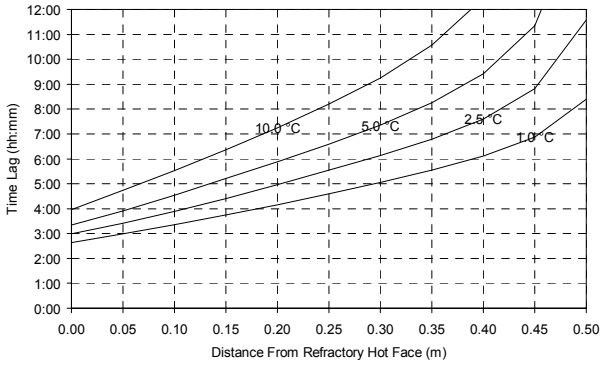

(e)

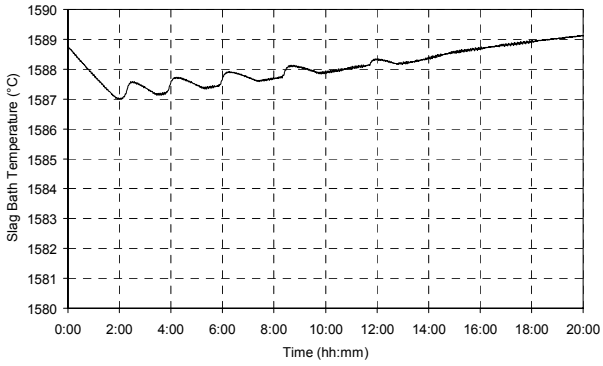

(f)

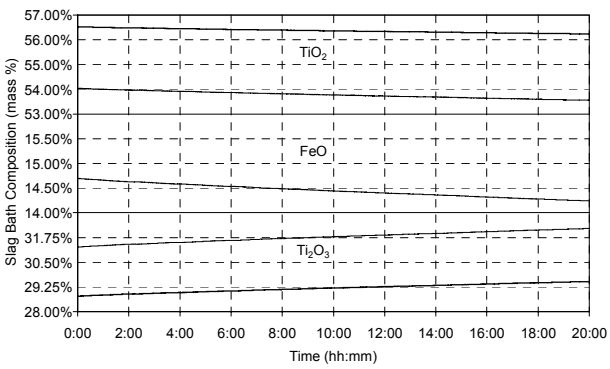

(g)

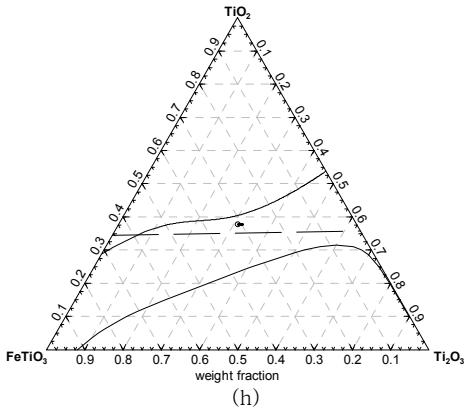

(h)

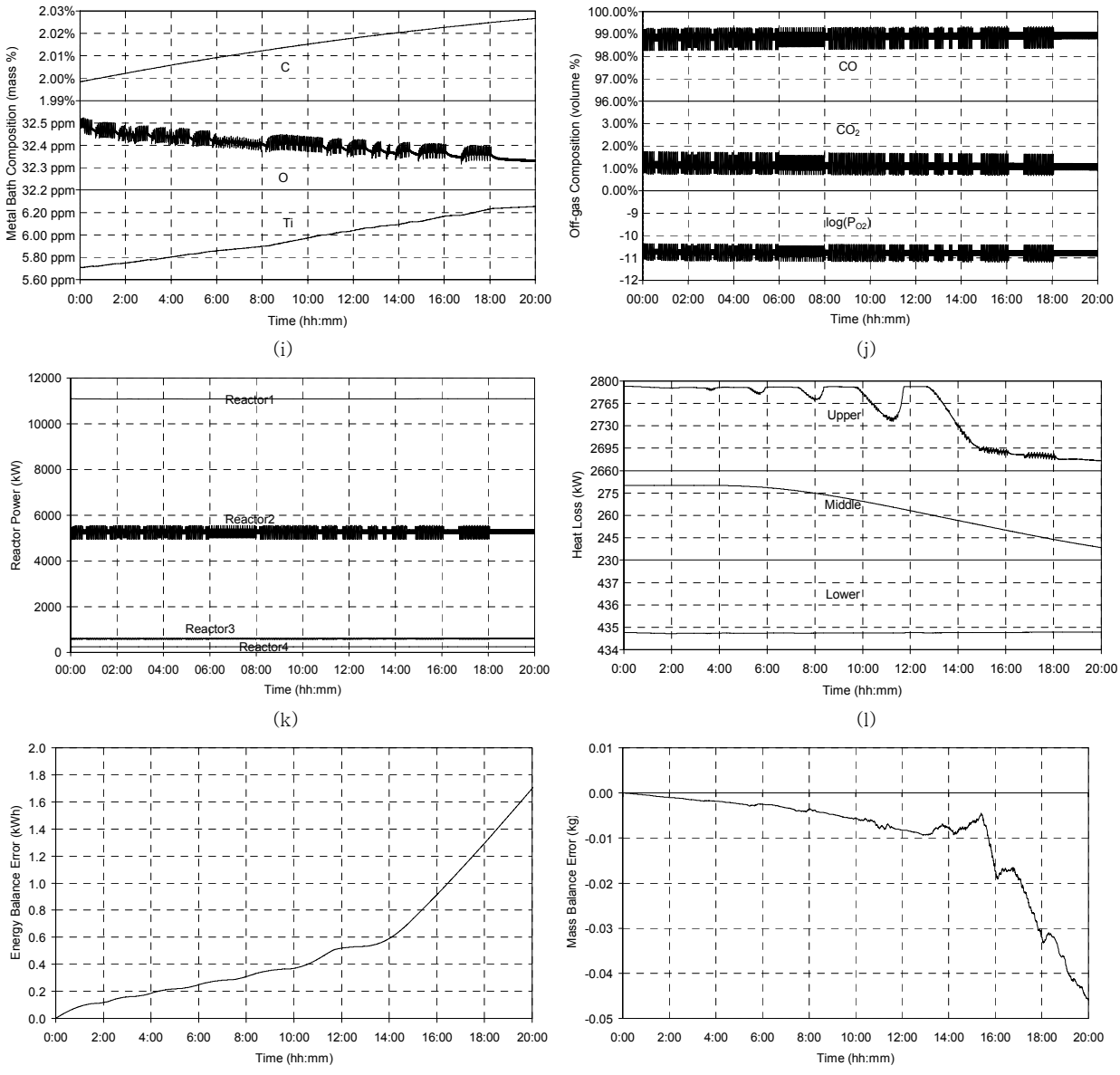

Figure 125 – Experiment 8.5 results.

8.3.6 Experiment 8.6

ILMENITE FEED RATE CHANGE	ILMENITE FEED RATE	REDUCTANT FEED RATE CHANGE	REDUCTANT FEED RATE	ELECTRICAL POWER CHANGE	ELECTRICAL POWER
-	20,000 kg/h	-2 kg/ton ilm.	1,660 kg/h	-	21,715 kW

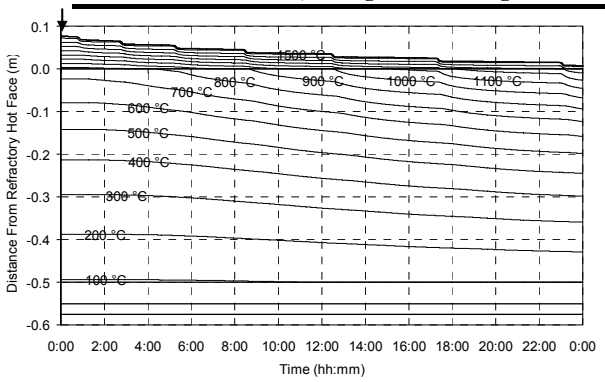

(a)

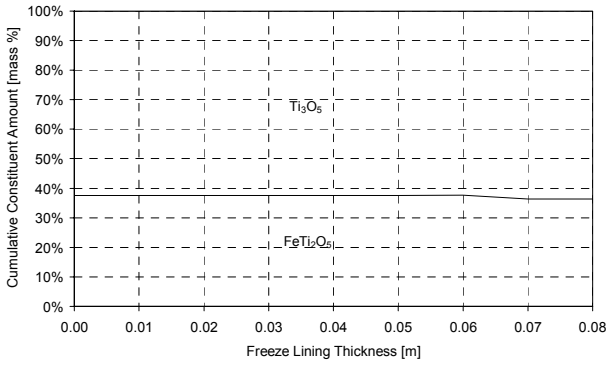

(b)

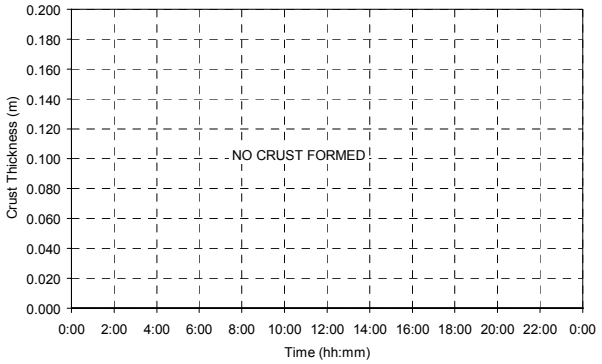

(c)

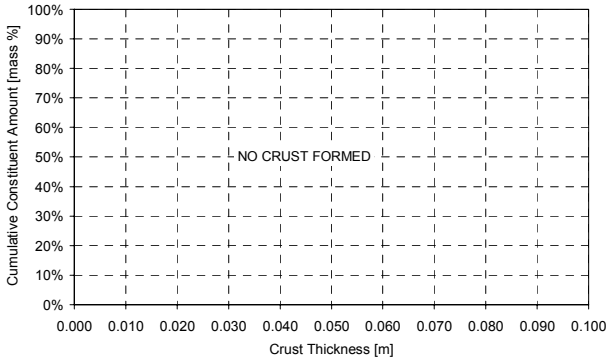

(d)

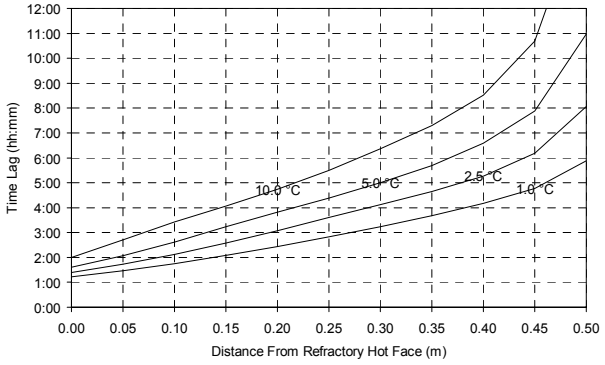

(e)

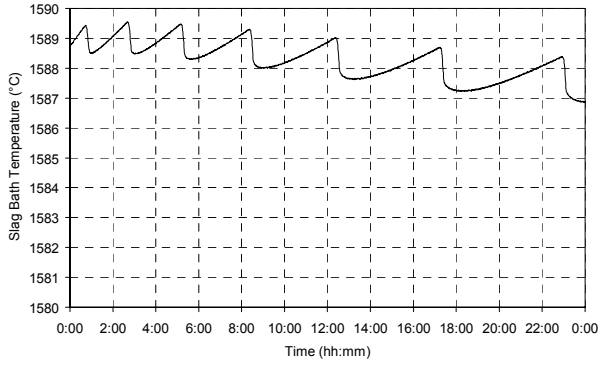

(f)

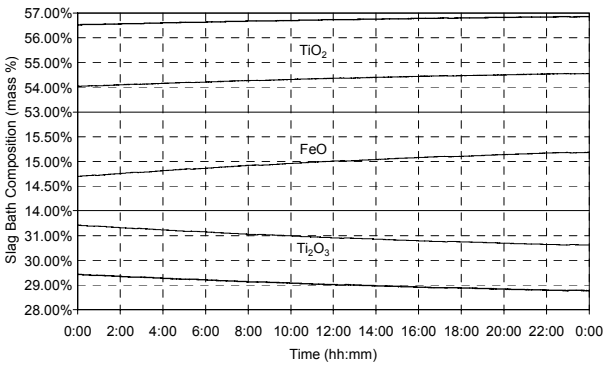

(g)

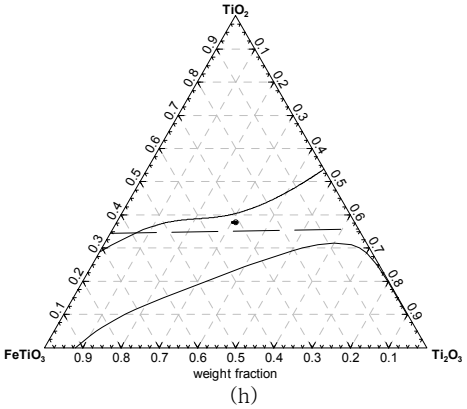

(h)

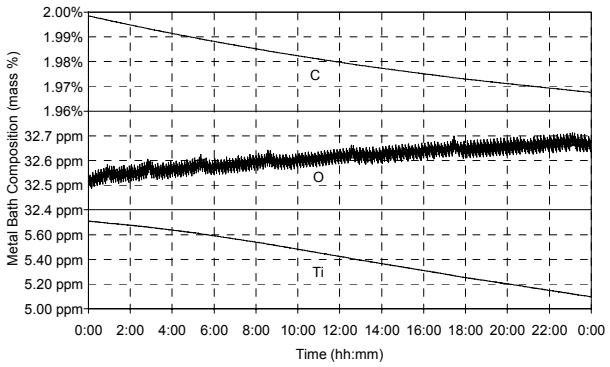

(i)

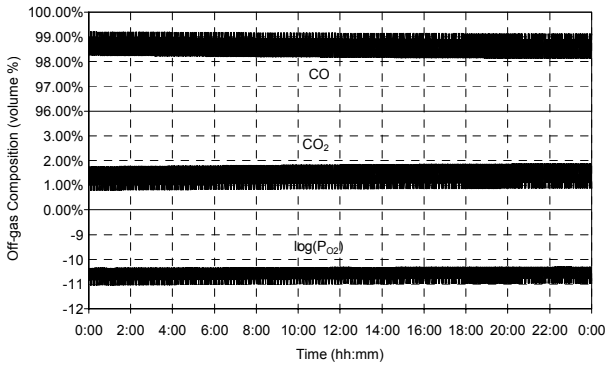

(j)

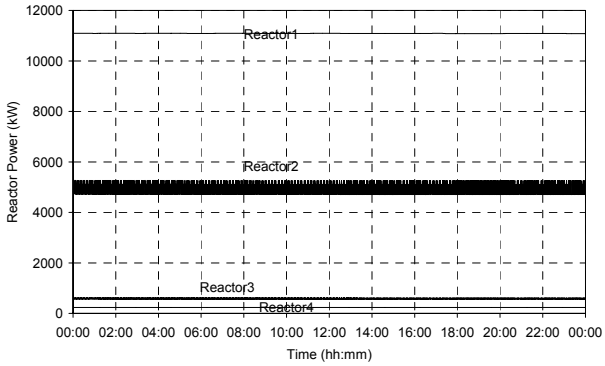

(k)

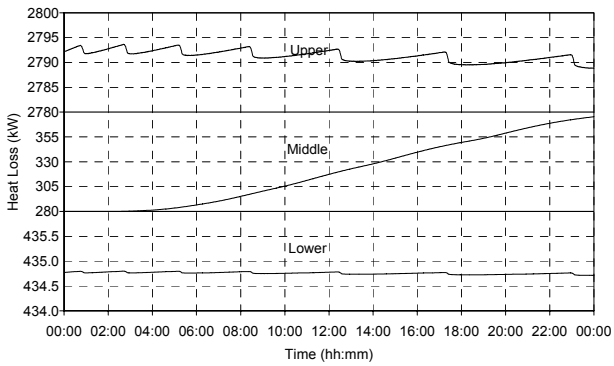

(l)

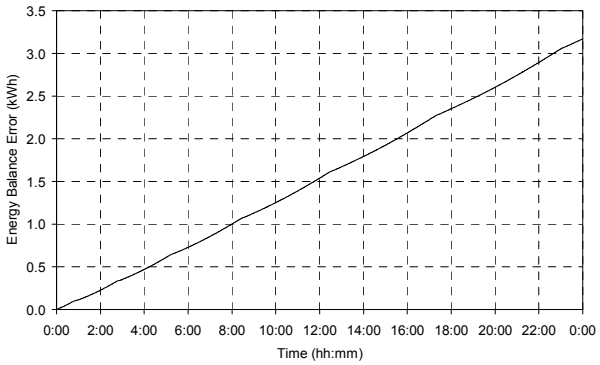

(m)

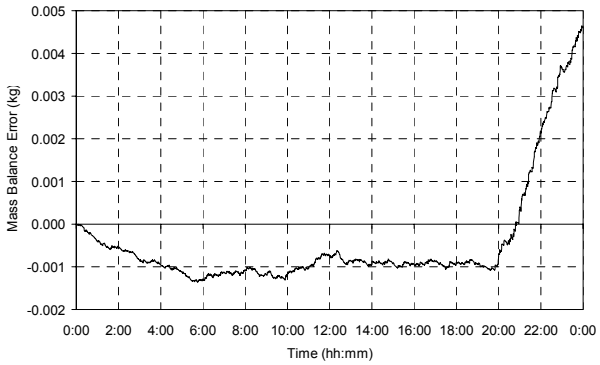

(n)

Figure 126 – Experiment 8.6 results.

8.3.7 Experiment 8.7

ILMENITE FEED RATE CHANGE	ILMENITE FEED RATE	REDUCTANT FEED RATE CHANGE	REDUCTANT FEED RATE	ELECTRICAL POWER CHANGE	ELECTRICAL POWER
–	20,000 kg/h	–	1,700 kg/h	+ 5 kWh/ton ilm.	21,815 kW

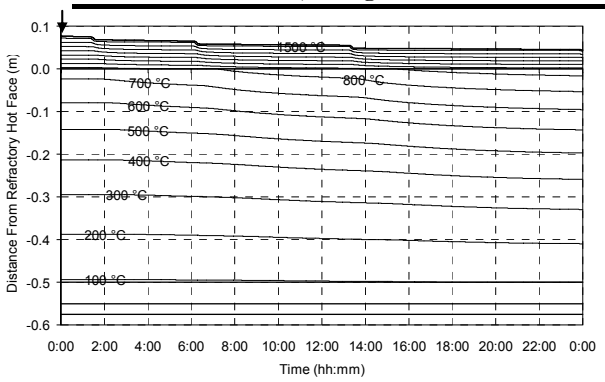

(a)

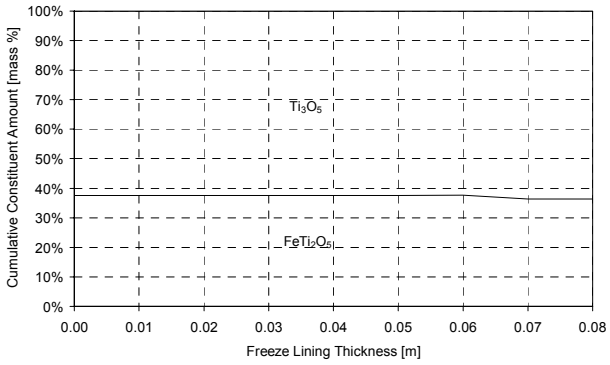

(b)

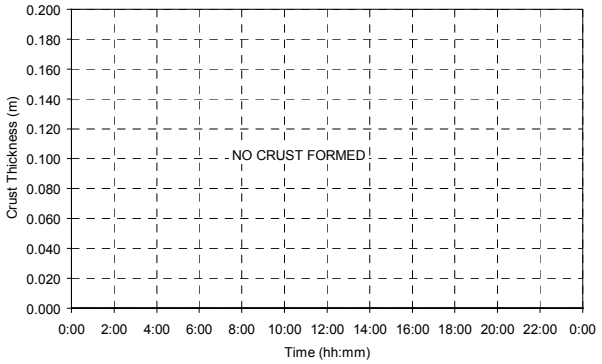

(c)

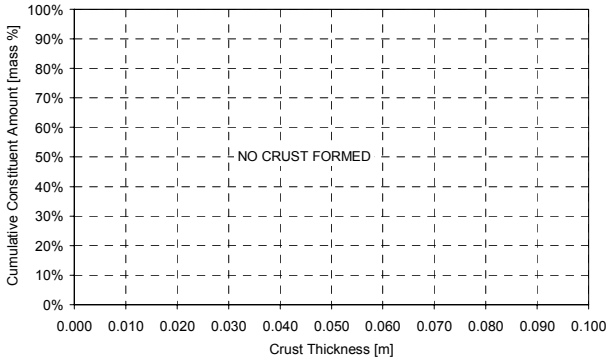

(d)

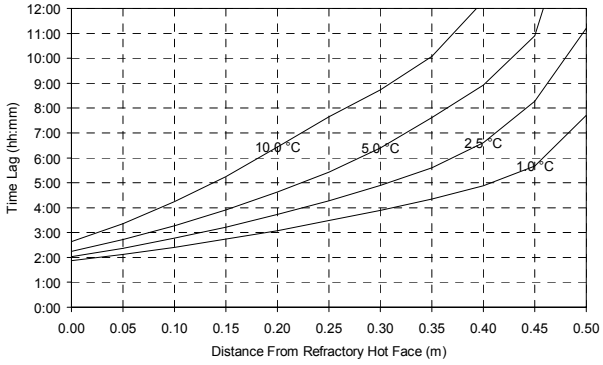

(e)

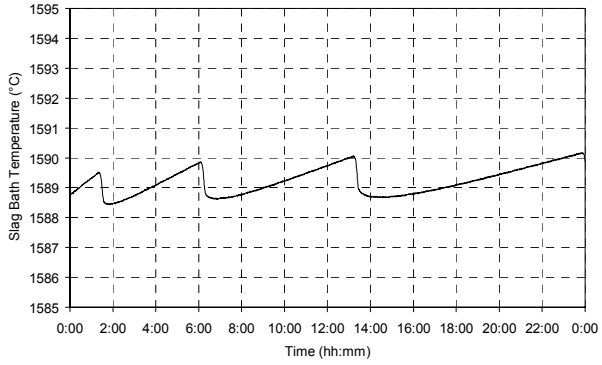

(f)

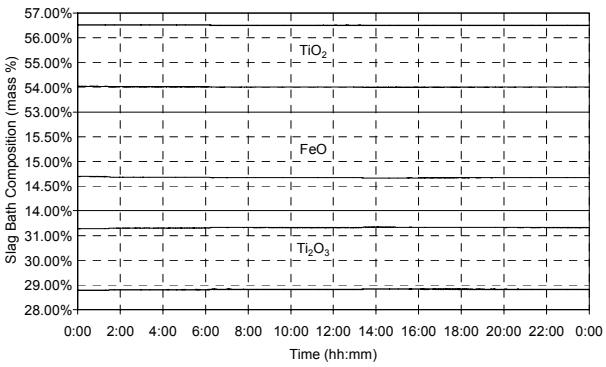

(g)

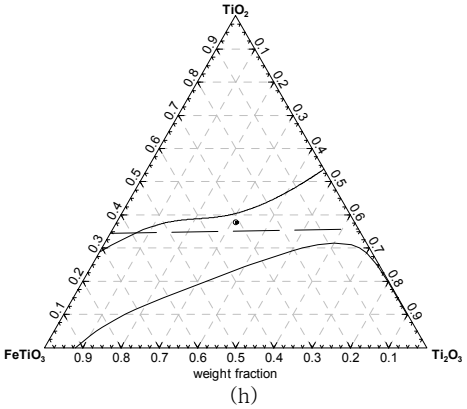

(h)

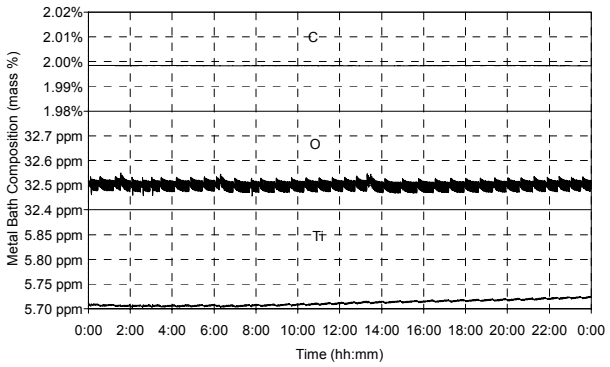

(i)

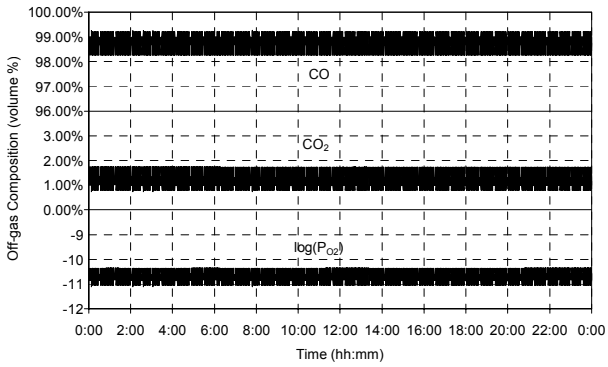

(j)

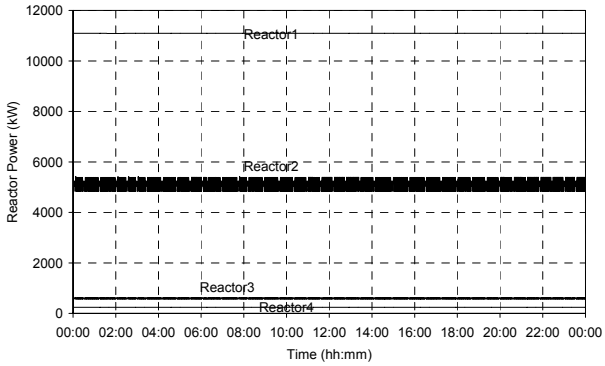

(k)

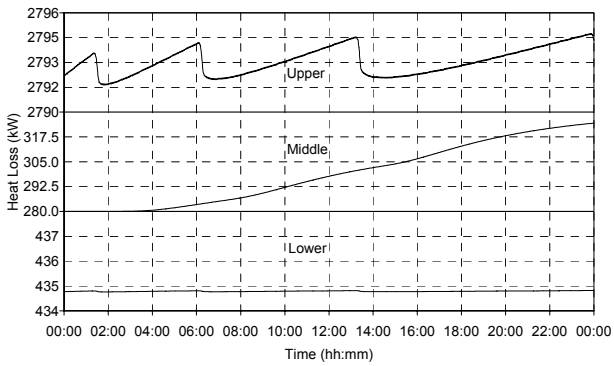

(l)

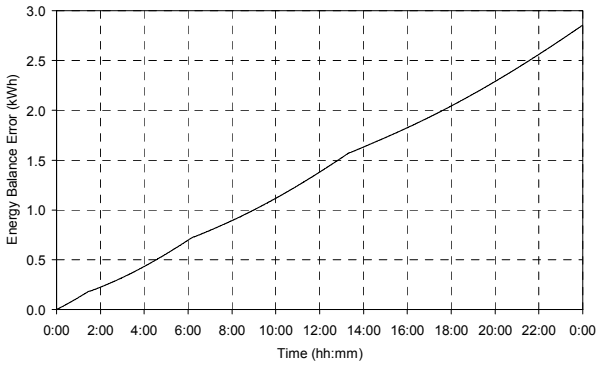

(m)

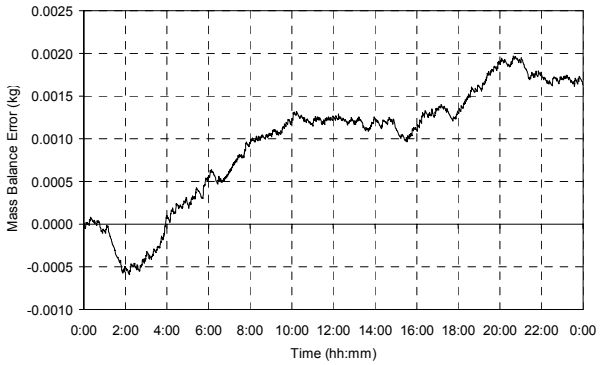

(n)

Figure 127 – Experiment 8.7 results.

8.3.8 Experiment 8.8

ILMENITE FEED RATE CHANGE	ILMENITE FEED RATE	REDUCTANT FEED RATE CHANGE	REDUCTANT FEED RATE	ELECTRICAL POWER CHANGE	ELECTRICAL POWER
-	20,000 kg/h	-	1,700 kg/h	-5 kWh/ton ilm.	21,615 kW

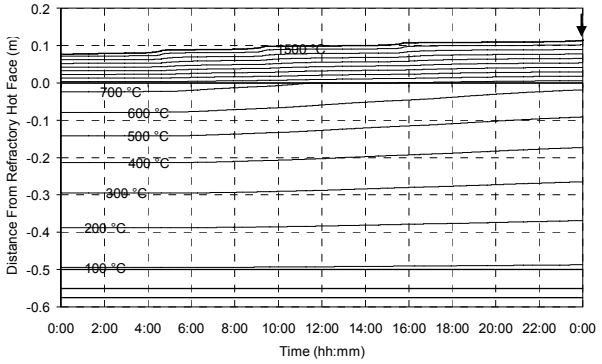

(a)

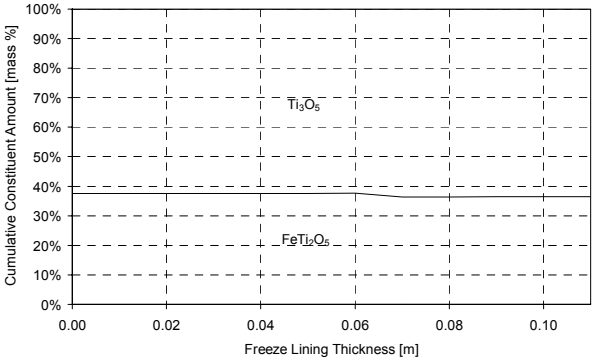

(b)

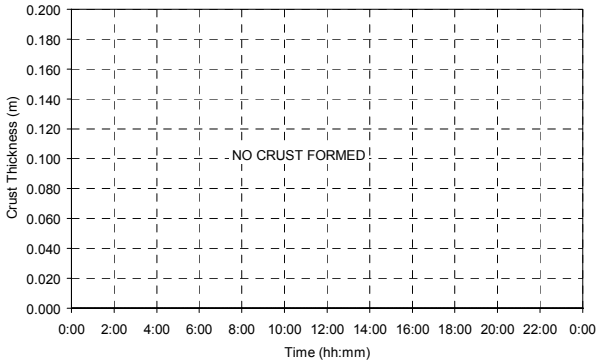

(c)

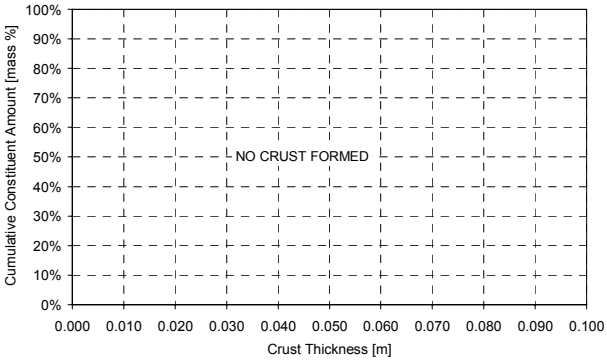

(d)

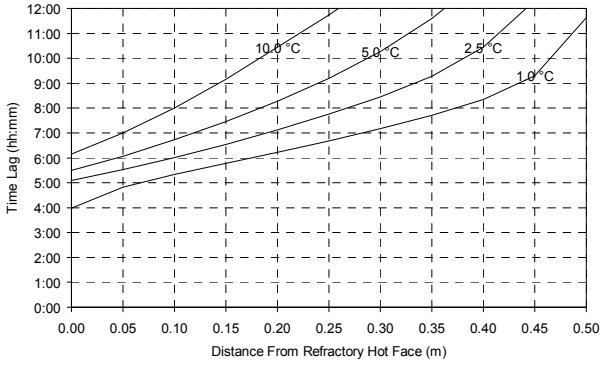

(e)

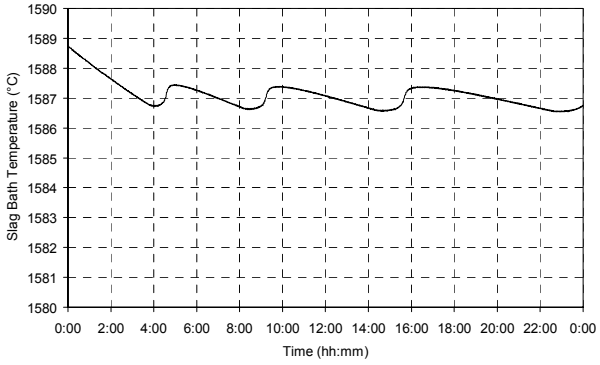

(f)

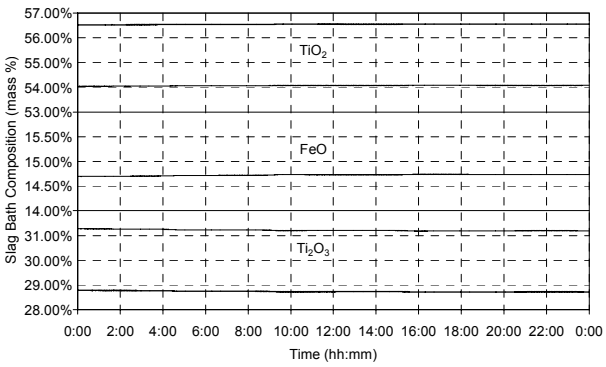

(g)

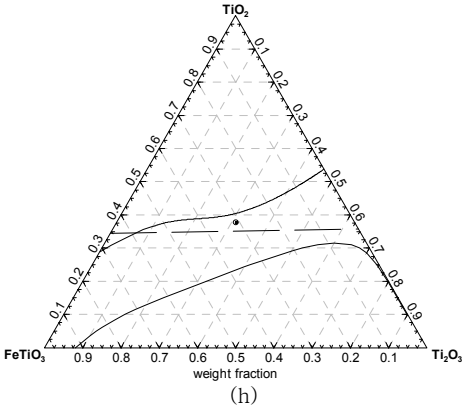

(h)

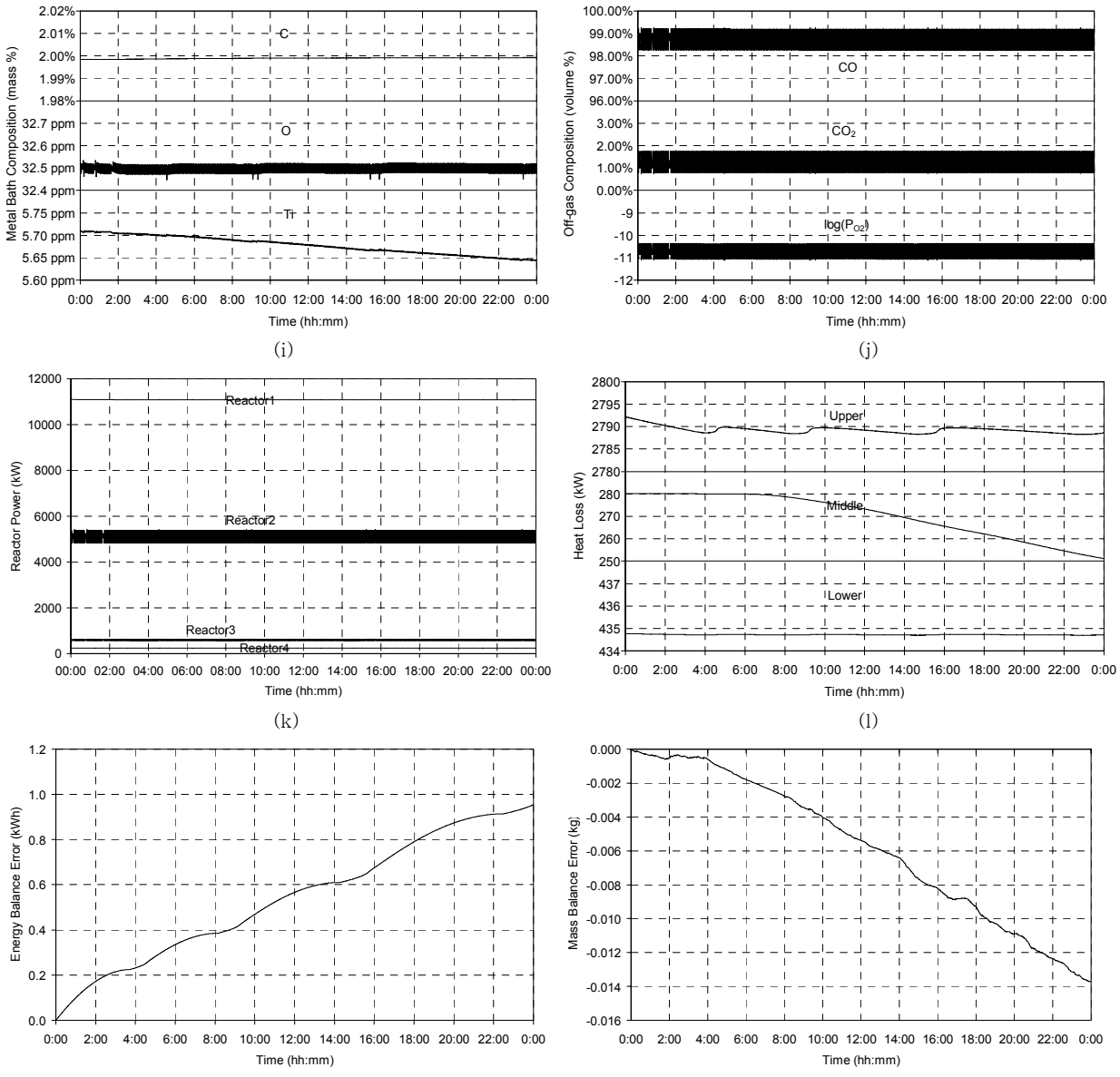

Figure 128 – Experiment 8.8 results.

8.3.9 Experiment 8.9

ILMENITE FEED RATE CHANGE	ILMENITE FEED RATE	REDUCTANT FEED RATE CHANGE	REDUCTANT FEED RATE	ELECTRICAL POWER CHANGE	ELECTRICAL POWER
–	20,000 kg/h	–	1,700 kg/h	+ 10 kWh/ton ilm.	21,915 kW

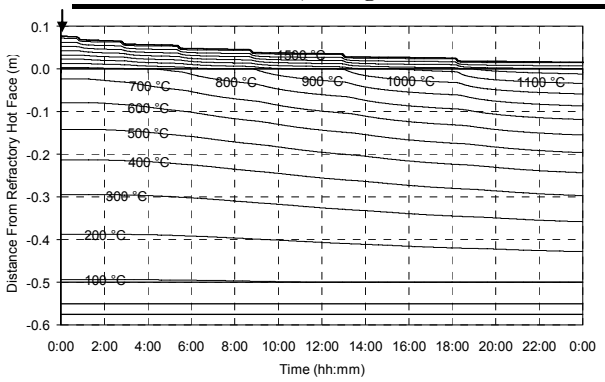

(a)

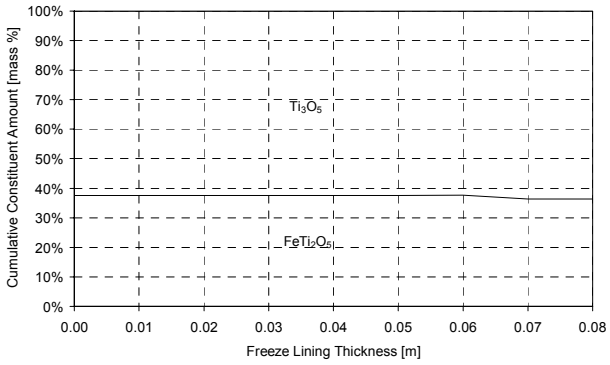

(b)

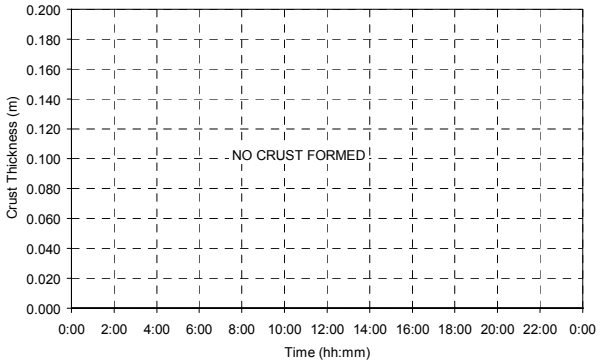

(c)

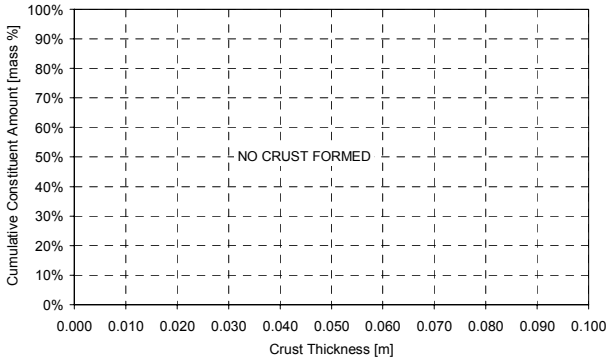

(d)

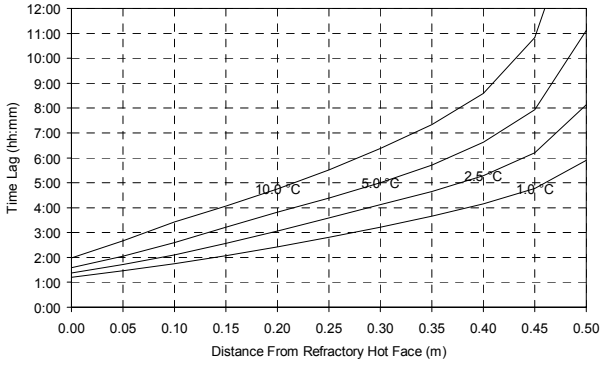

(e)

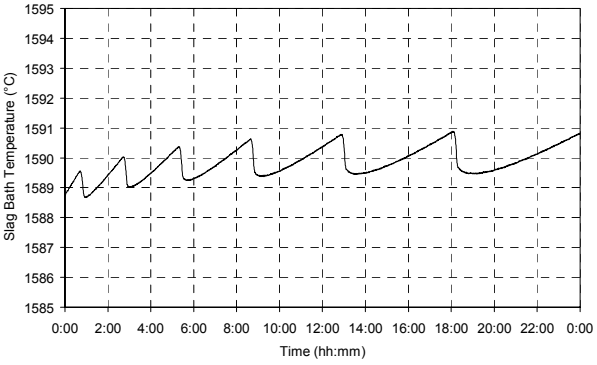

(f)

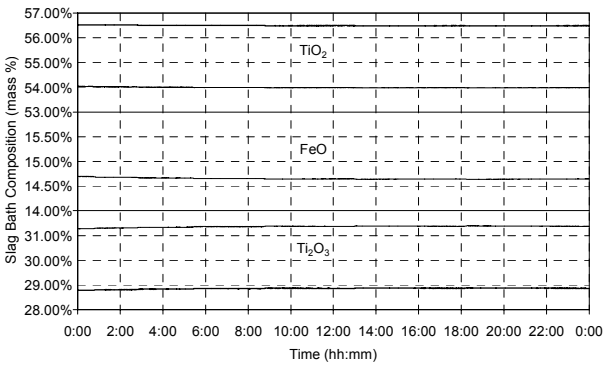

(g)

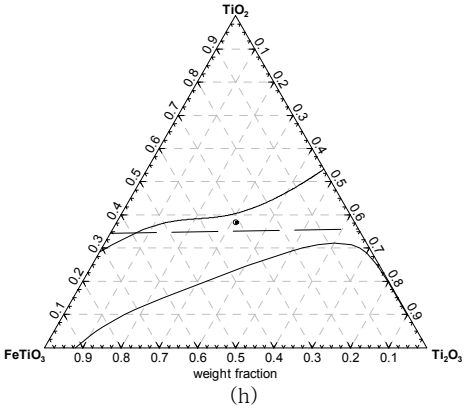

(h)

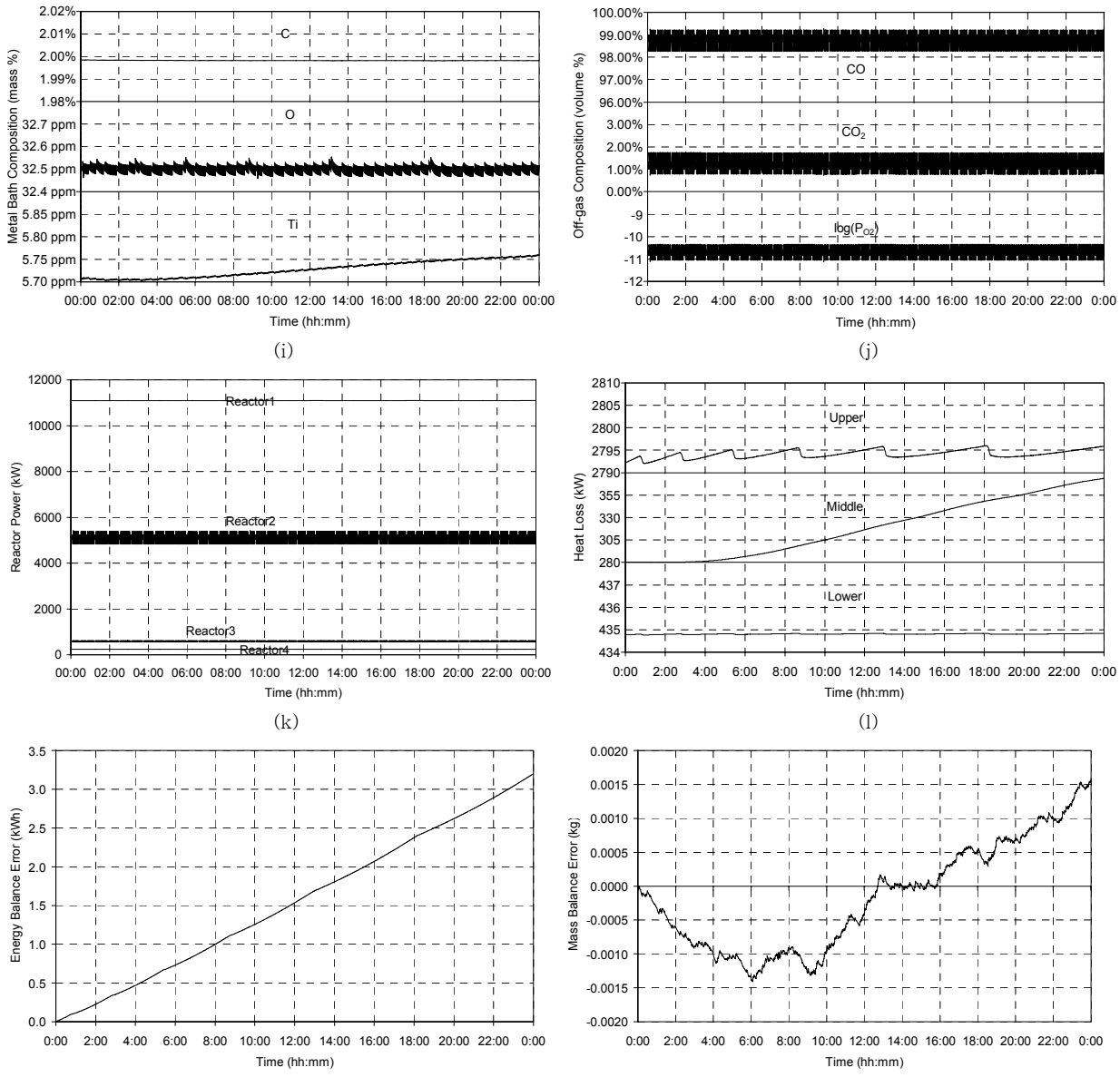

Figure 129 – Experiment 8.9 results.

8.3.10 Experiment 8.10

ILMENITE FEED RATE CHANGE	ILMENITE FEED RATE	REDUCTANT FEED RATE CHANGE	REDUCTANT FEED RATE	ELECTRICAL POWER CHANGE	ELECTRICAL POWER
-	20,000 kg/h	-	1,700 kg/h	-10 kWh/ton ilm.	21,515 kW

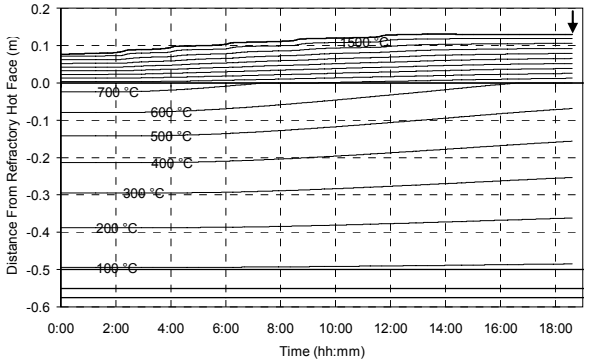

(a)

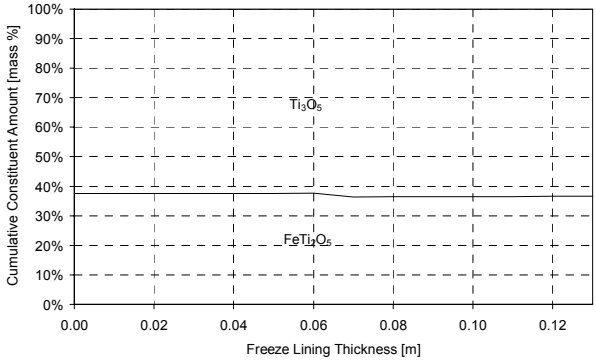

(b)

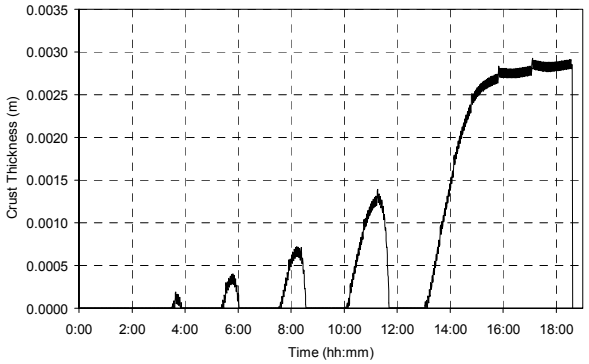

(c)

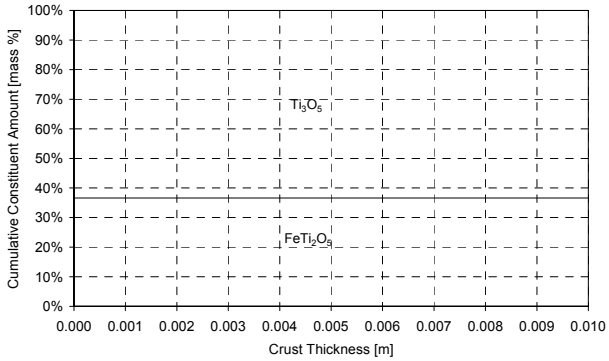

(d)

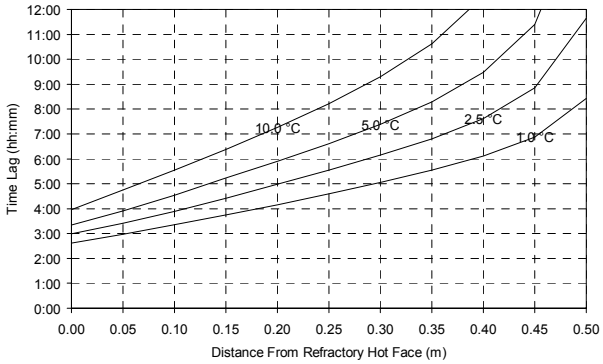

(e)

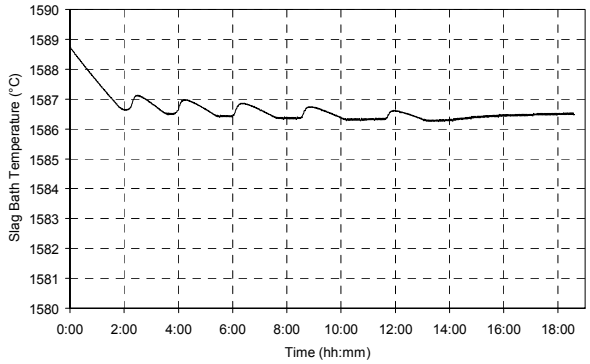

(f)

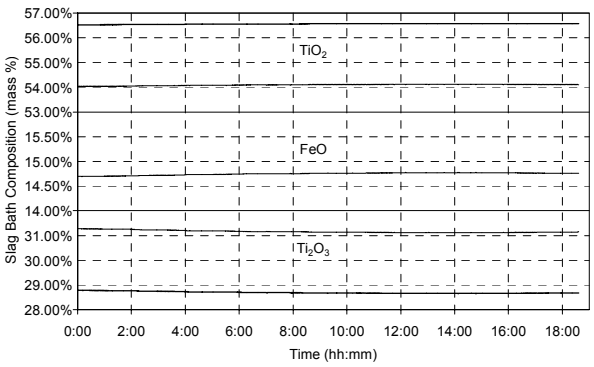

(g)

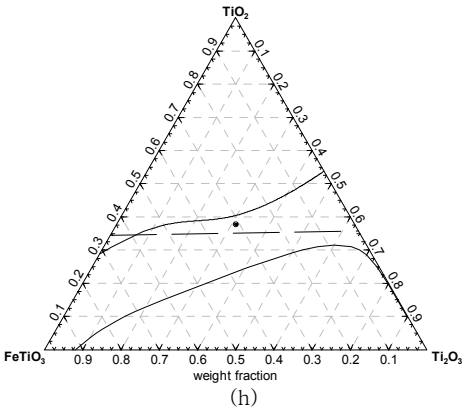

(h)

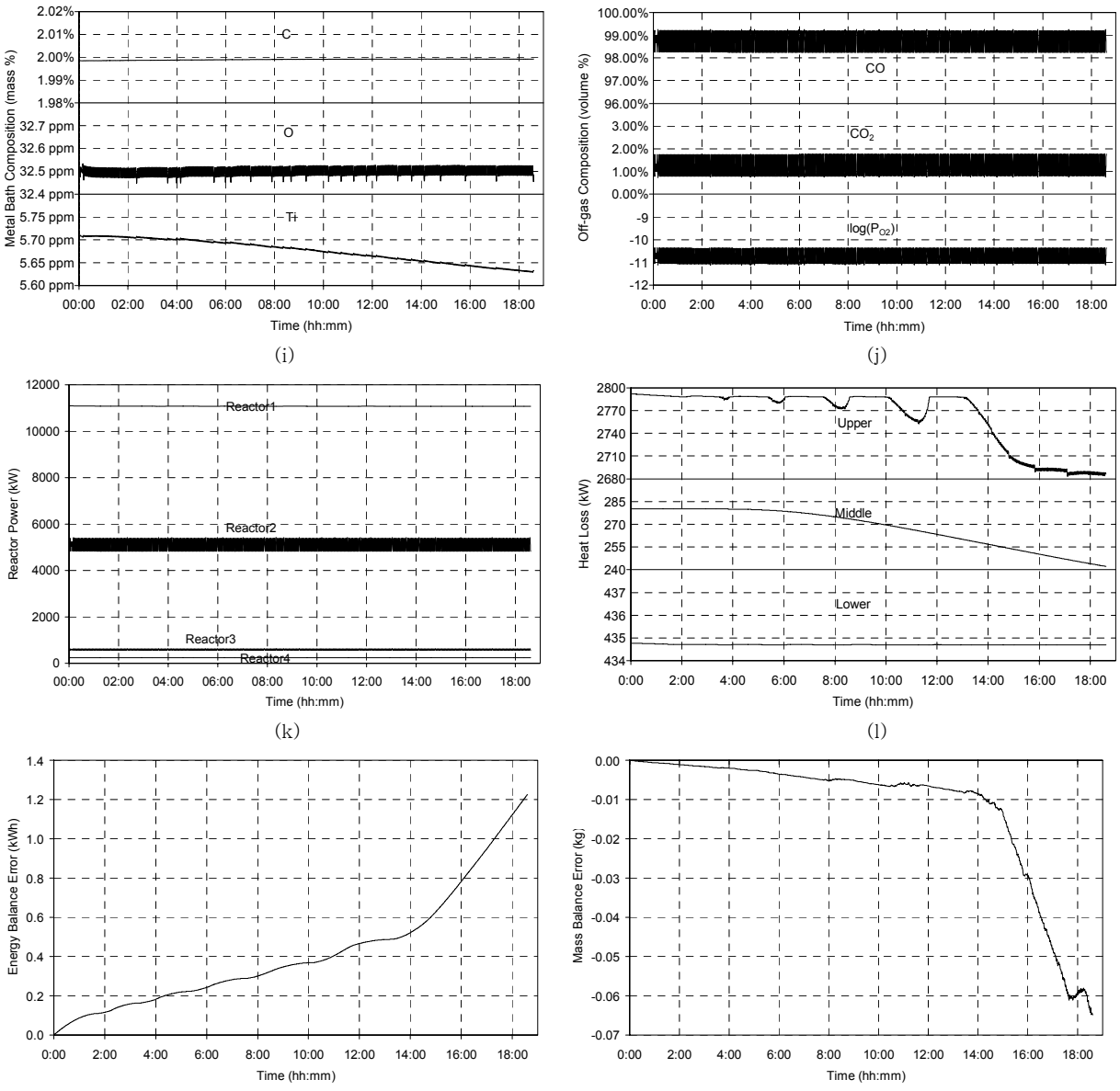

Figure 130 – Experiment 8.10 results.

8.3.11 Experiment 8.11

ILMENITE FEED RATE CHANGE	ILMENITE FEED RATE	REDUCTANT FEED RATE CHANGE	REDUCTANT FEED RATE	ELECTRICAL POWER CHANGE	ELECTRICAL POWER
–	20,000 kg/h	+ 1 kg/ton ilm.	1,720 kg/h	+ 5 kWh/ton ilm.	21,815 kW

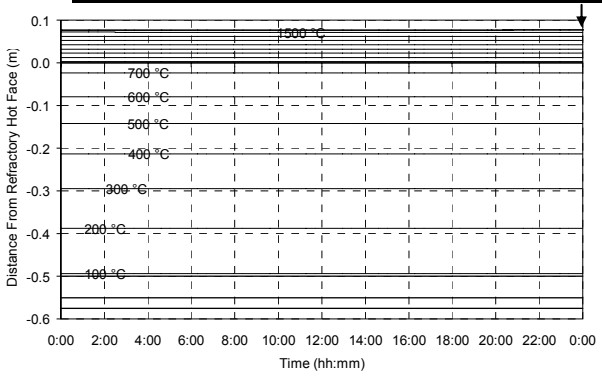

(a)

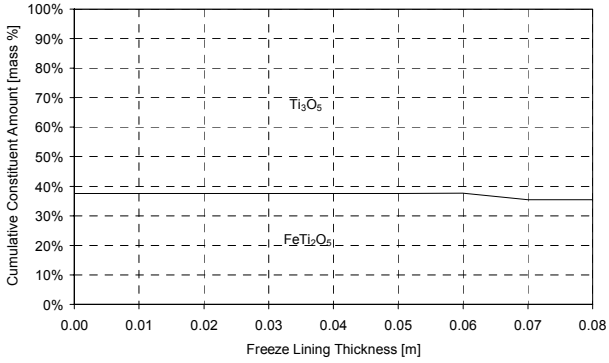

(b)

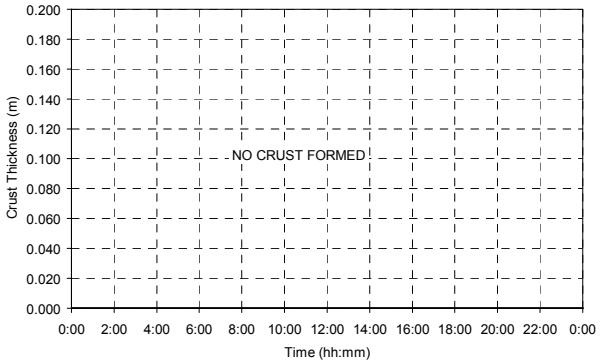

(c)

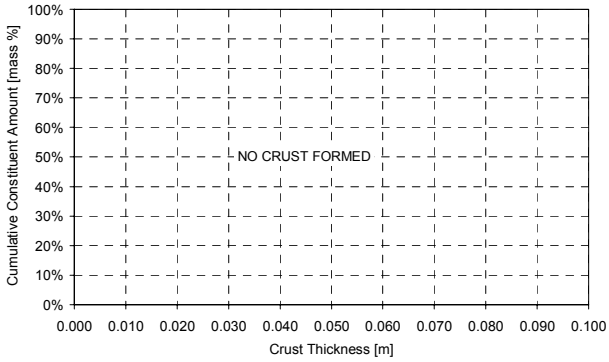

(d)

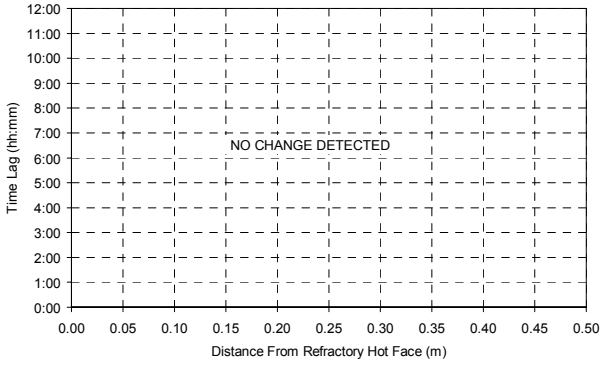

(e)

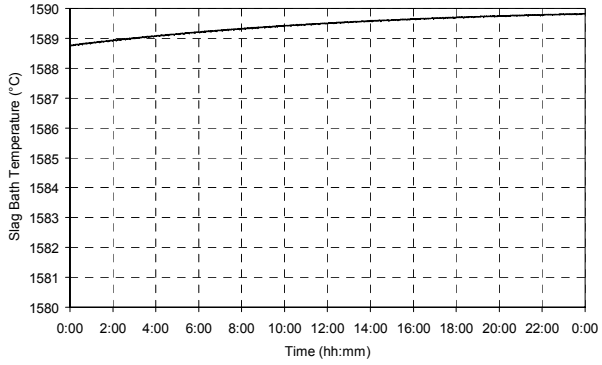

(f)

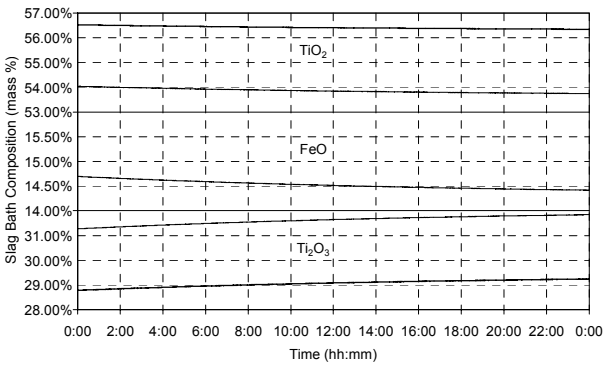

(g)

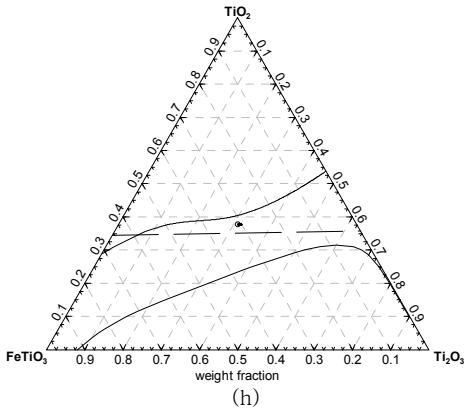

(h)

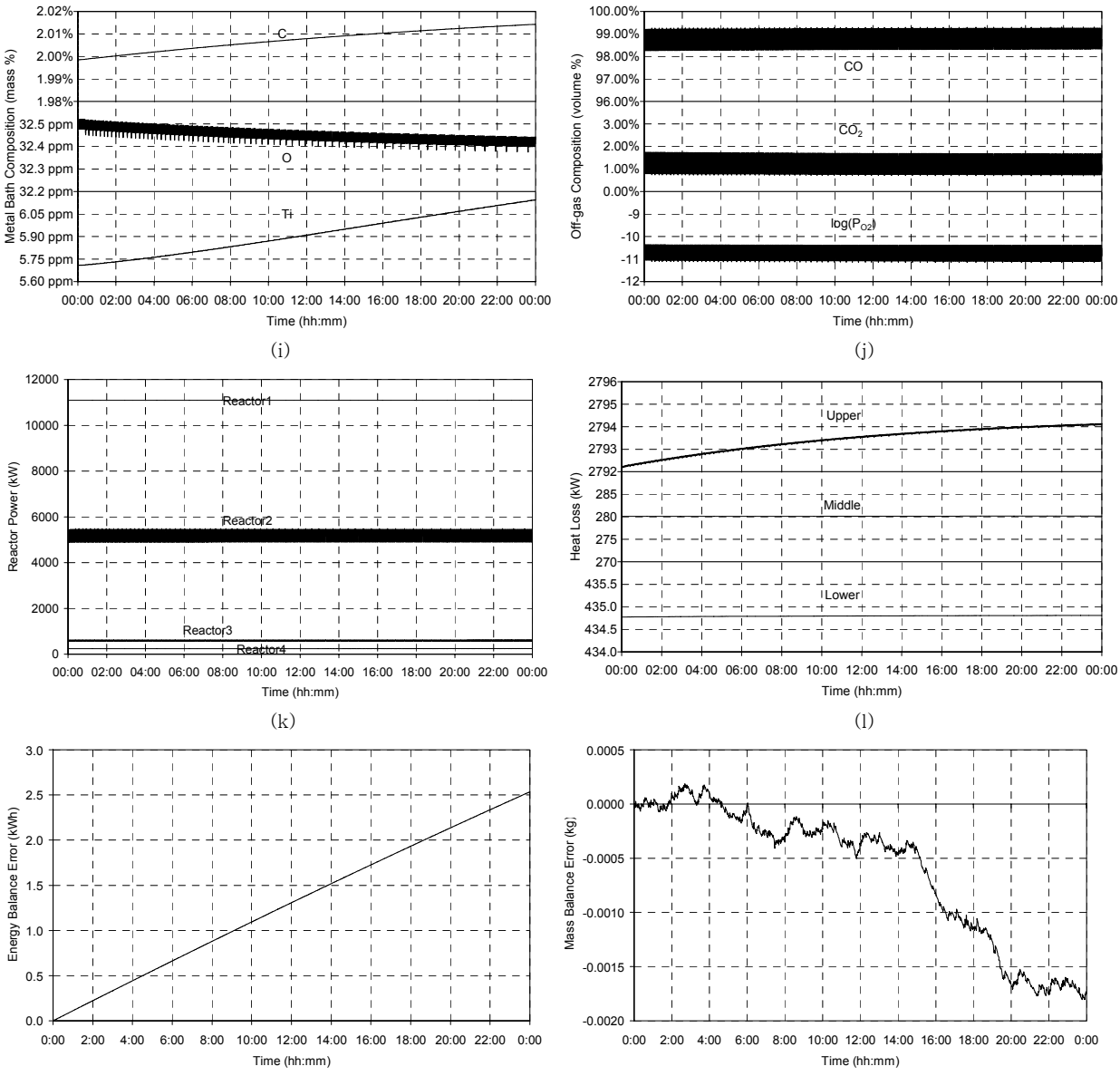

Figure 131 – Experiment 8.11 results.

8.3.12 Experiment 8.12

ILMENITE FEED RATE CHANGE	ILMENITE FEED RATE	REDUCTANT FEED RATE CHANGE	REDUCTANT FEED RATE	ELECTRICAL POWER CHANGE	ELECTRICAL POWER
–	20,000 kg/h	−1 kg/ton ilm.	1,680 kg/h	−5 kWh/ton ilm.	21,615 kW

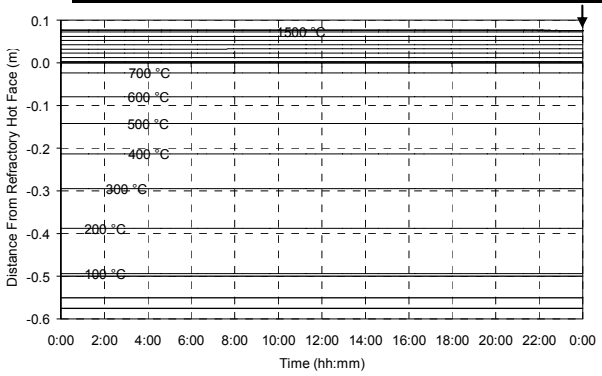

(a)

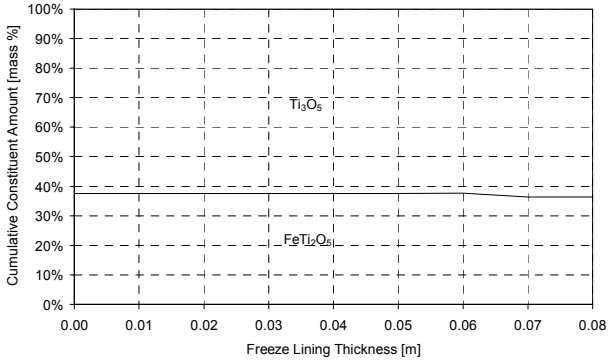

(b)

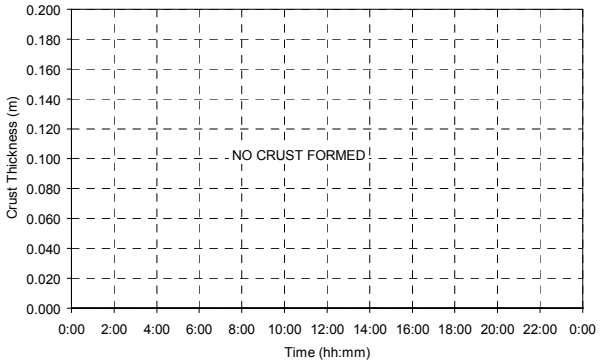

(c)

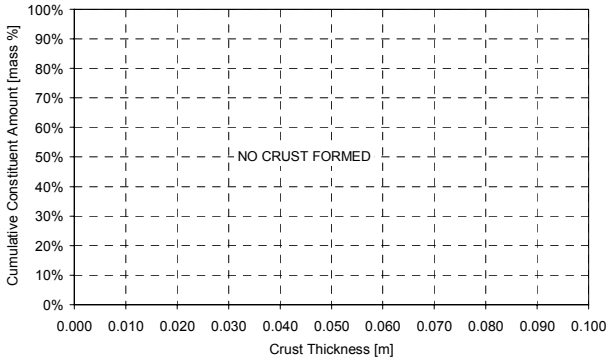

(d)

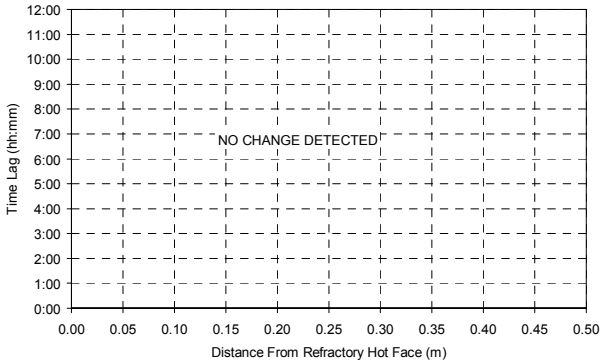

(e)

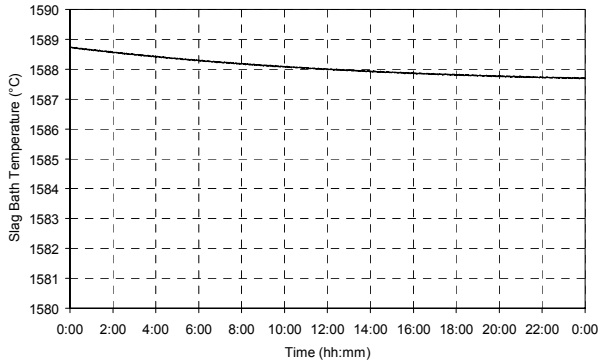

(f)

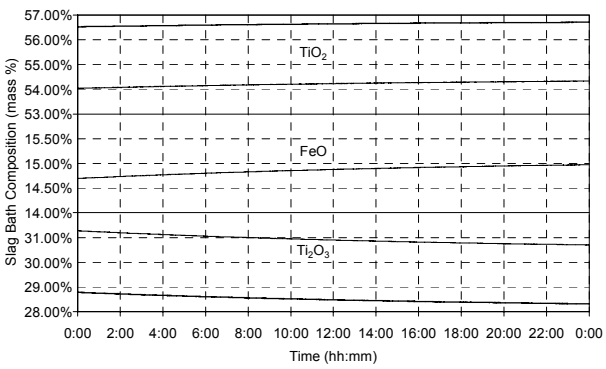

(g)

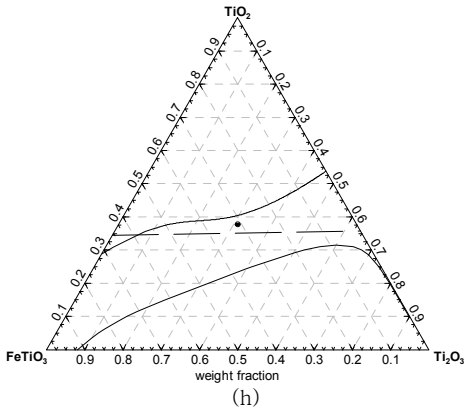

(h)

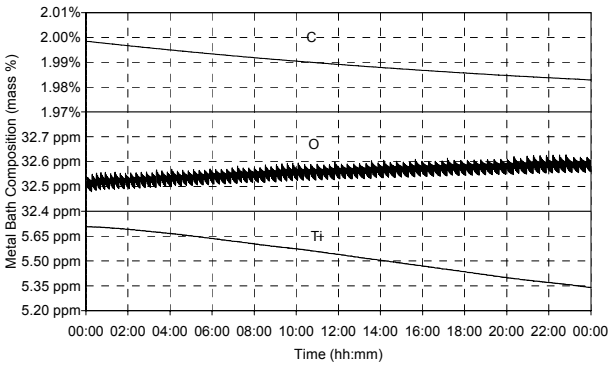

(i)

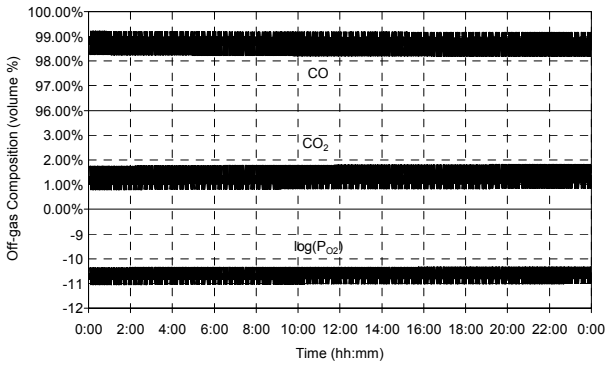

(j)

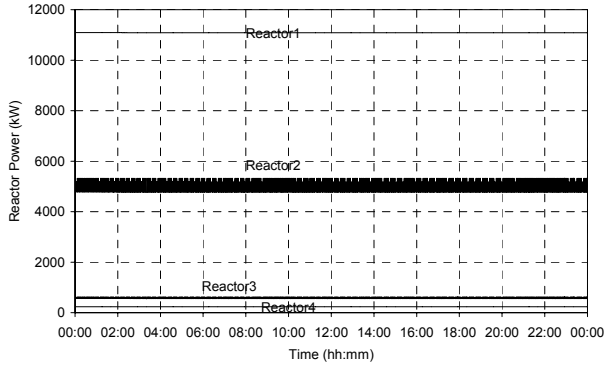

(k)

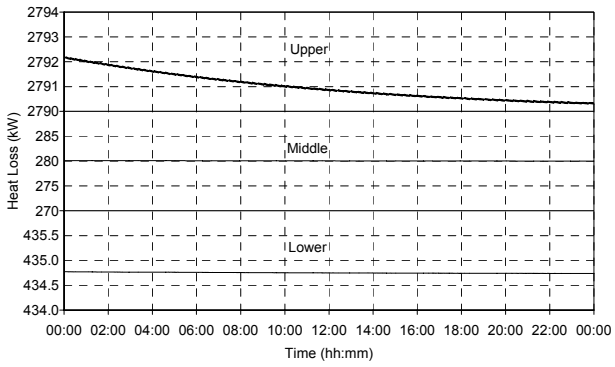

(l)

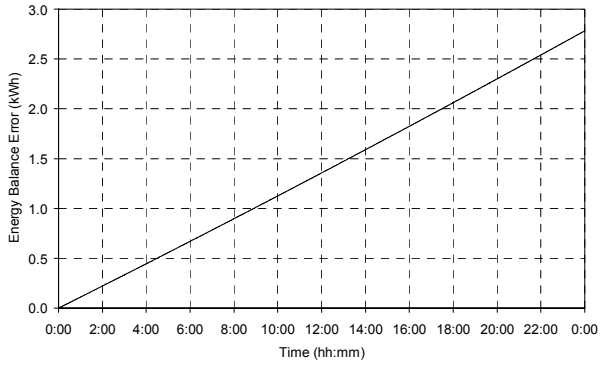

(m)

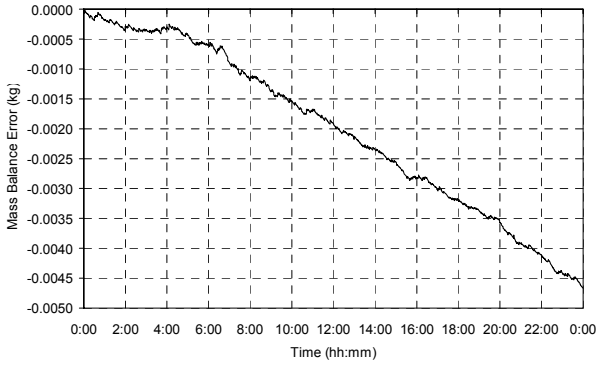

(n)

Figure 132 – Experiment 8.12 results.

8.3.13 Experiment 8.13

ILMENITE FEED RATE CHANGE	ILMENITE FEED RATE	REDUCTANT FEED RATE CHANGE	REDUCTANT FEED RATE	ELECTRICAL POWER CHANGE	ELECTRICAL POWER
–	20,000 kg/h	+ 2 kg/ton ilm.	1,740 kg/h	+ 10 kWh/ton ilm.	21,915 kW

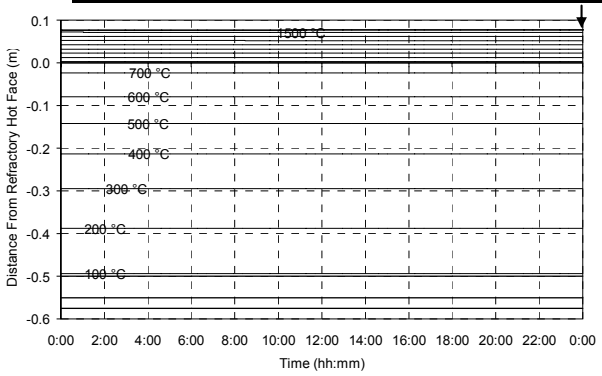

(a)

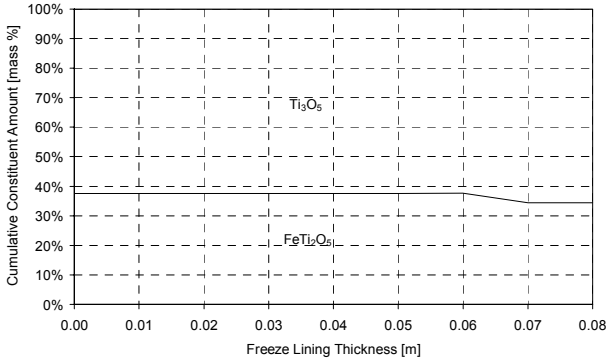

(b)

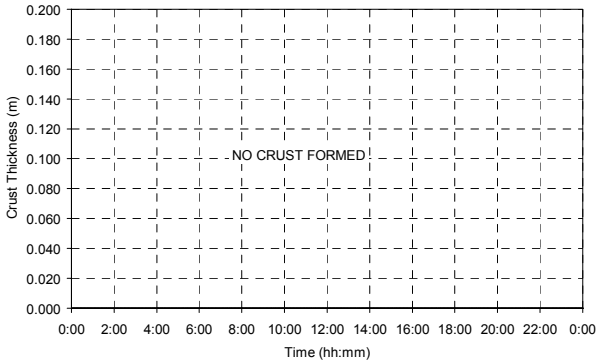

(c)

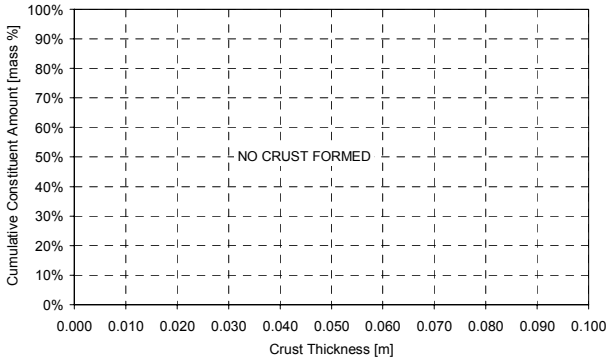

(d)

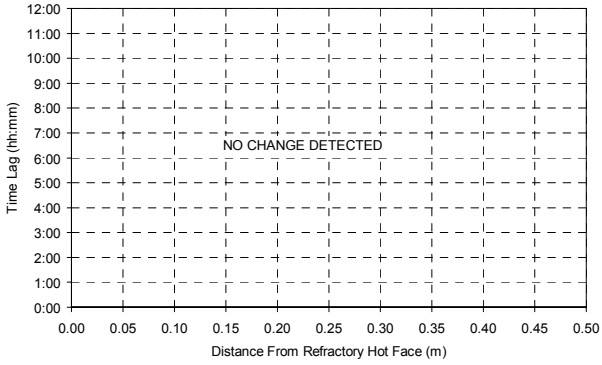

(e)

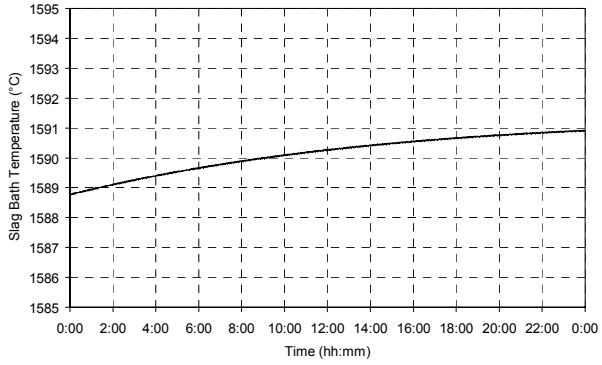

(f)

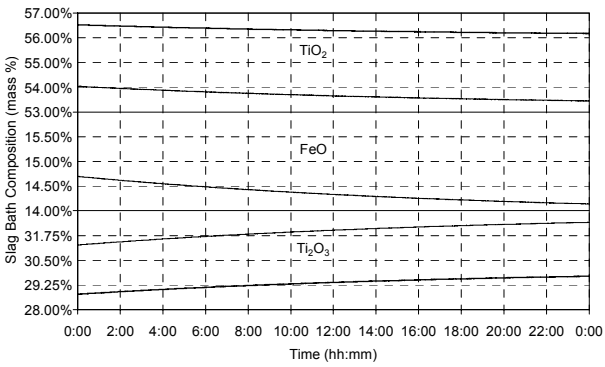

(g)

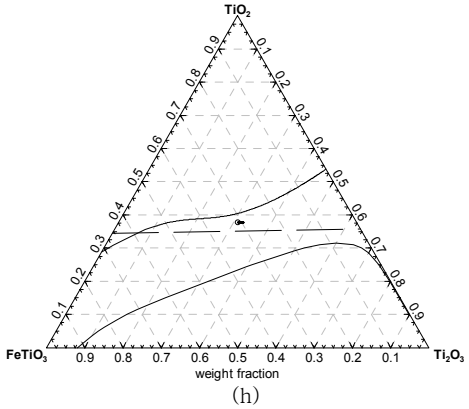

(h)

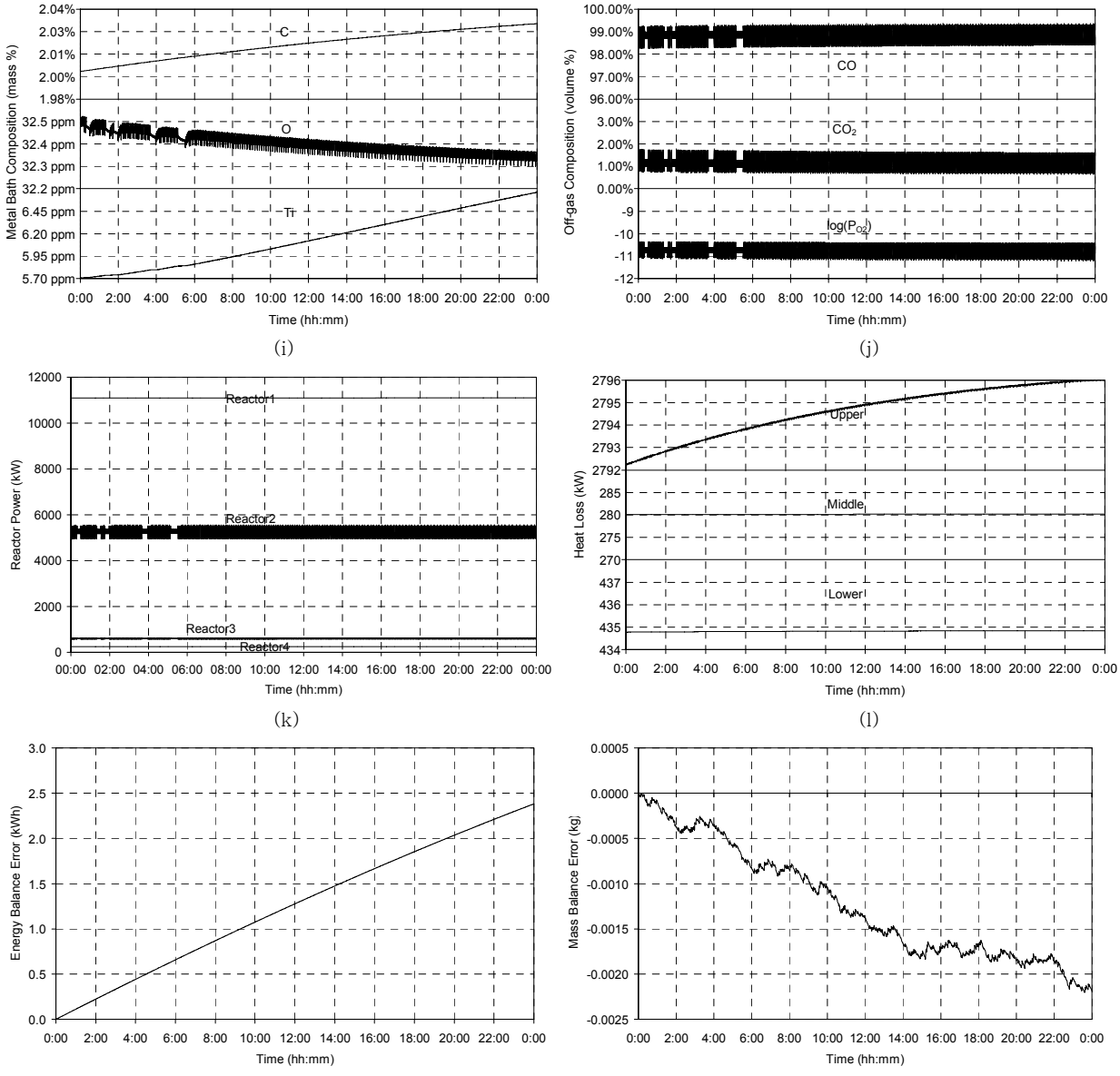

Figure 133 – Experiment 8.13 results.

8.3.14 Experiment 8.14

ILMENITE FEED RATE CHANGE	ILMENITE FEED RATE	REDUCTANT FEED RATE CHANGE	REDUCTANT FEED RATE	ELECTRICAL POWER CHANGE	ELECTRICAL POWER
–	20,000 kg/h	-2 kg/ton ilm.	1,660 kg/h	-10 kWh/ton ilm.	21,515 kW

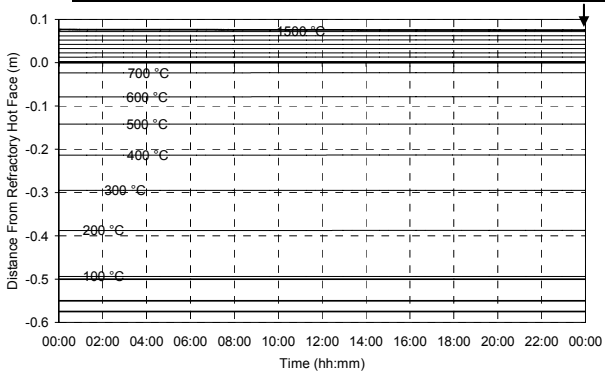

(a)

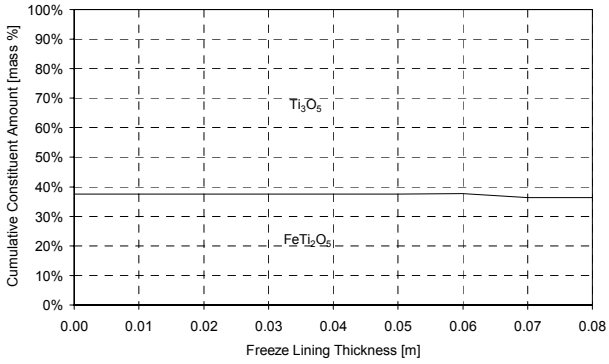

(b)

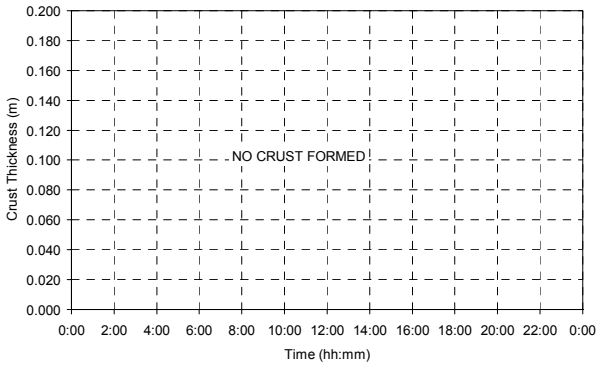

(c)

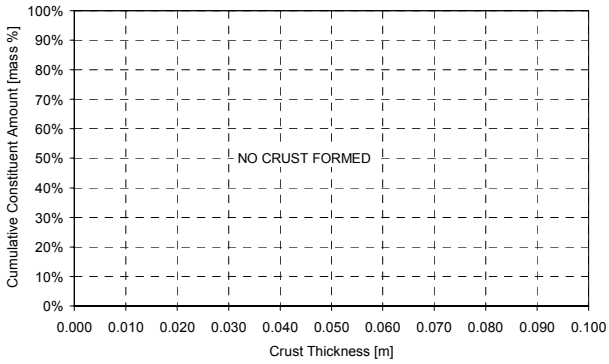

(d)

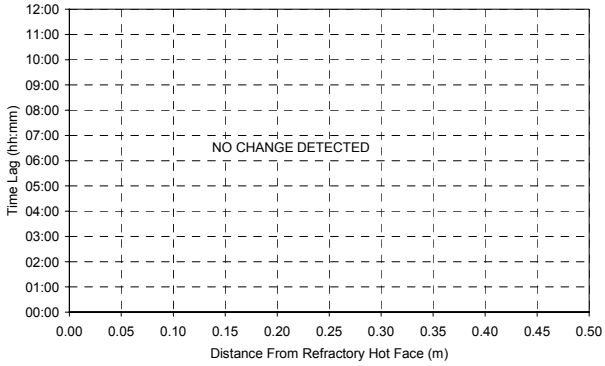

(e)

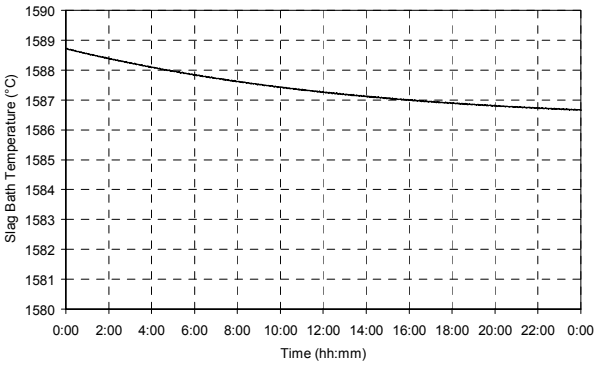

(f)

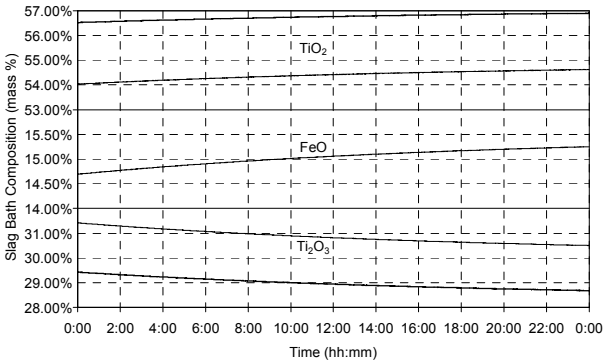

(g)

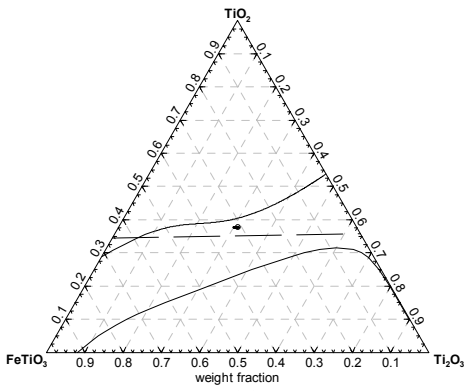

(h)

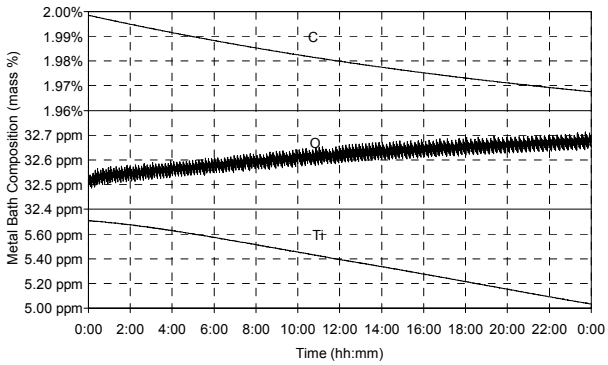

(i)

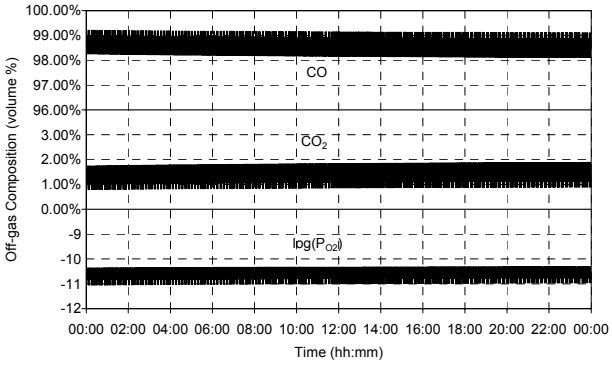

(j)

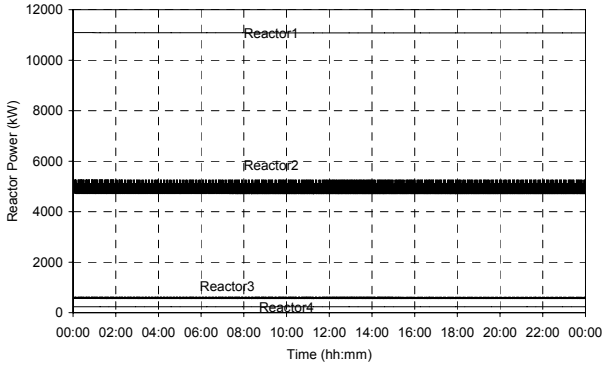

(k)

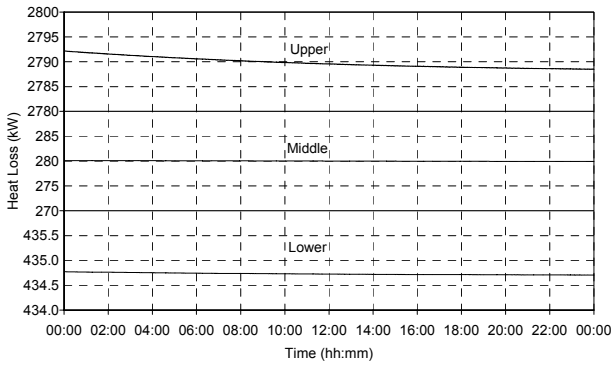

(l)

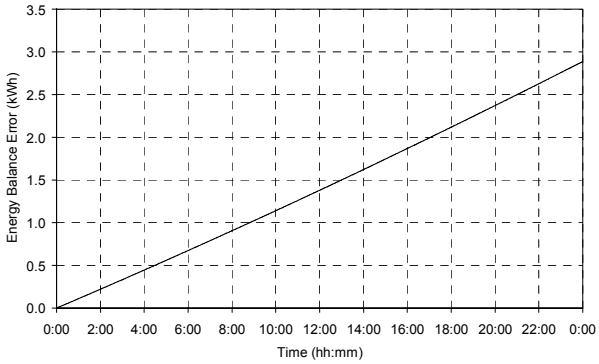

(m)

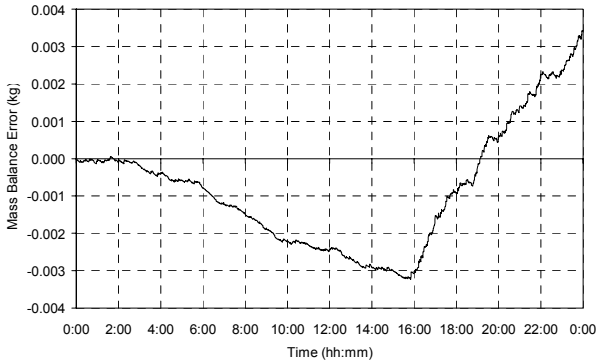

(n)

Figure 134 – Experiment 8.14 results.

8.3.15 Experiment 8.15

ILMENITE FEED RATE CHANGE	ILMENITE FEED RATE	REDUCTANT FEED RATE CHANGE	REDUCTANT FEED RATE	ELECTRICAL POWER CHANGE	ELECTRICAL POWER
–	20,000 kg/h	+ 5 kg/ton ilm.	1,800 kg/h	+ 25 kWh/ton ilm.	22,215 kW

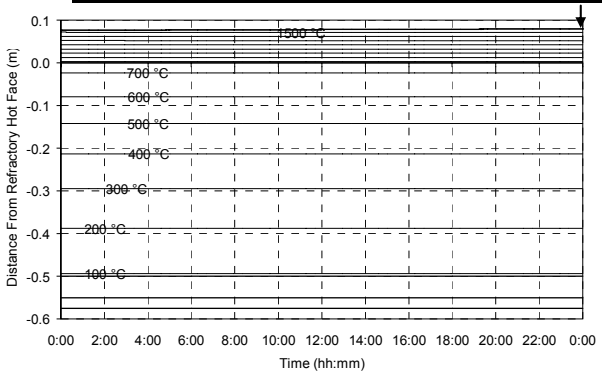

(a)

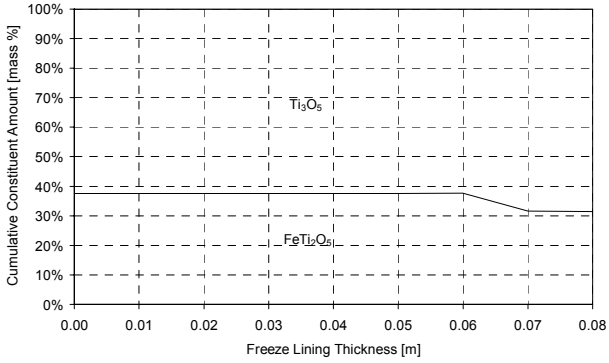

(b)

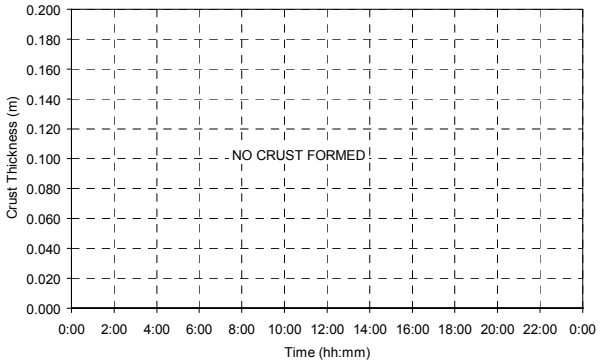

(c)

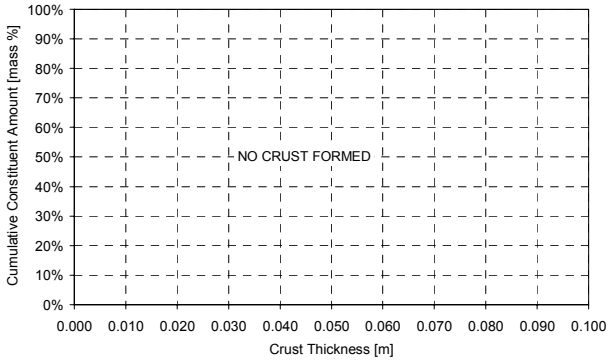

(d)

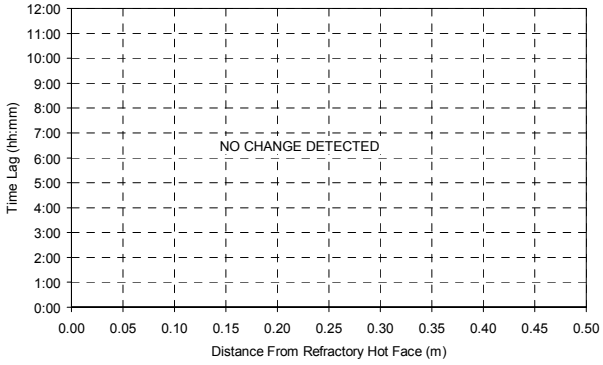

(e)

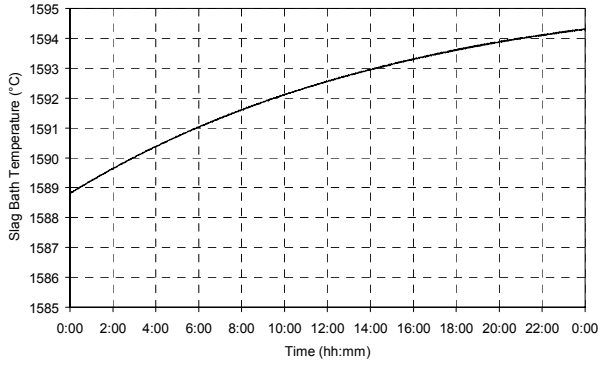

(f)

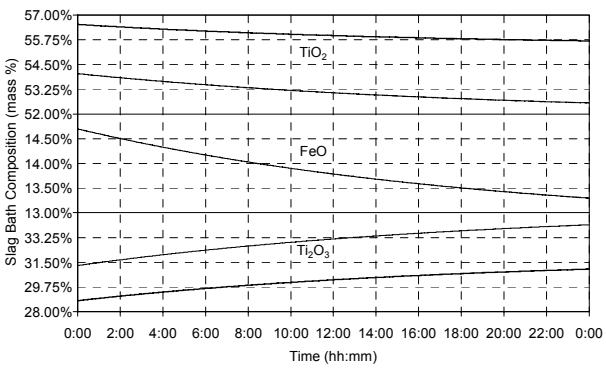

(g)

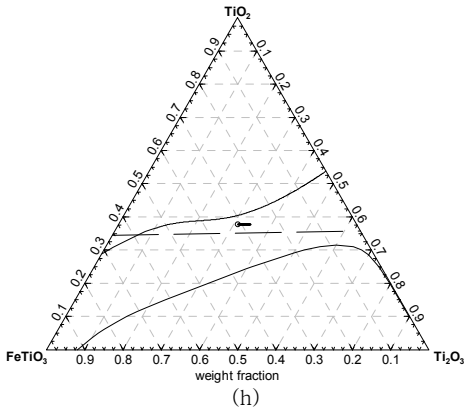

(h)

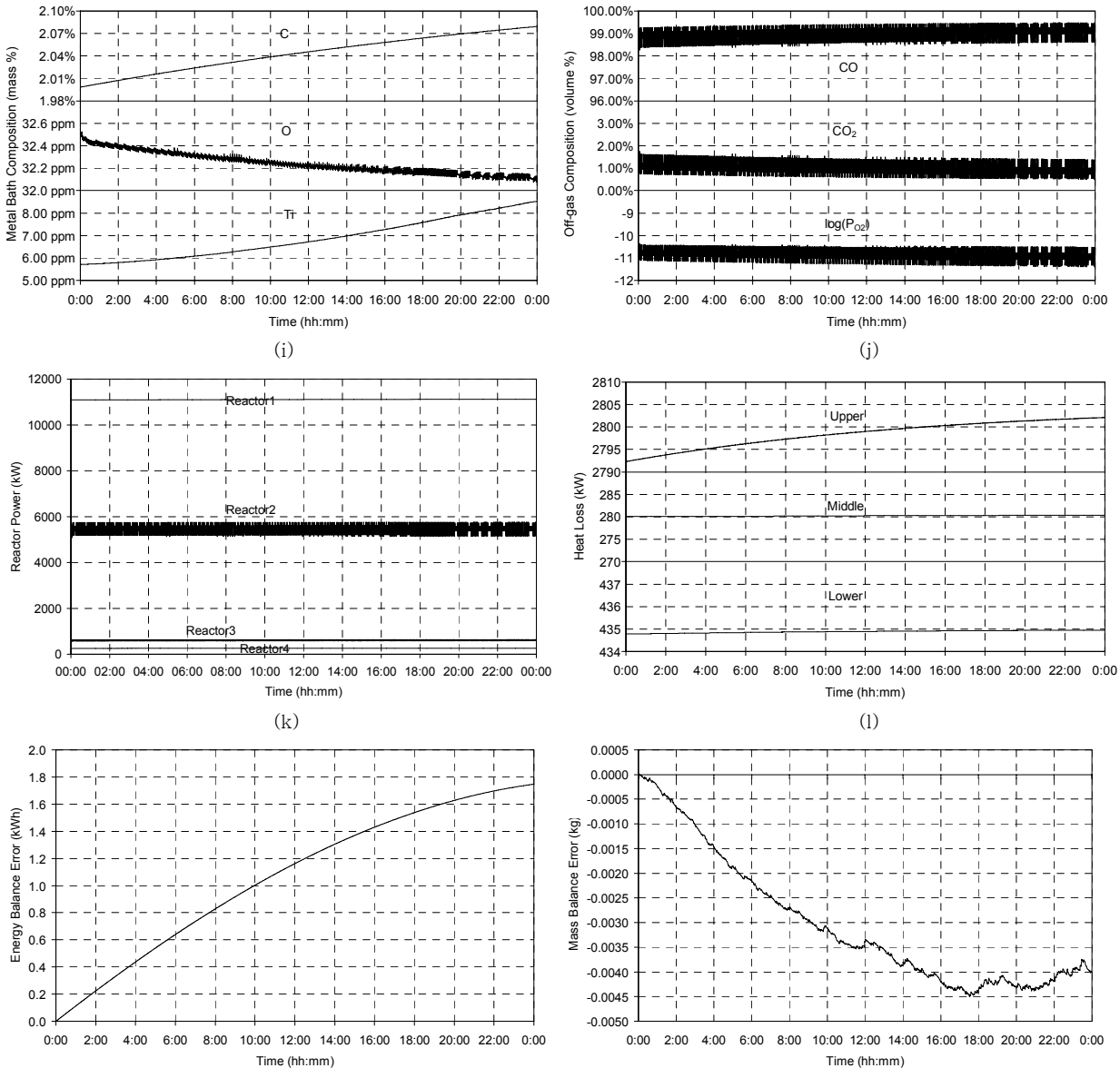

Figure 135 – Experiment 8.15 results.

8.3.16 Experiment 8.16

ILMENITE FEED RATE CHANGE	ILMENITE FEED RATE	REDUCTANT FEED RATE CHANGE	REDUCTANT FEED RATE	ELECTRICAL POWER CHANGE	ELECTRICAL POWER
–	20,000 kg/h	-5 kg/ton ilm.	1,600 kg/h	-25 kWh/t ilm	21,215 kW

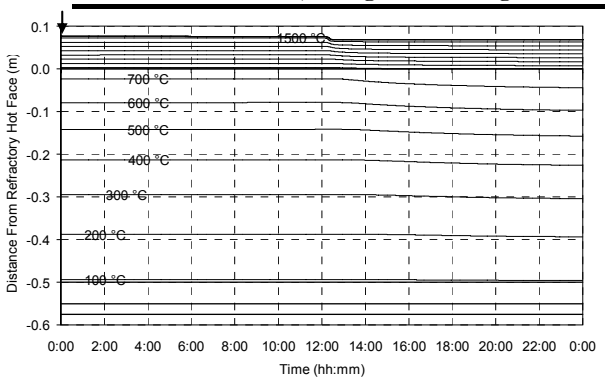

(a)

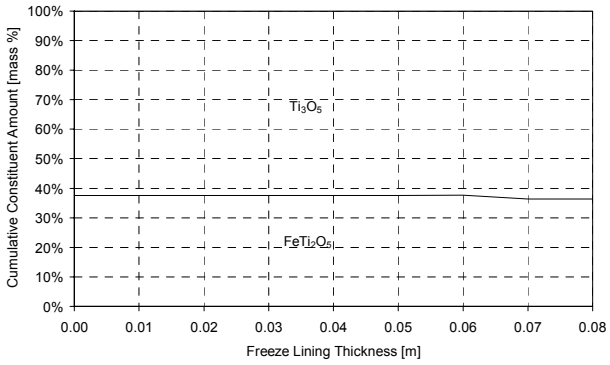

(b)

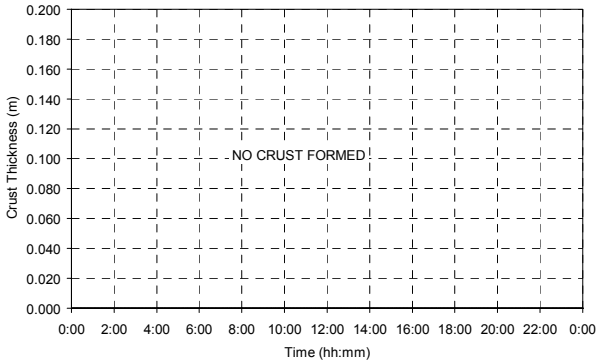

(c)

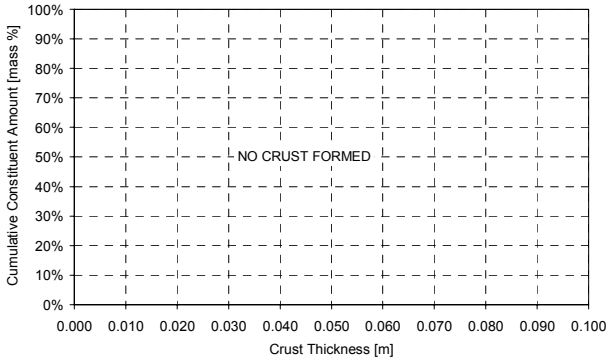

(d)

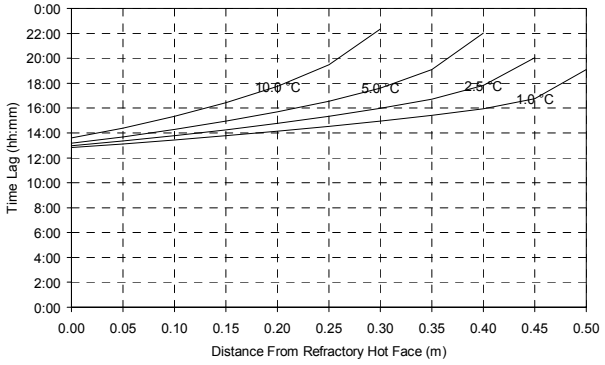

(e)

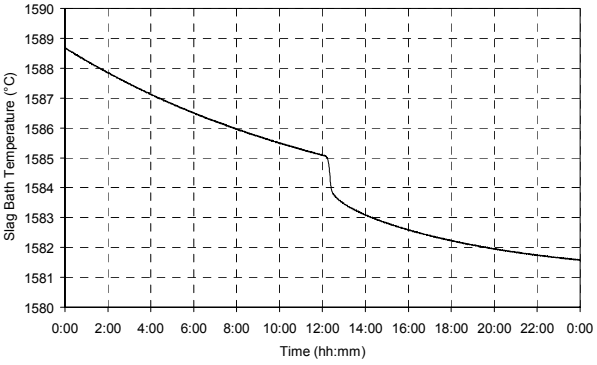

(f)

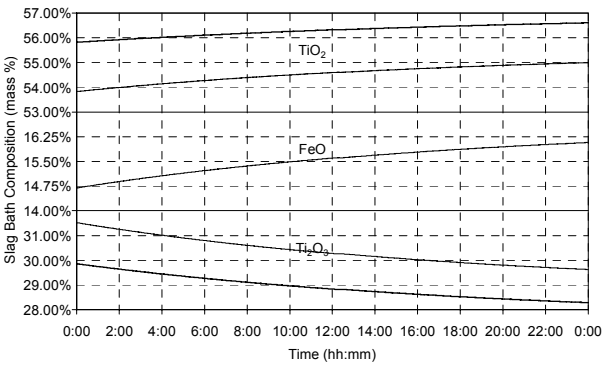

(g)

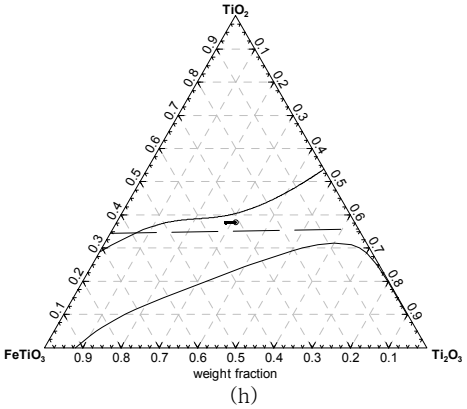

(h)

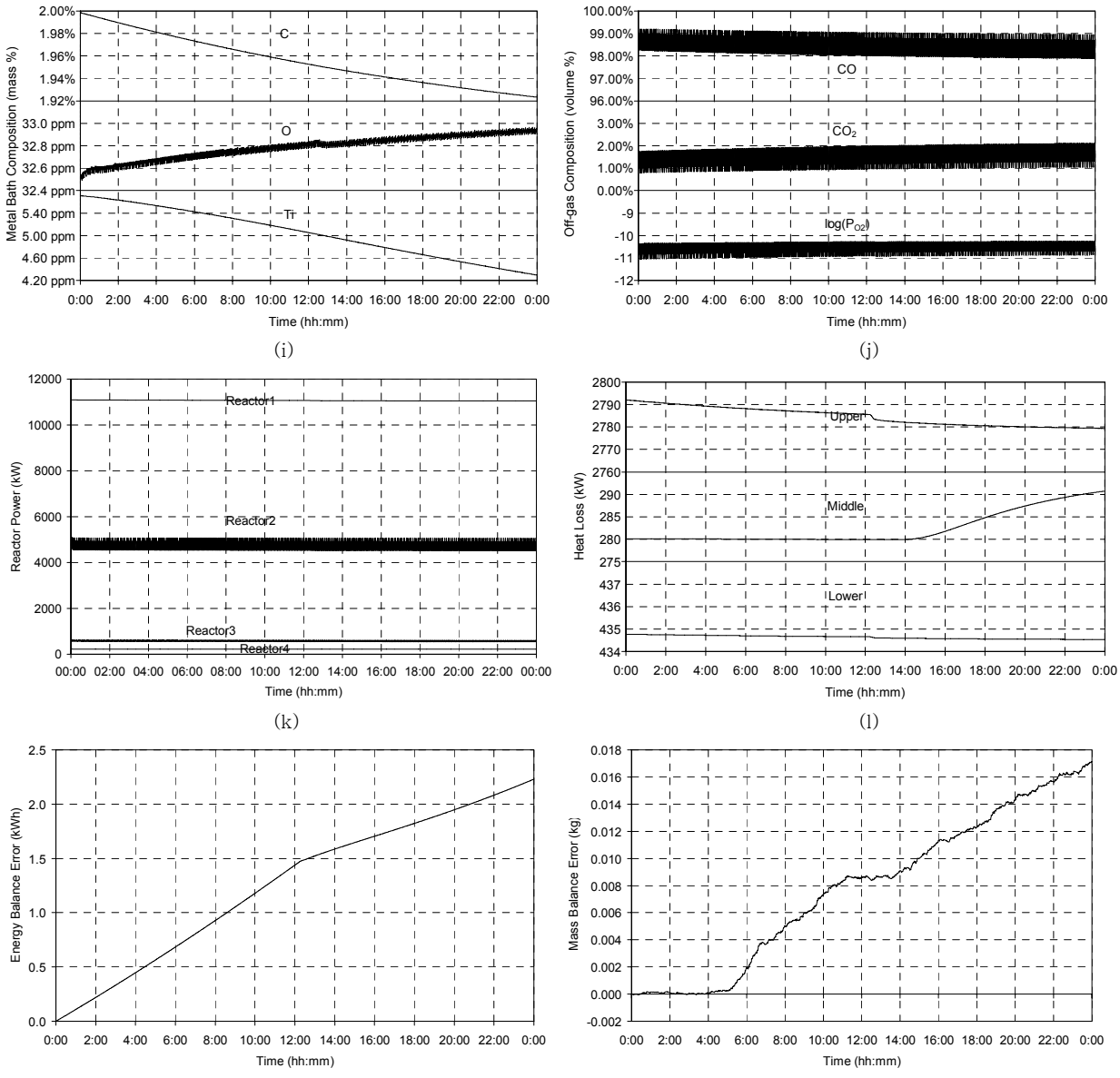

Figure 136 – Experiment 8.16 results.

8.3.17 Experiment 8.17

ILMENITE FEED RATE CHANGE	ILMENITE FEED RATE	REDUCTANT FEED RATE CHANGE	REDUCTANT FEED RATE	ELECTRICAL POWER CHANGE	ELECTRICAL POWER
–	20,000 kg/h	+ 10 kg/ton ilm.	1,900 kg/h	+ 50 kWh/ton ilm.	22,715 kW

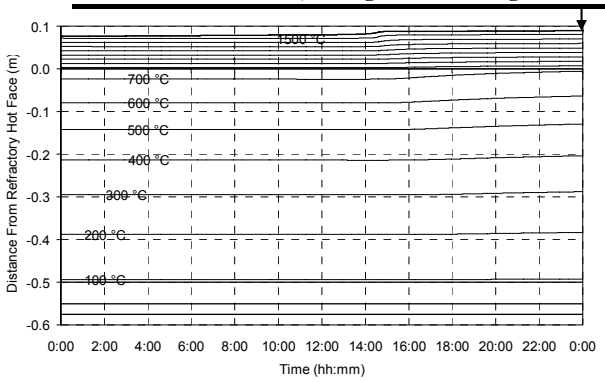

(a)

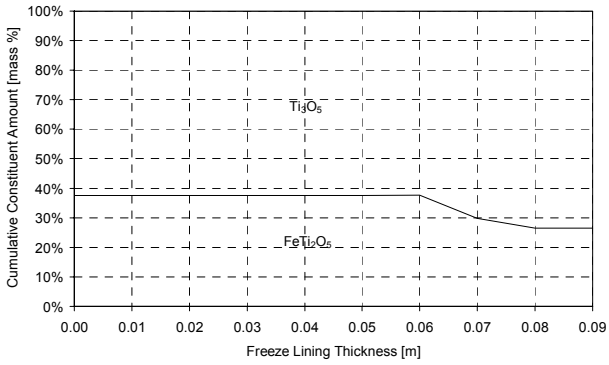

(b)

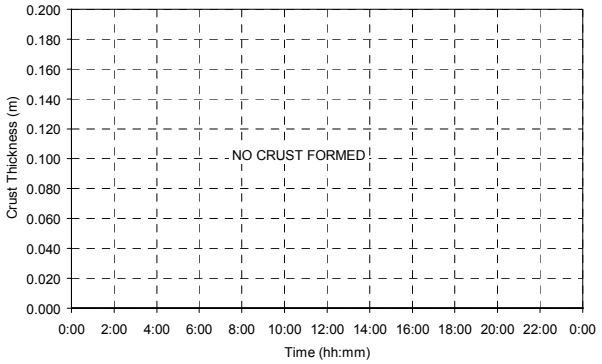

(c)

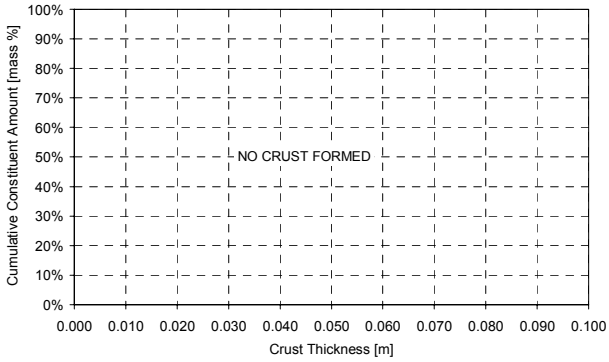

(d)

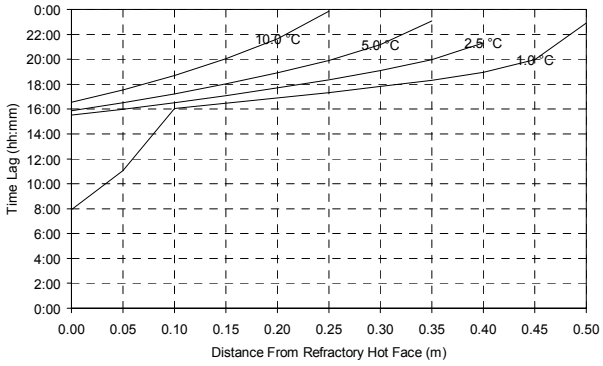

(e)

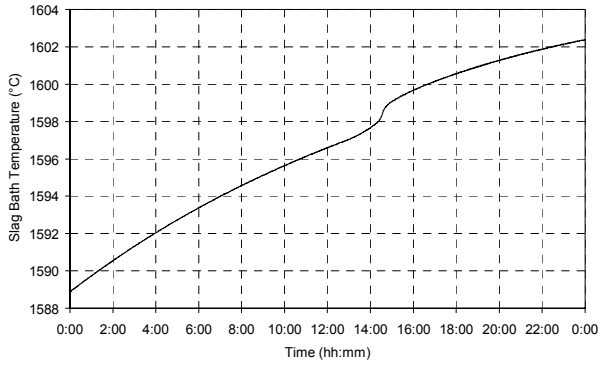

(f)

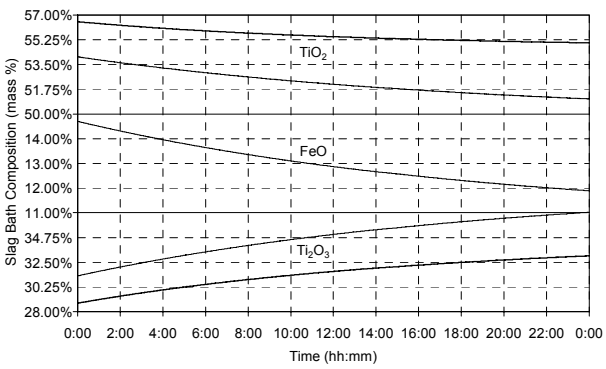

(g)

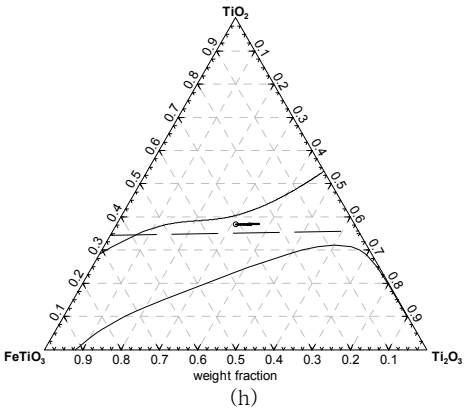

(h)

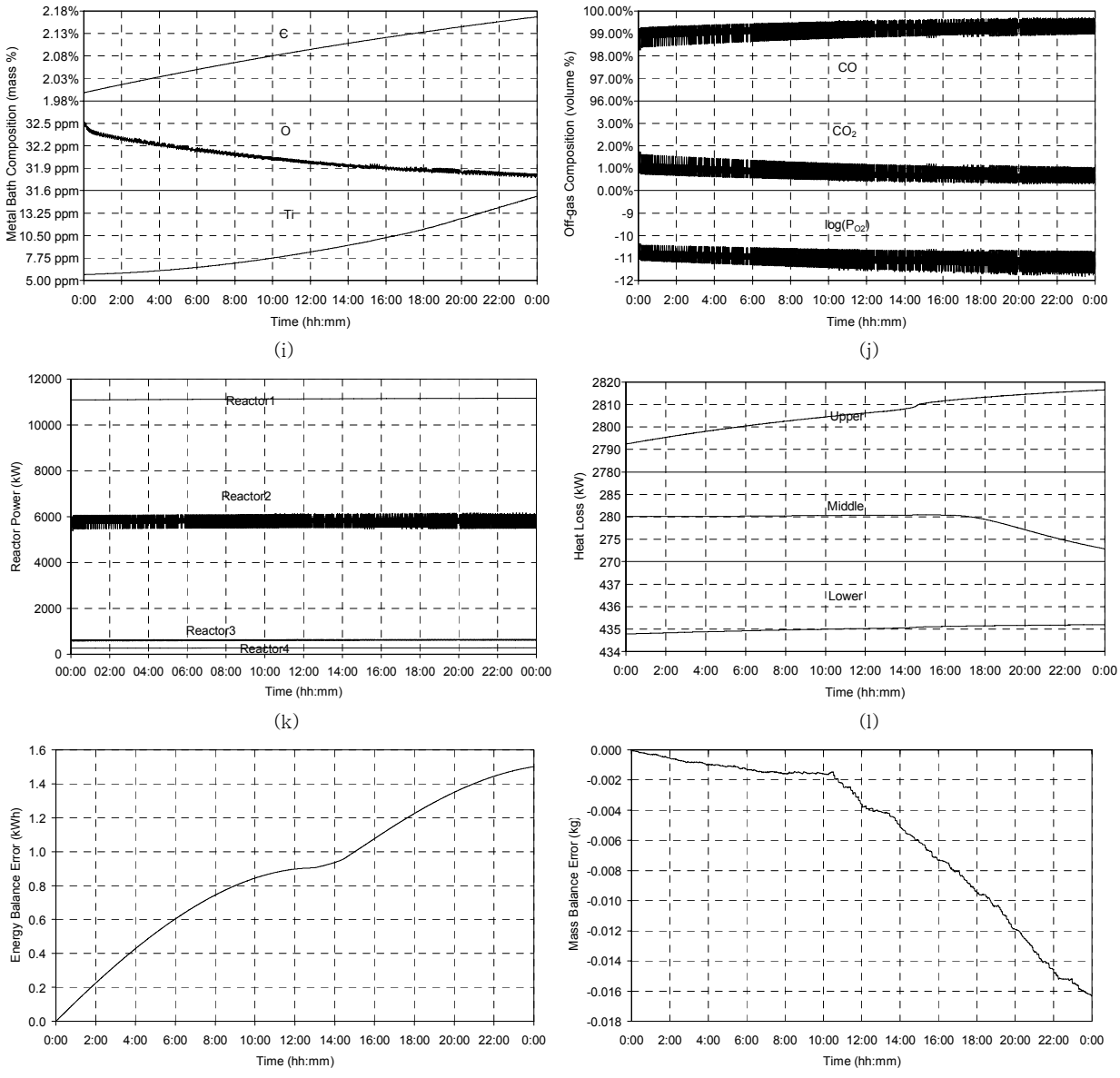

Figure 137 – Experiment 8.17 results.

8.3.18 Experiment 8.18

ILMENITE FEED RATE CHANGE	ILMENITE FEED RATE	REDUCTANT FEED RATE CHANGE	REDUCTANT FEED RATE	ELECTRICAL POWER CHANGE	ELECTRICAL POWER
-	20,000 kg/h	-10 kg/ton ilm.	1,500 kg/h	-50 kWh/ton ilm.	20,715 kW

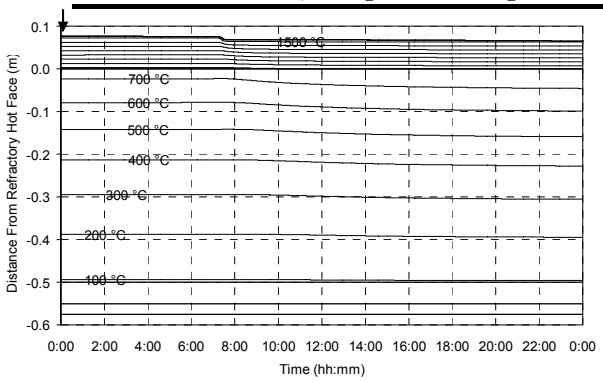

(a)

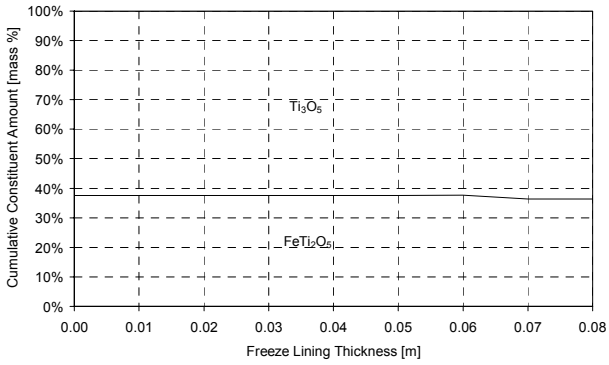

(b)

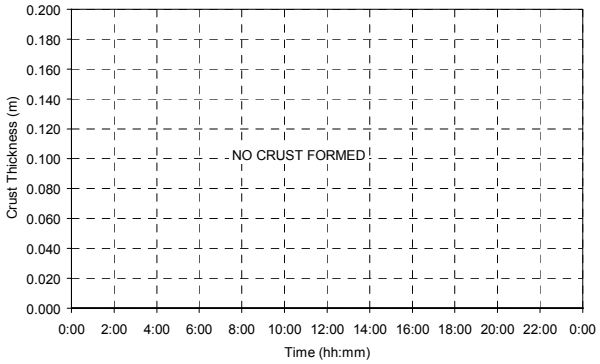

(c)

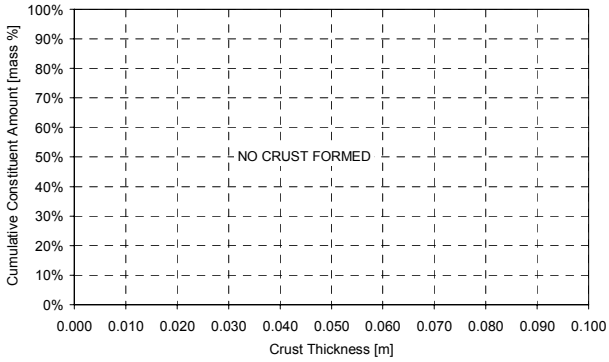

(d)

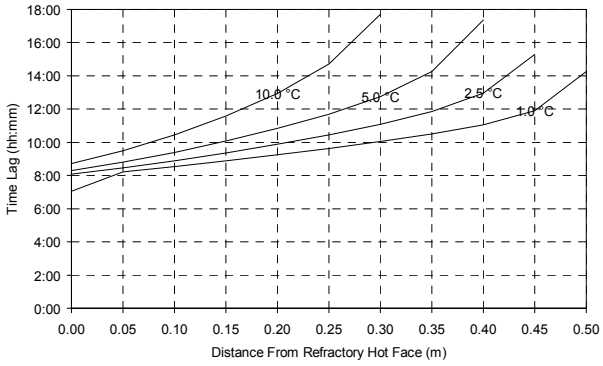

(e)

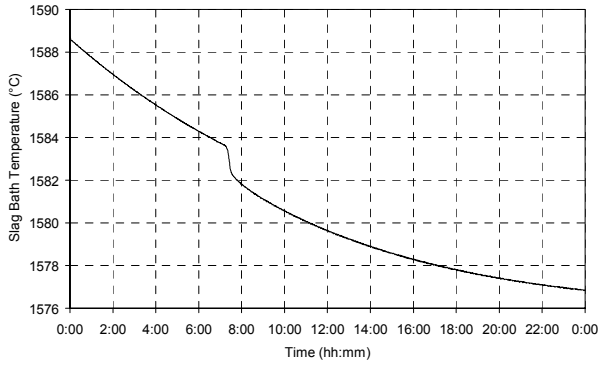

(f)

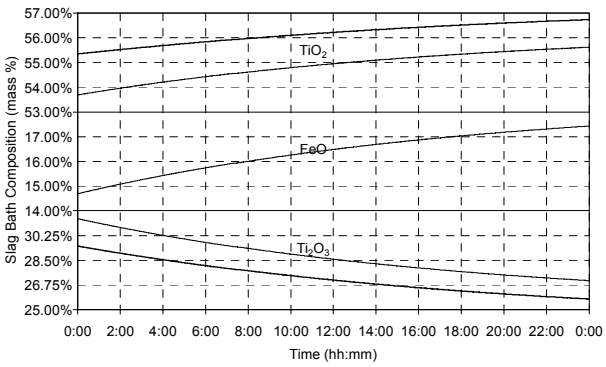

(g)

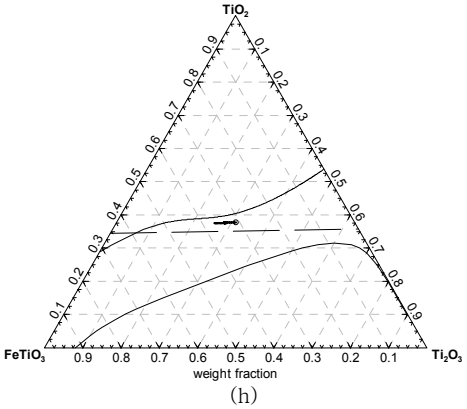

(h)

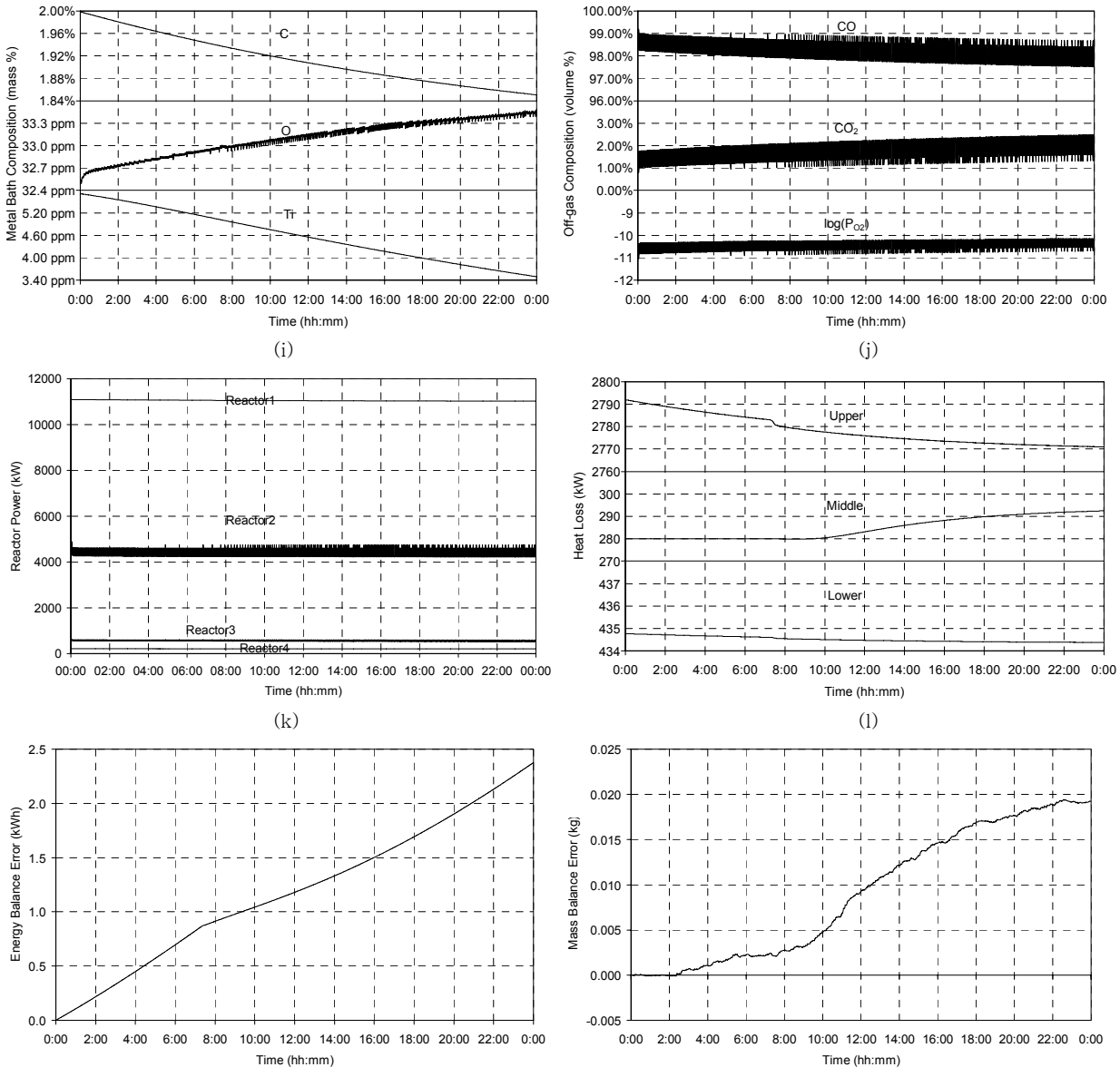

Figure 138 – Experiment 8.18 results.

8.3.19 Experiment 8.19

ILMENITE FEED RATE CHANGE	ILMENITE FEED RATE	REDUCTANT FEED RATE CHANGE	REDUCTANT FEED RATE	ELECTRICAL POWER CHANGE	ELECTRICAL POWER
–	20,000 kg/h	+ 10 kg/ton ilm.	1,900 kg/h	+ 52 kWh/ton ilm.	22,755 kW

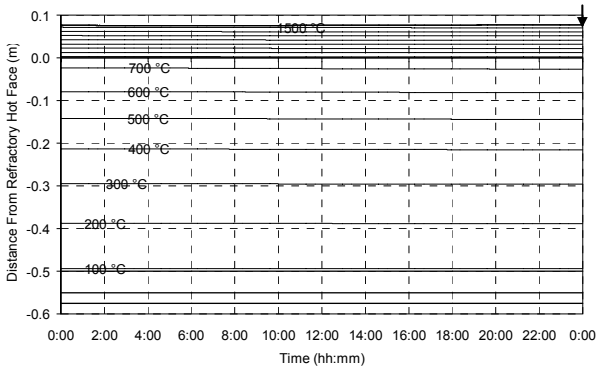

(a)

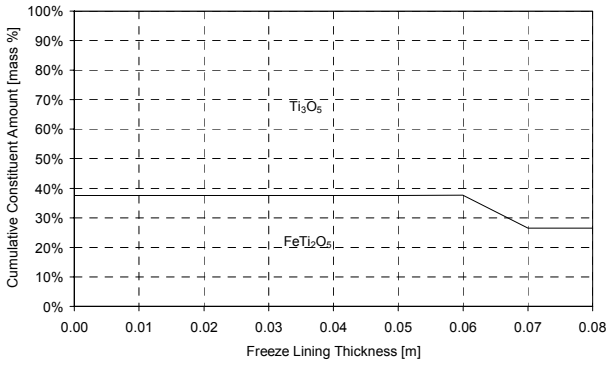

(b)

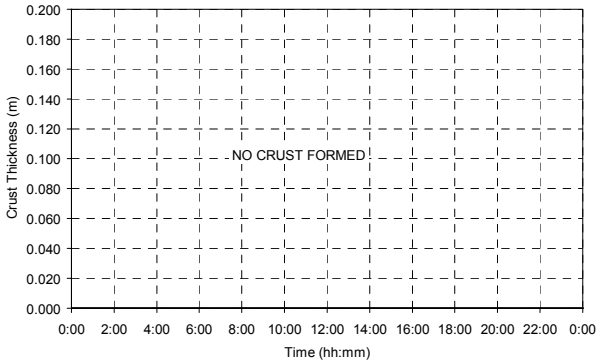

(c)

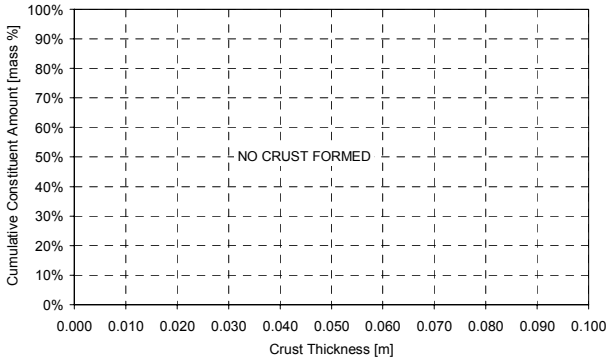

(d)

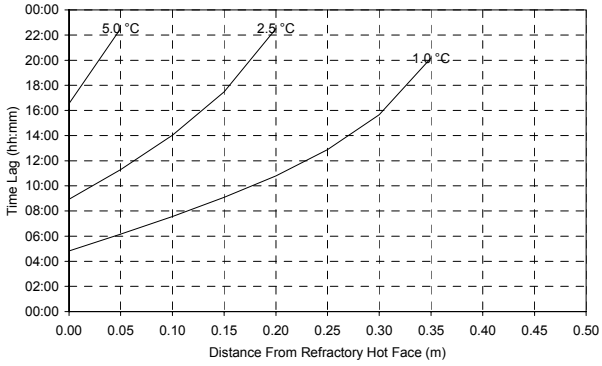

(e)

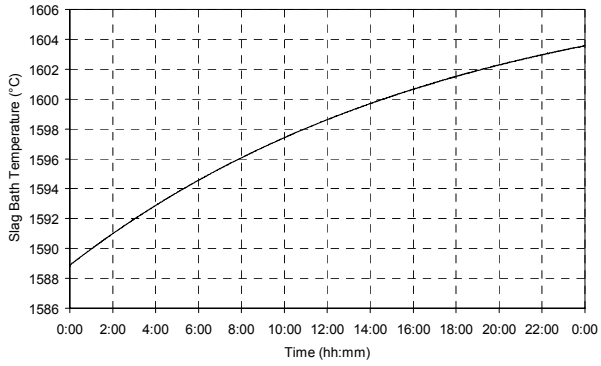

(f)

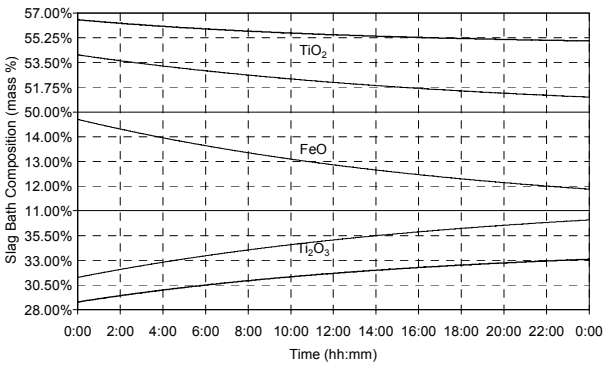

(g)

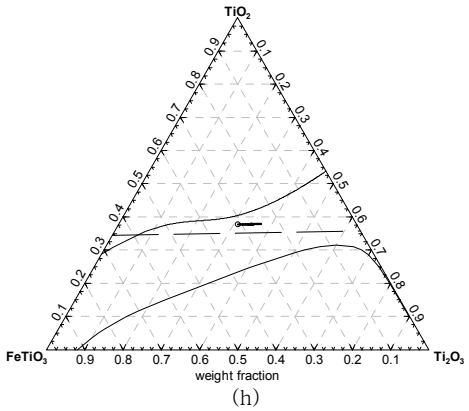

(h)

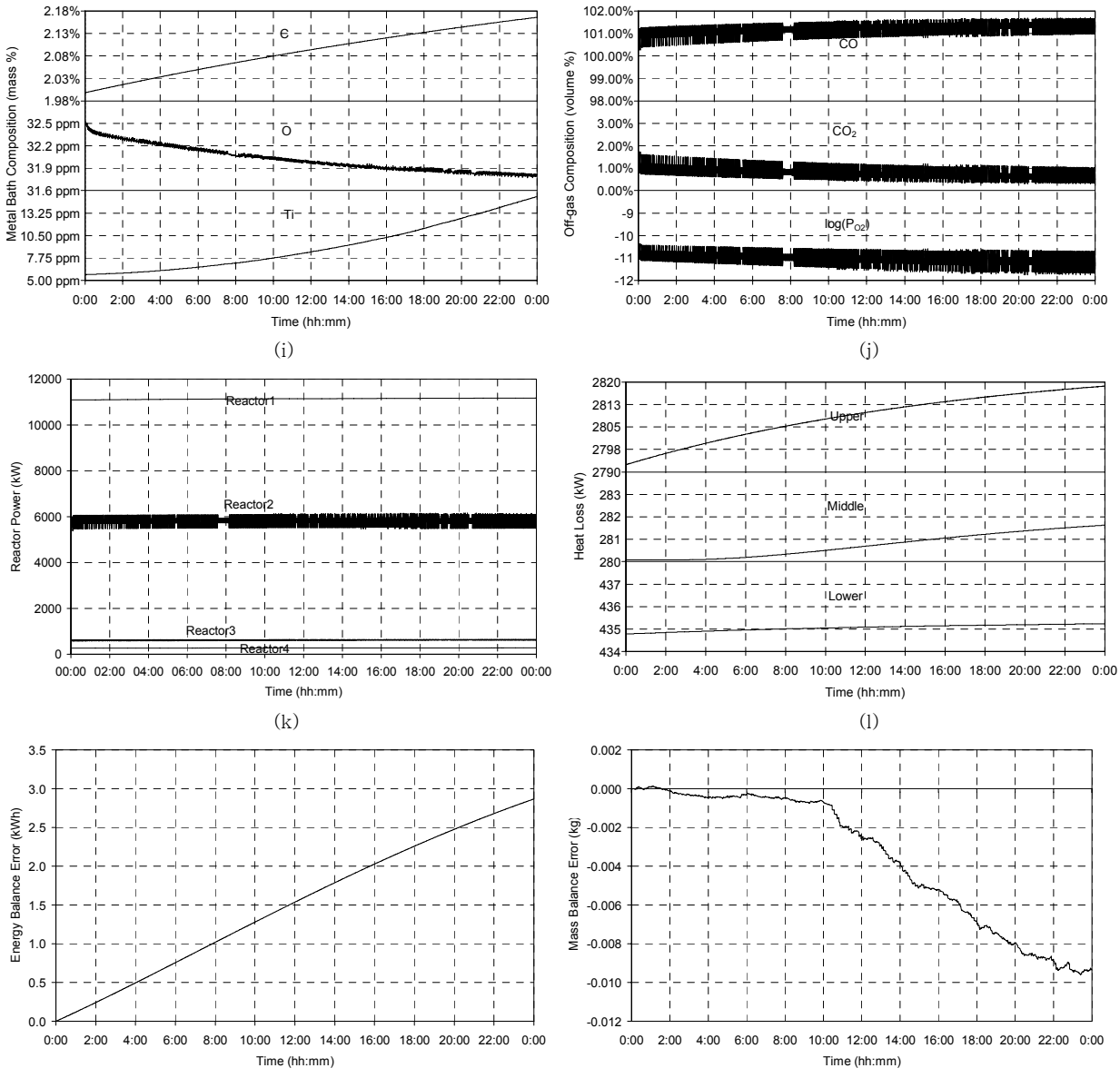

Figure 139 – Experiment 8.19 results.

8.3.20 Experiment 8.20

ILMENITE FEED RATE CHANGE	ILMENITE FEED RATE	REDUCTANT FEED RATE CHANGE	REDUCTANT FEED RATE	ELECTRICAL POWER CHANGE	ELECTRICAL POWER
–	20,000 kg/h	−10 kg/ton ilm.	1,500 kg/h	−53 kWh/ton ilm.	20,655 kW

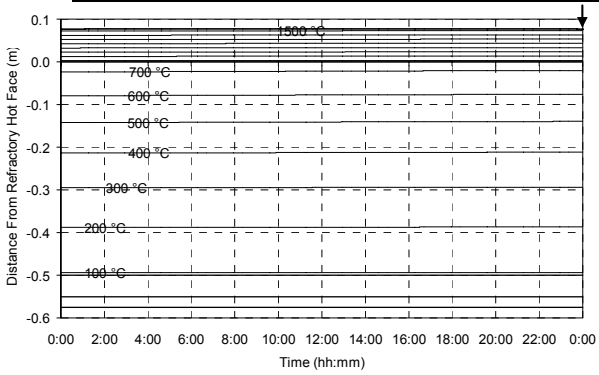

(a)

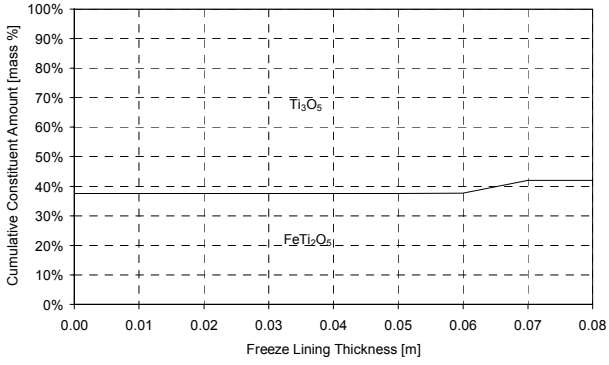

(b)

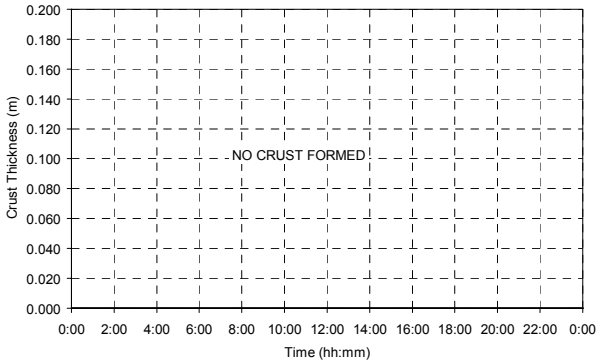

(c)

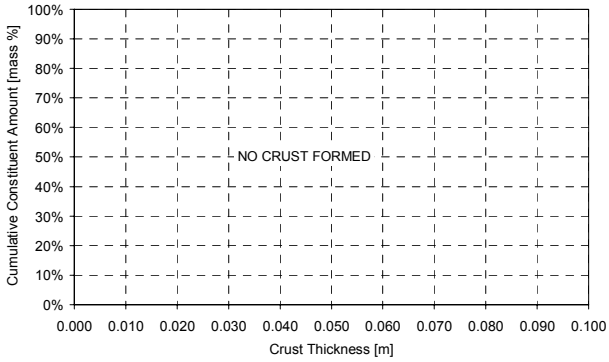

(d)

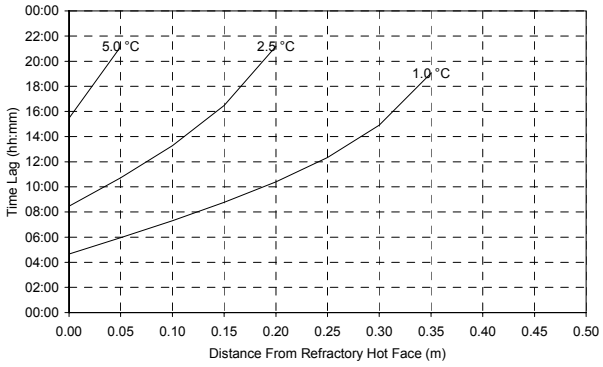

(e)

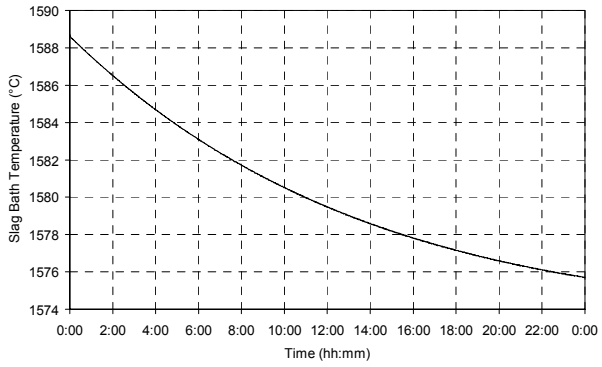

(f)

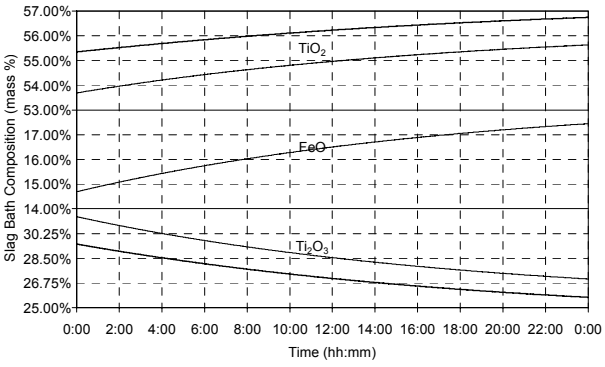

(g)

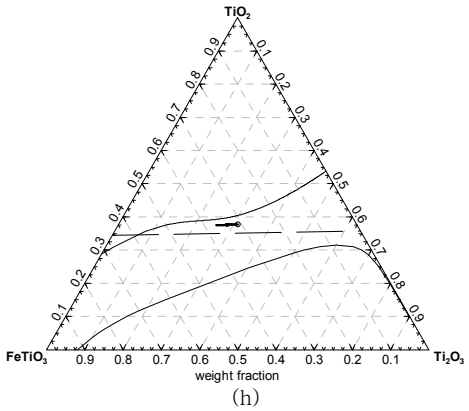

(h)

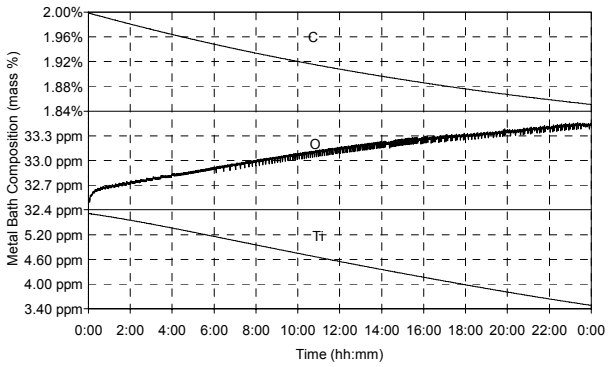

(i)

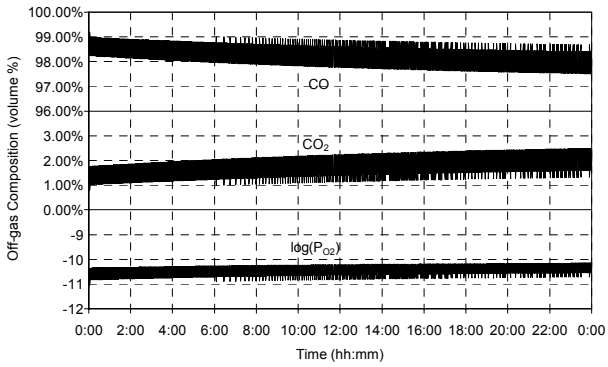

(j)

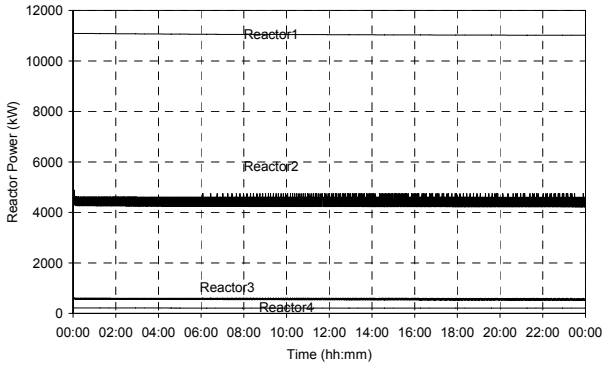

(k)

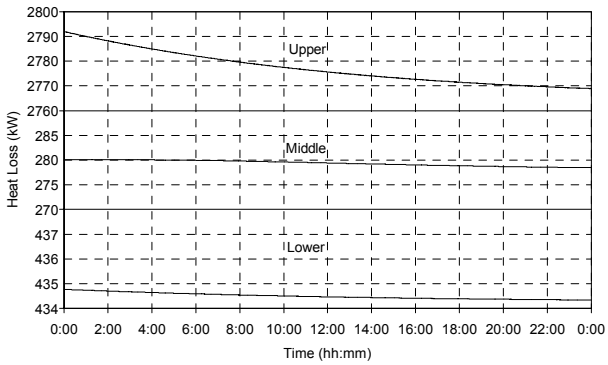

(l)

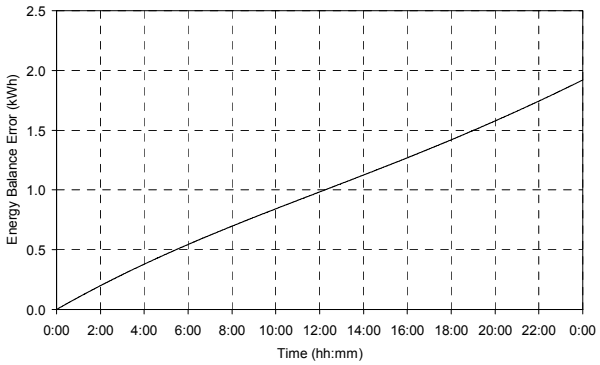

(m)

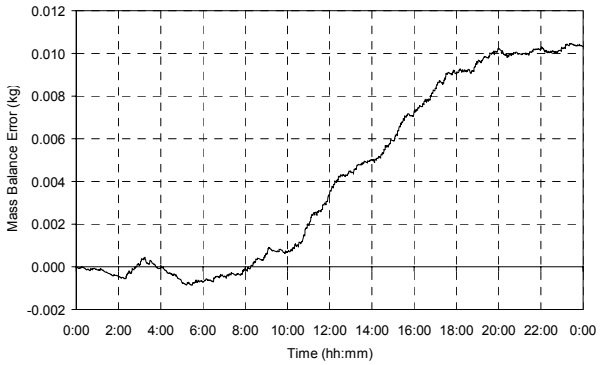

(n)

Figure 140 – Experiment 8.20 results.

8.4 DISCUSSION

The experimental results are discussed in the following paragraphs under these headings:

- The impact of severe operational errors
- Independent adjustment of reductant and energy inputs
- Combined adjustment of reductant and energy inputs

8.5 THE IMPACT OF SEVERE OPERATIONAL ERRORS

Experiments 8.1 and 8.2 simulated two scenarios in which severe operational errors occurred. Although industrial plants usually have a variety of measures in place to avoid these errors, there is always still the possibility of these or similar errors occurring. For this reason studying the impact of such errors remains relevant.

In the case of experiment 8.1 all feed (ilmenite and reductant) was stopped while the initial electrical power was maintained. This scenario is very similar to those simulated in CHAPTER 6, except that a much more complete process model was used here for conducting the simulation. In the situation described by this experiment, the electrical energy that is normally consumed by heating and melting of ilmenite, and by reduction reactions between slag and reductant suddenly becomes available for heating the slag. The consequences of this situation became clear in the experimental results.

Experiment 8.2 simulated a less severe error. Only the reductant feed was completely stopped and the ilmenite feed and electrical power was maintained. The only heat sinks removed from the system were therefore the reduction reactions between slag and reductant, and dissolution of carbon in the zone beneath the electrode.

8.5.1 Freeze Lining Thickness

The freeze lining disappeared completely 19 minutes after all feed was stopped in experiment 8.1. This is comparable to the results achieved in CHAPTER 6, where 10,000 kW of electrical power removed a 102 mm freeze lining in around 20 minutes and a 66 mm freeze lining in 13 minutes. One would expect the freeze lining in experiment 8.1 to melt away faster given the electrical power input of 21,715 kW. The effect of this power input was however reduced by heat losses from the slag bath surface, lower sidewalls and heart. The energy consumed by Reactor2 and Reactor4 in the initial stages of the experiment, and by Reactor3 throughout the experiment further reduced the effective power input. The rate at which the freeze lining disappeared can therefore be understood.

In experiment 8.2 it took 36.5 minutes for the freeze lining to melt away after reductant feed was stopped. The difference of 17.5 minutes compared with experiment 8.1 can be explained by the sustained energy consumption of Reactor1. Because the ilmenite feed rate was maintained, Reactor1 continued consuming in excess of 11,000 kW to heat and melt ilmenite. This reduced the rate at which the freeze lining melted away.

In both cases (experiment 8.1 and 8.2) the freeze lining disappeared at an alarming rate. If an operational error similar to those simulated goes unnoticed for a period longer than the time required for melting away the freeze lining, serious damage to the furnace lining can occur. Another point of concern is that the

freeze lining in an actual furnace does not have a constant thickness around the circumference of the furnace. This creates the possibility that damage may start to occur some time earlier than what is indicated above.

8.5.2 Freeze Lining Composition

Because graph (b) shows the composition of the freeze lining as a function of position at the point in time when the freeze lining was at its thickest, and because the freeze lining was at its thickest at the start of both experiments 8.1 and 8.2, no observations could be made from the results of these experiments.

8.5.3 Thermal Response of Freeze Lining and Furnace Wall

The thermal response of specifically the furnace wall is important when one considers the use of sidewall thermocouple signals for the purpose of controlling freeze lining thickness. Within the context of the situations simulated in experiments 8.1 and 8.2, it would be valuable if such thermocouple signals provided early warning of the impending damage.

From graph (e) in the experimental results of experiment 8.1 it is evident that a thermocouple capable of detecting and transmitting a 1 °C change in temperature must be installed at a position 5.7 cm away from the refractory hot face if it is to provide a warning within 19 minutes. However, after 19 minutes some damage would already have occurred. Deciding on a safety margin of 5 minutes would then mean that the thermocouple would have to be installed at the hot face of the refractory material. Even then it would only be able to warn 4 minutes before damage sets in.

In the case of experiment 8.2 the thermocouple would have to be installed 11.4 cm from the refractory hot face if its warning is to coincide with refractory damage; and 7.5 cm from the hot face if it is required to warn 5 minutes before.

From graph (a) it is apparent that if a thermocouple is installed 5 cm away from the hot face, it would be reading around 650 °C. The temperature at the hot face is just below 800 °C. At 10 cm the temperature is roughly 560 °C. All of these temperatures are comfortably within the range of type K thermocouples.

Organisations operating ilmenite-smelting furnaces are often conservative when it comes to the depth of insertion of thermocouples in furnace refractory materials. This can be understood because the refractory lining must last for a period of up to 10 years. However, from the results of experiments 8.1 to 8.2 it can be concluded that thermocouples installed at positions further than 5 cm from the refractory hot face would be of little use as warning signals in situations such as those simulated.

8.5.4 Slag Bath Temperature

As has been explained in previous chapters, slag bath temperature in an ilmenite-smelting furnace cannot vary independent from liquid slag composition while a freeze lining is present. The slag bath temperature is expected to closely follow the liquidus temperature of the slag. This was demonstrated by the experimental results presented in CHAPTER 6 and CHAPTER 7.

It is evident from graph (f) of experiments 8.1 and 8.2 that the temperature of the liquid slag had risen quite appreciably. The increase was 37 °C for experiment 8.1 and 16 °C for experiment 8.2. What is not evident

from these graphs is the difference between the slag bath temperature and the liquidus temperature of the slag.

Graph (h) of experiment 8.1 shows that only a slight change in slag composition occurred. Given such a small change and an increase of 37 °C in liquid slag temperature, one must conclude that either the liquidus temperature surface is very steep, or that there is an appreciable difference between the slag bath temperature and the liquidus temperature of the slag.

In the case of experiment 8.2 the change in composition is substantially greater, but towards the $FeTiO_3$ corner of the graph. One would expect that the liquidus temperature would fall when the composition moves in that direction.

To make interpretation easier, the two (h) graphs were superimposed on the mass fraction version of the liquidus diagram presented in Figure 11.

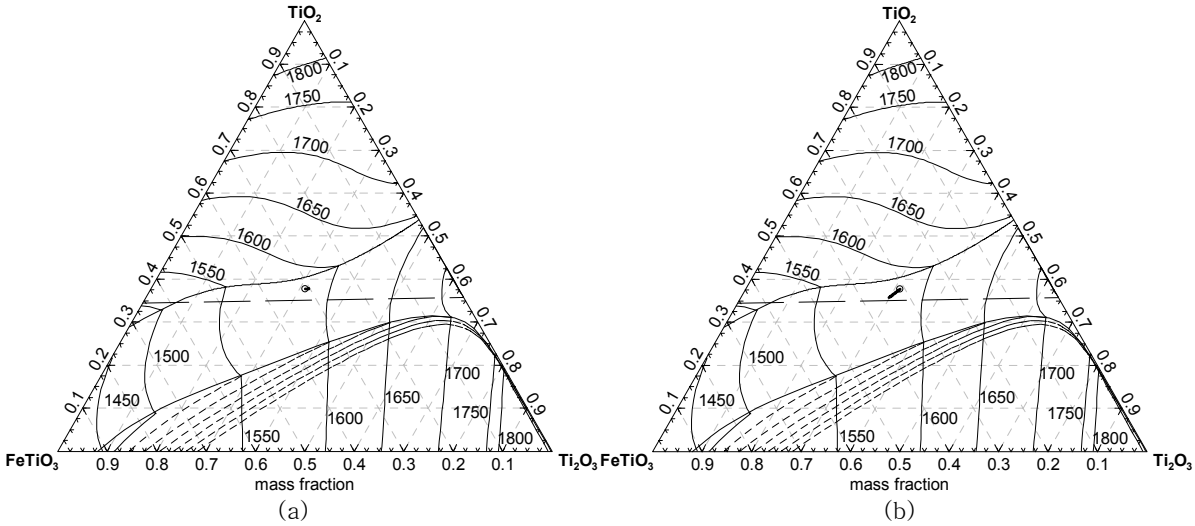

Figure 141 – Graph (h) of experiments 8.1 (a) and 8.2 (b) superimposed on the liquidus diagram.

From Figure 141 it is clear that the slag liquidus temperature in neither experiment went beyond 1600 °C. This means that the flow conditions created in the model by the FreezeLiningFlow and CrustFlow sub-models resulted in a significantly superheated slag bath. Because the model could not be validated on actual plant data, it is uncertain how well the model describes these aspects of the real process. The fact that the model described the freeze lining and crust parts of the process fairly well according to the knowledge and experience of the author about the ilmenite-smelting process, does however lend some confidence to these results. The results are expected to deviate quantitatively from reality, but should display qualitatively what can be expected from an actual process.

8.5.5 Slag Bath Composition

The change in liquid slag composition in experiment 8.1 was largely the result of solid slag from the freeze lining entering into the slag bath. Some reduction at the interface between the slag and metal baths also contributed to the change in composition.

A more pronounced change in liquid slag composition occurred during experiment 8.2. The situation in this experiment is comparable (in terms of material inputs) to experiment 7.20. In experiment 8.2 the slag composition also moved towards the $FeTiO_3$ corner of graph (h). The direction of the movement seemed to be offset to some degree by the composition of the freeze lining material melted into the bath and, to a lesser degree, reduction taking place at the interface between the slag and metal baths.

8.5.6 Metal Bath Composition

The rate of change in carbon content of the metal bath was virtually identical for experiments 8.1 and 8.2. After 10 minutes both had reached 1.99% and after 20 minutes both were at 1.98%. The carbon content dropped further during the second half of experiment 8.2 because of the longer duration.

It is evident from the metal bath O and Ti contents of the two experiments that the oxidation potential in the furnace changed in different directions. During experiment 8.1 the oxygen content of the metal decreased and the Ti content increased with time as a result of reduction reactions between the slag and metal baths removing oxygen from the system.

In the case of experiment 8.2 the trend was in the opposite direction even though the same reduction reactions were active at roughly the same rate, as was evident from the change in carbon content. The reason for the difference is the large quantity of oxygen carried into the furnace with the ilmenite feed.

8.5.7 Off-gas Composition

The off-gas composition echoed the observations made from the metal bath composition results. The partial oxygen pressure during experiment 8.2 was clearly higher at 10^{-10} atm compared with that of experiment 8.1 at $10^{-10.6}$ atm.

8.5.8 Reactor Power

The reactor power results shown in graph (k) of experiments 8.1 and 8.2 presented no surprises. Reactor1 power dropped off suddenly during experiment 8.1, but was maintained during experiment 8.2. This is as a result of ilmenite feed being stopped in experiment 8.1.

The power of Reactor2 and Reactor4 diminished during both experiments. This happened because reductant feed was stopped at the start of both experiments. No reductant was therefore available after some time for reaction in these two reactors.

Reactor3 maintained its power in both experiments because contact between the slag and metal baths remained unchanged during both experiments.

8.5.9 Heat Losses

Experiment 8.1 and 8.2 furnace heat loss results as shown in graph (l) also behaved as expected. The losses from the lower part of the furnace increased in both cases as a result of an increase in iron temperature. The losses from the middle of the furnace remained virtually constant because of the lag inherent in the heat transfer path through the freeze lining and furnace wall. Similar inertia should have been evident in the lower-furnace heat loss results because conduction also takes place through a

refractory layer. The simplified way in which this heat transfer was modelled however eliminated this lag. The upper-furnace losses rose steadily because of the increase in the temperature of the slag bath.

8.6 INDEPENDENT ADJUSTMENT OF REDUCTANT AND ENERGY INPUTS

In experiments 8.3 to 8.10 the suggested 1:5 ratio of reductant input to energy input was deliberately ignored to determine the influence of independent adjustment of these two process inputs. The following four independent adjustments were studied:

- Increase in reductant feed rate (experiments 8.3 and 8.5).
- Decrease in reductant feed rate (experiments 8.4 and 8.6).
- Increase in energy input rate (experiments 8.7 and 8.9).
- Decrease in energy input rate (experiments 8.8 and 8.10).

Experiments 8.5 and 8.10 were run for a period shorter than 24 hours due to software instabilities.

8.6.1 Freeze Lining Thickness

The behaviour of the freeze lining during the experiments presented no surprises. In cases where more energy became available (experiments 8.4, 8.6, 8.7 and 8.9), the freeze lining became thinner. During the other four experiments where additional energy was consumed by reduction reactions or simply removed from the electrical power input, the freeze lining became thicker.

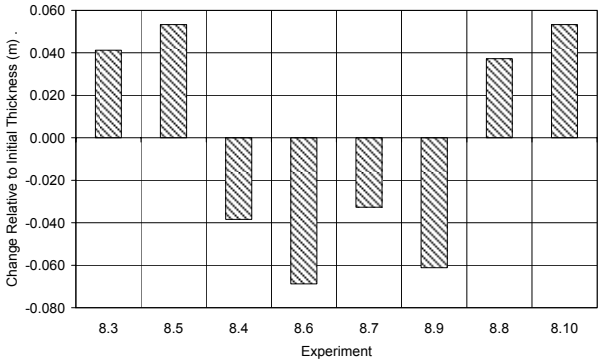

Figure 142 – Chapter 8 subset 2 change in freeze lining thickness.

From the experimental results it is evident that an independent increase in reductant feed rate has, in terms of freeze lining thickness, an influence that is very similar to a decrease in energy input rate given that the ratio between the set points is 1:5. The same similarity was observed between a decrease in reductant feed rate and an increase in energy input rate. This similarity is understandable since an increase in reductant feed rate causes additional energy to be consumed, and a decrease in reductant feed rate causes energy to become available for heating and melting of slag.

8.6.2 Freeze Lining Composition

Graph (b) in the result sets could only be used for interpretation in the case of experiments 8.3, 8.5, 8.8 and 8.10 because these were the only experiments that showed an increase in freeze lining thickness.

In all these cases the solidified material consisted of only pseudobrookite and no rutile. After close inspection, it was found that the pseudobrookite $FeTi_2O_5$ content decreased with time during experiments 8.3 and 8.5, and increased in the case of experiments 8.8 and 8.10. These tendencies are not visible in graph (b) because of the scale that was selected. The change in $FeTi_2O_5$ content was dominated by the increase in reduction during experiments 8.3 and 8.5; and by the enrichment of the liquid slag in FeO due to solidification during experiments 8.8 and 8.10.

8.6.3 Thermal Response of Freeze Lining and Furnace Wall

The thermal response of the furnace wall as described by graph (e) in each result set varied visibly between the various experiments. The pattern that is present in the data shows that larger set point changes causes quicker response than smaller changes. The response of the wall was also quicker in cases where the freeze lining became thinner compared with cases where the freeze lining grew thicker. Both these observations are consistent with the observations made in paragraph 6.4.2 (page 170).

8.6.4 Crust Thickness

Crust formation only occurred during experiments 8.5 and 8.10 (graph (c)). The reason for the crust formation was the relatively large change in energy input rate that resulted from the set point changes applied during these experiments. In both cases the energy input rate was effectively reduced by 200 kW. This reduction in energy input rate firstly caused the freeze lining to grow thicker. This solidification was however not enough to prevent the slag bath temperature from falling below its liquidus. The result was that solid slag was also formed in the Crust conductor module.

The indication of crust formation given by the model may indeed be accurate in that a crust would form in reality. Another possibility is that the solid slag would actually precipitate throughout the slag bath away from the zone close to the arc. Such precipitation would lead to an increase in effective slag viscosity, and an increased probability of slag foaming. Such process instabilities have been known to accompany incorrect set point changes that cause the furnace to become colder and 'close up'.

The volume fraction of solids in the slag bath can be calculated simply by dividing the crust thickness by the slag bath thickness (1 m). The solids content gives an indication of the effective slag viscosity.

8.6.5 Crust Composition

The solid slag in the crust consisted of only pseudobrookite and no rutile, similar to the freeze lining. The composition of the pseudobrookite was also very similar to that of the freeze lining. This is to be expected because liquid slag from the slag bath is the source for both the freeze lining and crust.

8.6.6 Slag Bath Temperature

Experiments 8.3 and 8.5 showed an initial drop in slag bath temperature, followed by a slow rise. The origin of the initial drop is not clear. The steady rise, however, can be attributed to the changing slag composition and the changing slag liquidus temperature.

The same initial drop in temperature was observed during experiments 8.8 and 8.10. Once again it is not known what the cause of this behaviour is. In these experiments the initial fall in temperature was followed

by a slow decrease in slag bath temperature. This is the result of the slight change in slag bath composition that was caused by slag solidification. In experiment 8.10 the slag bath temperature started increasing slightly once the freeze lining had reached a new stable thickness. This was the result of the slag bath composition starting to change in the opposite direction compared with before.

The slag bath temperature decreased during experiments 8.4 and 8.6 as a result of the decrease in reductant feed rate causing an increase in FeO content. During experiments 8.7 and 8.9 the change was in the opposite direction because of the dominant influence being the introduction of higher melting point material entering into the slag bath from the freeze lining.

8.6.7 Slag Bath Composition

Relative changes in slag bath composition for the subset of experiments being discussed here are shown in Figure 143. All changes were calculated as a percentage of the initial composition of each phase constituent.

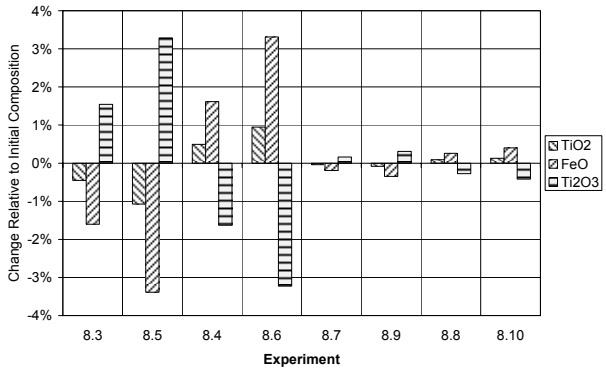

Figure 143 – Slag bath composition change relative to initial composition.

The variations in slag bath composition for the range of experiments were expected. Experiments 8.3 to 8.6 showed an increase in Ti_2O_3 content and a decrease in FeO and TiO_2 content when the reductant feed rate was increased (experiments 8.3 and 8.5). The opposite was observed when the reductant feed rate was reduced (experiments 8.4 and 8.6).

In the case of experiments 8.7 to 8.10, the only influence on slag bath composition was that of solidification and melting. The FeO and TiO_2 content increased and the Ti_2O_3 content decreased when the freeze lining became thicker (experiments 8.8 and 8.10). When the freeze lining melted away (experiments 8.7 and 8.9), the change in composition was in the opposite direction.

8.6.8 Metal Bath Composition

The reason for the noisy signals in this graph is the approach followed to constrain the slag bath composition close to the M_3O_5 composition. See paragraphs 5.6.8a and 5.6.8b for details.

Relative changes in slag bath composition for the subset of experiments being discussed here are shown in Figure 144. All changes were calculated as a percentage of the initial composition of each phase

constituent. The results for oxygen in this figure are less accurate, especially for the small changes in composition during experiments 8.7 to 8.10. This is the result of the noise in the oxygen content signal. The change in oxygen content was therefore ignored when interpreting the results of these four experiments.

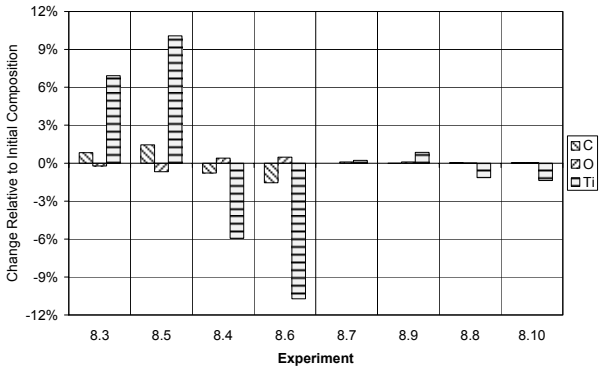

Figure 144 – Metal bath composition change relative to initial composition.

The first four experiments in the subset again did not present any surprises. The increase in reductant feed rate in experiments 8.3 and 8.5 resulted in more reducing conditions in the slag bath. This is evident from the increase in carbon and titanium content, and the reduction in oxygen content for these experiments. The decrease in reductant feed rate in experiments 8.4 and 8.6 had the opposite effect.

The change in composition during experiments 8.7 to 8.10 was expected to be minimal because only the power set point was changed. This was certainly the case for the carbon content. As mentioned before, the oxygen content will not be discussed here. The change in Ti content was also small, but more noticeable than what was expected.

The reason for the increase in Ti content during experiments 8.7 and 8.9 was the composition of the freeze lining that was being melted into the slag bath. This solid slag had a Ti_2O_3 content of roughly 40% and was situated on the stoichiometric M_3O_5 line indicated on graph (h) of the experimental results. This composition is significantly more reduced than the liquid slag in the furnace throughout the duration of the experiment. This resulted in the newly melted slag acting as a 'reductant' when entering the slag bath.

The explanation for the decrease in Ti content during experiments 8.8 and 8.10 can be explained similarly. Because the power set point was reduced during these experiments, liquid slag started to solidify. Because solidification tends to enrich the slag bath in FeO and TiO_2 and reduce the Ti_2O_3 content, the metal bath is gradually exposed to a more oxidised slag bath. This resulted in Ti being oxidised from the metal bath by the slag bath.

8.6.9 Off-gas Composition

The reason for the noisy signals in this graph is the approach followed to constrain the slag bath composition close to the M_3O_5 composition. See paragraphs 5.6.8a and 5.6.8b for details.

The off-gas composition results as shown in graph (j) of the experimental results were consistent with expectations. The partial oxygen pressure dropped when the reductant feed rate was increased (experiments 8.3 and 8.5) and increased when the reductant feed rate was decreased (experiments 8.4 and 8.6).

Virtually no change in partial oxygen pressure was observed for experiments 8.7 to 8.10. This is to be expected, because the greatest influence on the off-gas composition comes from Reactor2. This reactor was only subjected to a slight change in slag composition resulting from solidification and melting.

8.6.10 Reactor Power

The reason for the noisy signals in this graph is the approach followed to constrain the slag bath composition close to the M_3O_5 composition. See paragraphs 5.6.8a and 5.6.8b for details.

The changes in reactor power relative to the initial steady state for experiments 8.3 to 8.10 are shown in Figure 145. The power values for the various experiments were calculated by taking an average over the duration of the experiment.

For all experiments in the subset, the power of Reactor1 (heating and melting of ilmenite feed) changed only slightly relative to the initial steady state. In the case of experiments 8.3 to 8.6 Reactor1 power was lower than the initial steady state. This was because the slag bath temperature was lower than the initial steady state value for most of the duration of all four of these experiments. In the case of experiments 8.7 to 8.10 Reactor1 power increased when the electrical power set point was increased, and decreased when the electrical power set point was decreased. The reason for this was again the temperature of the slag bath relative to the initial steady state value.

The origin of the relationship between slag temperature and Reactor1 power lies in the fact that this reactor heats up the entering ilmenite to the temperature of the IsoMod1 isothermal module and transforms it to the liquid state. Since the SlagBath mixer module is contained in IsoMod1, it assumes the IsoMod1 temperature. Changes in this temperature influence the enthalpy required to heat up the molten ilmenite, and therefore directly influence Reactor1's power.

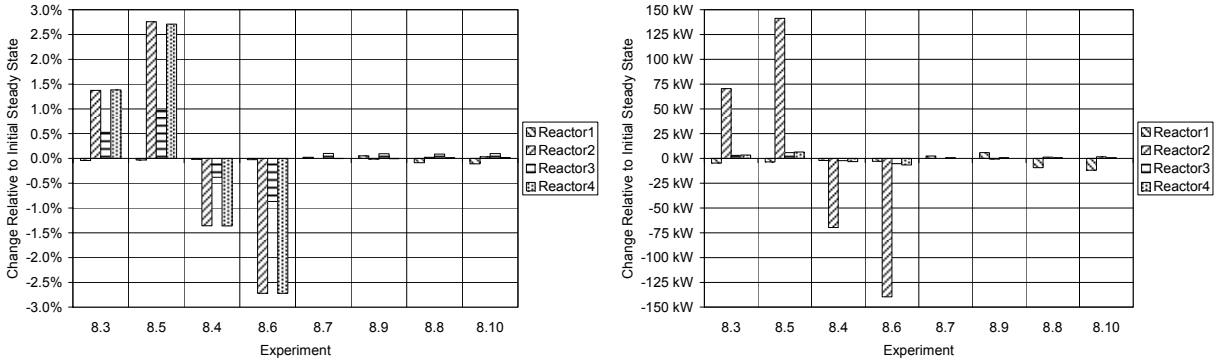

Figure 145 – Changes in reactor power values relative to initial steady state.

In graph (a) the change was calculated as a percentage of the initial steady state value. In graph (b) it was calculated by simply subtracting the kW values.

As expected, Reactor2 (slag-reductant reaction) power increased significantly when the reductant feed rate set point was increased (experiments 8.3 and 8.5) and decreased by roughly the same amount when the reductant feed rate set point was decreased (experiments 8.4 and 8.6). Virtually no change in Reactor2 power was detected when only the electrical power set point was adjusted (experiments 8.7 to 8.10).

Graph (a) of Figure 145 shows Reactor4 (carbon dissolution in metal) power changing by roughly the same percentage as the corresponding Reactor2 power, and in the same direction. This is because both these reactors are directly influenced by the reductant feed rate. The model was configured to dissolve more reductant into the metal bath (Reactor4) when more reductant is fed.

Reactor3 (metal-slag reaction) power increased in cases where the carbon content of the metal bath increased (experiments 8.3 and 8.5), and decreased in cases where the carbon content of the metal bath decreased (experiments 8.4 and 8.6).

8.6.11 Heat Losses

Heat loss rate results are shown in graph (l) of the experimental results.

The upper-furnace heat loss rate was a function of the surface temperature of the slag bath. In cases where no crust formed, this temperature was equal to the slag bath temperature. In cases where a crust did form (experiments 8.5 and 8.10), it was equal to the Crust conductor module's outer temperature.

The middle-furnace heat loss rate was determined by the thickness of the freeze lining. A thinner freeze lining resulted in a higher heat loss rate. This increase however lagged in time behind the thinning of the freeze lining due to the thermal inertia of the furnace wall.

Due to the method used to estimate the lower-furnace heat loss rate, this rate was directly proportional to the temperature of the metal bath.

8.7 APPROPRIATELY COMBINED ADJUSTMENT OF REDUCTANT AND ENERGY INPUTS

8.7.1 Freeze Lining Thickness

Figure 146 shows the change in freeze lining thickness relative to the initial value for experiments 8.11 to 8.20. The aim of these experiments was to obtain a more accurate value of the required ratio of changes in reductant and energy inputs (to maintain a stable freeze lining). Note that in experiments 8.11 to 8.18 the ratio of 1 kg to 5 kWh was maintained, for increasing sizes of perturbation. From this figure it is evident that the proposed 1:5 ratio of reductant input to energy input does not keep the process in complete balance. Experiments 8.17 and 8.18 show this most clearly. The ratio was therefore adjusted to 1:5.2 for experiment 8.19 and 1:5.3 for experiment 8.20. This caused the freeze lining thickness to remain more constant.

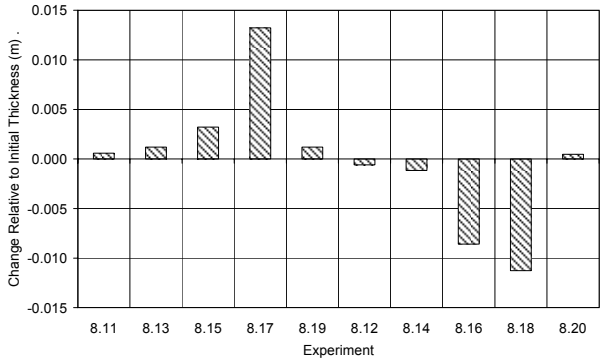

Figure 146 – Chapter 8 subsets 3 and 4 change in freeze lining thickness.

8.7.2 Freeze Lining Composition

It is evident from graph (b) of the experimental results that the composition of the freeze lining at the solid–liquid interface was influenced by the change in slag bath composition during the various experiments. During those experiments where the reductant and energy input rates were increased (experiments 8.11, 8.13, 8.15, 8.17 and 8.19), the freeze lining at the interface became richer in Ti_3O_5. The opposite was evident from the other experiments where the input rates were reduced.

In all cases the freeze lining consisted of only pseudobrookite with no rutile.

8.7.3 Thermal Response of Freeze Lining and Furnace Wall

Because the changes made to reductant and energy input rate set points resulted in only slight changes in freeze lining thickness, temperatures in the furnace wall either did not change to any significant degree, or it changed very slowly. This is shown in graph (e) of the experiment result sets.

8.7.4 Slag Bath Temperature

The change in slag bath temperature relative to the initial steady state value for the third and fourth experiment subsets are summarised in Figure 147.

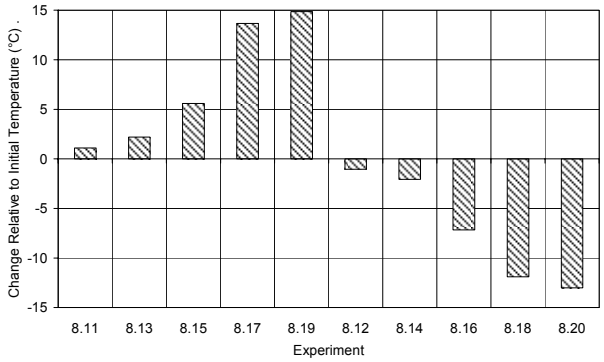

Figure 147 – Chapter 8 subsets 3 and 4 change in slag bath temperature relative to initial steady state.

The tendencies visible in these results were expected. The first five experiments shown in the Figure 147 represent conditions of progressively more reduction. This caused the liquidus temperature of the slag to increase. The opposite was true of the last five experiments in the figure.

8.7.5 Slag Bath Composition

Figure 148 shows a summary of the change in slag bath composition for experiments 8.11 to 8.20. The change is expressed as a percentage of the initial content value of each phase constituent.

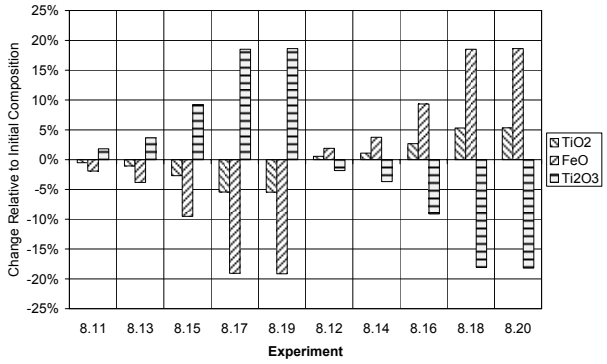

Figure 148 – Chapter 8 subsets 3 and 4 change in slag bath composition relative to initial steady state.

The first five experiments showed in Figure 148 shows an increase in Ti_2O_3 content and a decrease in TiO_2 and FeO content. This is consistent with the increased reductant and energy feed rate set points associated with these experiments. The last five experiments in this figure show the opposite change in composition. This is the result of the decreased reductant and energy feed rate set points used during these experiments.

In graph (h) of the experimental results it is evident that the direction in which the slag bath composition is changing, is parallel to the stoichiometric M_3O_5 line. This is a result of the formulation of the Reactor2Flow and Reactor3Flow sub-models. These sub-models were formulated in such a way that the model was able to reproduce the observed compositional invariance of the slag.

8.7.6 Metal Bath Composition

Figure 149 summarises the change in metal bath composition of experiments 8.11 to 8.20. The change is again expressed as a percentage of the initial content value of each phase constituent.

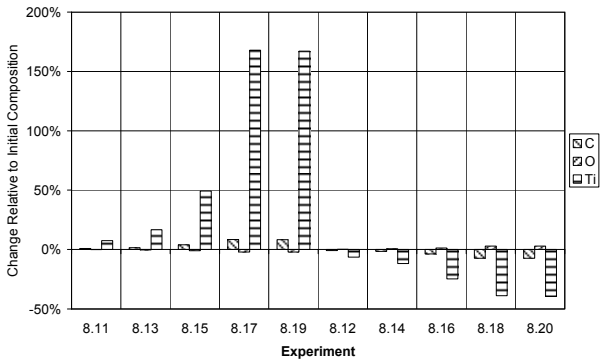

Figure 149 – Chapter 8 subset 3 and 4 change in metal bath composition relative to initial steady state.

The tendencies visible in Figure 149 are as expected. More reducing conditions associated with the first five experiments result in more carbon and titanium and less oxygen in the metal. The opposite was observed from the last five experiments that were executed with progressively less reducing conditions.

8.7.7 Off-Gas Composition

The off-gas composition results as presented in graph (j) of the experimental results showed an increase in partial oxygen pressure for experiments in which conditions were adjusted to be less reducing (experiments 8.12, 8.14, 8.16, 8.18 and 8.20). The opposite tendency is evident in the results of the remaining five experiments in which more reducing conditions were used.

8.7.8 Reactor Power

Figure 150 summarises the changes in reactor power relative to the initial steady state values. The power values for the various experiments were calculated by taking an average over the duration of the experiment.

The power of Reactor1 changed only slightly due to relatively small changes in slag bath temperature.

The power of Reactor2 increased as the reductant feed rate was increased, and decreased when the reductant feed rate was reduced. Graph (a) shows that the power of Reactor4 changes with the same percentage as Reactor2. This is due to both these reactors being influenced strongly by changes in reductant feed rate.

Reactor3 power increased when the carbon content of the metal bath increased, and decreased when the carbon content of the metal dropped.

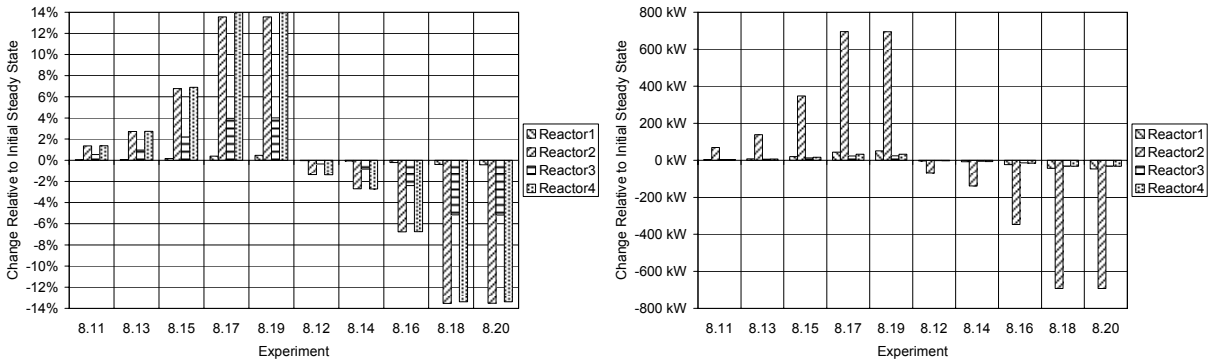

(a) (b)

Figure 150 – Chapter 8 subsets 3 and 4 changes in reactor power values relative to initial steady state.

In graph (a) the change was calculated as a percentage of the initial steady state value. In graph (b) it was calculated by simply subtracting the kW values.

8.7.9 Heat Losses

The heat losses as shown in graph (l) of the experimental results of experiments 8.11 to 8.20 presented no new insights. The upper-furnace and lower-furnace heat losses were determined by the temperature of the slag bath, and the middle-furnace heat loss by the thickness of the freeze lining.